OFDM based Time Difference Of Arrival Estimation

Ahmed Abudabbousa

Sorbonne Université

Ecole doctorale : EDITE 103

Laboratoire d'Électronique et Électromagnétisme

OFDM based Time Difference Of Arrival Estimation

Par Ahmed **Abudabbousa**

Thèse de doctorat d'Électronique

Dirigée par M. Aziz Benlarbi-Delaï

Présentée et soutenue publiquement le 17/04/2018

Devant un jury composé de :

Mme Boukour Fouzia, Directrice de recherche	rapporteur
M. Loyez Christophe, Directeur de Recherche	rapporteur
M. De Donker Philippe, Professeur	Examinateur
M. Kokabi Hamid, Professeur	Examinateur
M. Benlarbi-Delaï Aziz, Professeur	Directeur de thèse
M. Sarrazin Julien, Maître de conférence	Encadrant

This research is dedicated:

To my parents: my dear father "Issa" who spent his life to grow mine, and my sweethearted mother "Boshra" who is the spring that never stops giving.

To my wife "Areej", there are no words that could describe how I am grateful for her support and encouragement throughout the years.

To "Nima", who has always been by my side and gave me assistance.

To my daughter "Boshra" for her patience and understanding.

My deepest gratitude to my brothers: "Tamer", "Ghassan", "Housam", and my sisters "Inas" "Faten" "Nesrean".

Finally, to all my family members who have been a constant source of motivation, inspiration, and support.

Acknowledgments

First and foremost, I would like to express my deep appreciation to my director Prof. Aziz Benlarbi-Delaï for providing advice, support and excellent guidance. The warm discussions and regular meetings I had with him during this research. His spirit of youth contributed greatly to the successful completion of this research.

I also thankful to the members of jury particularly the reviewers Mme Boukour Fauzia, M. Loyez Christophe who their recommendations were very useful. In continue, thanks to M. De Donker Philippe, M. Kokabi Hamid and M. Sarrazin Julien.

I owe a deep debt of gratitude to the Islamic university of Gaza, Sorbonne University, the Phoenix project for giving me an opportunity to complete this work by providing me all the efforts and facilities.

Finally, I would like to take this opportunity to thank warmly all my beloved friends, who have been very supportive during my thesis, especially my best friend Amine Rabehi.

Abstract

Wireless technologies make possible the emergence of smart environment where different things are interconnected to each other to give people more services and flexibility. Due to that, a huge number of connected objects, expected to reach tens of billions by 2030, will be attached to the network and will need a huge amount of energy. This energy, usually expressed in time and frequency domains, needs to be reduced and may benefit from the optimal exploitation of the third domain: the spatial resource.

We focus on this last domain, since finding the position of the connected objects can help to perform multi-hop communication, or to achieve energy and data focalization, leading to energy efficient communication. Finding the position means generally performing triangulation, through pseudo-distances, which in turn means time delay management. So far, among several time estimation techniques, Time Difference Of Arrival (TDOA) seems to be a good candidate to combine accuracy and ease of use, especially for the short-range indoor application.

In order to help the emergence of a low added complexity indoor location system, our contribution consists of a TDOA based solution that exploits the OFDM based popular communication signals. In this work, we perform, using a Multiple Inputs Simple Output, channel characterization and modeling for TDOA estimation. By handling these channel frequency responses in different ways, we minimize different cost functions expressed as the difference between measured channel response and a predefined direct model. For validation, the simulation based on different topologies exhibit results pointing out the property of super-resolution of such approach. The performance of the proposed TDOA estimation is compared to the Cramer Rao Lower Bound. The effects of the multipath are taken into account and some proposed solutions are discussed and simulated. Moreover, the experimental part of this work validates both the direct and inverse models in different channel configurations.

Contents

Acknowledgments iv

Abstract vi

Contents viii

General Introduction 1

Chapter 1: Context and State of the art of Indoor Positioning 5

1.1 Introduction 5
1.2 Indoor positioning: a critical need 5
1.2.1 Context 5
1.2.2 General definitions 6
1.3 Indoor Positioning Systems 8
1.3.1 Infrared (IR) Positioning Systems 8
1.3.2 Ultra-sound Positioning Systems 8
1.3.3 Radio Frequency (RF) Positioning Systems 9
1.3.4 Alternative systems 11
1.4 Measuring Principles 14
1.4.1 RF Metrics for Wireless Localization 14
1.4.2 Scene Analysis 21
1.4.3 Proximity 21
1.4.4 Conclusion 21
1.5 Objectives 22
1.6 Conclusion 23
Bibliography 24

Chapter 2: Multi carrier communication signals 29

2.1 Introduction 29
2.2 General principle of MC based TDOA estimation 29
2.3 Multi carrier based positioning systems and OFDM solutions 30
2.3.1 Blind solution 30
2.3.2 Training solution 30
2.3.3 Alternative solution 31
2.3.4 OFDM based positioning 31

2.3.5 Conclusion 31
2.4 Data modulation 32
2.4.1 QPSK Based Communication System 32
2.4.2 SNR calculation 33
2.4.3 Simulation results 35
2.5 OFDM communication system 38
2.5.1 Transmitter/Receiver module 38
2.5.2 Guard Interval 39
2.5.3 Guard Band and roll of factor 43
2.6 MATLAB implementation 44
2.6.1 Transmission part 44
2.6.2 Reception part 45
2.7 Channel Estimation 46
2.7.1 Pilot block 47
2.7.2 Mathematical derivation 48
2.7.3 Channel estimation testing 50
2.8 Conclusion 51
Bibliography 52
Chapter 3: OFDM based TDOA estimation 55
3.1 Introduction 55
3.2 Algorithms for TDOA-based positioning 55
3.3 Definition of the direct model 56
3.3.1 Frequency limitation 57
3.3.2 Signal model 58
3.3.3 Energy based approach 59
3.3.4 Channel based approach 59
3.4 Inverse problem: TDOA extraction 64
3.4.1 Large TDOA 64
3.4.2 Small TDOA 65
3.4.3 Very small TDOA 72
3.4.4 Cramer Rao Bound Limit 75
3.5 Communication parameters effect 76
3.5.1 Estimation of the coefficients $\boldsymbol{\alpha 1}, \boldsymbol{\alpha 2}$ 76
3.5.2 Number of pilots 77
3.6 Communication environment effect 78

3.6.1 Multipath modeling 78
3.6.2 Emulating Multipath 79
3.6.3 Multipath effect reduction 80
3.7 Conclusion 82
Bibliography 83
Chapter 4: Experimental setup and results 85
4.1 Presentation of the environment 85
4.1.1 The controlled electromagnetic room 85
4.1.2 Radiating devices 87
4.1.1 Amplifier 87
4.1.2 Arbitrary waveform generator 88
4.1.3 Digital storage oscilloscope 88
4.1.4 Conclusion 89
4.2 SISO communication system setup 89
4.2.1 The transmitter 89
4.2.2 The receiver 91
4.2.3 Signal acquisition and I-Q constellation 92
4.2.4 OFDM communication performances 95
4.2.5 Channel estimation 96
4.3 Direct and Inverse models validation 98
4.3.1 MISO configuration 98
4.3.2 Baseline calculation 99
4.3.1 Calibration MISO system 100
4.3.2 MISO configuration for TDOA estimation 101
4.3.3 Direct model validation 102
4.3.4 Inverse model validation 104
4.3.5 Multipath effects 105
4.4 Conclusion 107
Conclusions and perspectives 109
Abbreviations 113
List of Figures 115
List of Tables 119

General Introduction

The vision of Internet of Things (IoT), making everyday objects readable, recognizable, locatable, addressable, and controllable, will plunge people in smart environments rich of new experiences and opportunities. Actually, due to the demand of increased mobility and flexibility in our daily life, we assist today to a widespread deployment of wireless local and personal area networks, which beside the upcoming billions of connected objects, appeal new radio solutions that 5G promises to offer.

In order to address these huge needs, the future development of 5G considers a greater number of base stations than today, and it is no doubt that this will involve massive additional power consumption. So it becomes clear that efficient energy communications are more than ever required to answer economic issues and sustainability.

It is well known that in current wireless local and personal area networks, the spectrum congestion, the low energy efficiency communications and the insufficient exploitation of the spatial resources are among the factors that may slow down the development of IoT or IoE (Internet of Everything). To overcome these forthcoming restrictions, wireless location technology, as the mechanism for discovering relationship between connected objects, appears as one of the key solutions. This is because dedicated localization techniques in wireless communication can help in developing more extensively the exploitation of spatial resources and allow driving optimized routing algorithms for low energy multi hops communication and spectrum decongestion for Green ICT (Information and Communication Technology) by means of cognitive radio. Beside this, location already starts playing a major role to promote another emerging vision: a spatio-temporal Internet of Places (IoP), which would be able to structure and organize the spatial content of Internet.

To be ubiquitous, and hence compliant with the so-called Intelligent Ambience, location systems need to be embedded in various connected objects, even the smallest ones, and to be infrastructure free solution. This requires a specific attention regarding the size of proposed solutions, and regarding the added complexity to already existing infrastructures.

However, to truly achieve ubiquitous positioning, proposed solutions should solve problems and challenges related to the Non Line-of-sight (NLOS) propagation, signal scattering and multipath effects, interferences, vulnerability to environment changes, computational complexity and fine resolution. Facing these challenges, the localization, seen as a multidimensional problem, appears more complicated to perform and therefore many scientific areas such as specific channel modeling, algorithmic, statistics, RF circuit, and system design, hard/soft approach should be simultaneously considered in order to define a veritable science of localization.

To address these needs, and in order to help the emergence of a low added complexity indoor accurate location, our contribution consists with a Time Difference Of Arrival (TDOA) based solution that exploits already existing popular communication signals involved in 4G, and compliant with upcoming new radio solutions proposed for 5G.

So it appears relevant to perform a specific channel characterization and modeling dedicated to TDOA estimation, and later to location. Actually as the channel acts as an important transfer function whose knowledge is required, the time delay estimation needs a deep understanding of the channel behavior, to enhance the performance of the numerous approaches we dealt with.

This thesis report is structured as follows: chapter 1 starts by introducing the critical needs of the indoor positioning, and give o brief overview of existing technologies. The main wireless RF metrics for location are exposed and finally, stating the objectives of this research ends this chapter.

Second Chapter starts with the literature review of using the multicarrier signals, in indoor position especially, for Time Difference of Arrival estimation. The implementation of communication systems using multicarrier signal will be illustrated mathematically which include OFDM transmitter and receiver based QPSK modulation, SNR calculation, cyclic prefix, and channel estimation.

In the third chapter, a new TDOA estimation method based on the channel estimation is presented. After presenting the state of the art of TDOA estimation, we develop all the mathematical derivations leading to the definition of the direct problem. With that, the simulation results, based on different topologies described by different block diagrams, are

presented, and the performance of the proposed TDOA estimation, stating the inverse problem, is compared to Cramer Rao Lower Band. At the end, the effects of the multipath are demonstrated and some proposed solution are discussed and simulated.

Finally, the fourth chapter, as experimental part of this work, validates both the direct and inverse models in different channel configurations. Conclusion and perspectives end this work.

Chapter 1: Context and State of the art of Indoor Positioning

1.1 Introduction

The indoor positioning (IP) seems to be a key piece to give Personal Networks a better functionality, meeting the requirements in terms of agility, configurability, connectivity, and energy efficient communication. The indoor positioning is also serving many applications in various domains (health, entertainment, military …) making it really relevant and almost unavoidable.

The present chapter gives a brief overview describing these needs and the technical means to achieve them. After exposing the main metrics and the state of the art, we define the objectives we target in this work and justify the main choices we made.

1.2 Indoor positioning: a critical need

1.2.1 Context

Personal Networks have been designed to meet the demands of users to interconnect their various personal devices at different places into a single network as shown in Figure 1-1.

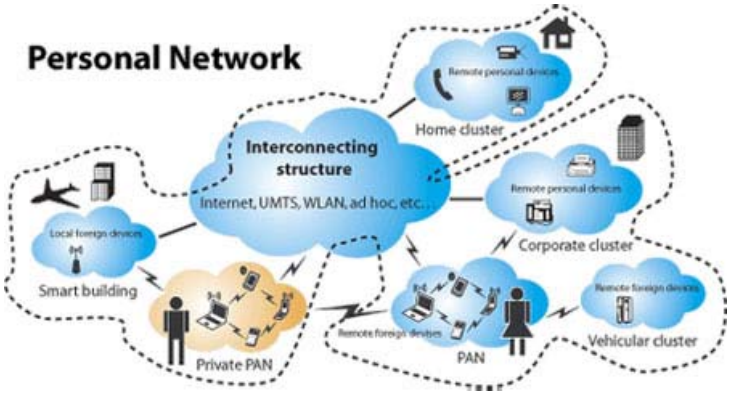

Figure 1-1: Personal Networks (PNs) [1]

This architecture will emerge new concepts and features for wireless data transmission and transponder systems. Some of the numerous possible application areas are: self-organizing sensor networks, ubiquitous computing, location sensitive billing, context dependent information services, tracking, and guiding.

So a well suited Personal Networks should include an accurate reliable and real-time indoor positioning protocols and services [2], [3], [4], especially for the future generation of communications networks in smart cities, where there is rapid development of integrated networks and services in PNs [5]. In addition, location information is one of the most important needs for several objectives since it helps to get better network planning [6], network adaptation [7], and load balancing [8] , etc.

Nowadays, IP Systems enable valuable position-based applications and services for users in Personal Networks such as homes, offices, sports centers, etc. For example, inside complex hospitals environments they provide guidance to the patients for efficient use of the limited medical resources system with achieving communication distance up to tens of meters away. Another example such as specifying a location of products stored in a warehouse may impact directly on storage costs. In addition, detecting firemen location in a building on fire, with maximum 3m accuracy and 95% accuracy, following up police dogs trained to find explosives in a building, and finding out tagged maintenance tools and equipment scattered all over a plant, remain relevant applications for IP. Another emerging field, requiring more precise positioning, deals with the Body Area Network [9]

1.2.2 General definitions

For positioning purpose, we need to distinguish between self-positioning, where the connected object or mobile unit (MU) itself determines its spatial coordinates relatively to fixed access or reference unit (RU), like for GPS, and remote positioning where the position of the MU is determined by a central point, like radar.

In some networks or for IoT purpose, one can also meet hybrid approaches leading to indirect remote positioning (IRP) or indirect self-positioning (ISP) system. For IRP system, each MU first performs a self-positioning and then transmits its position to a central point. For ISP the central point disseminates in the network the position of all objects. IRP and ISP are of great importance in updating the neighborhood tables highly required for routing algorithms.

Depending on different applications, IP Systems assign different types of location information mainly classified as [10]:

- Physical location which expresses a location in the form of coordinates;

- Symbolic location which expresses a location in a natural-language way such as : in the office, in the third-floor, in the bedroom, etc.;
- Absolute location which uses a shared reference grid for all located objects;
- Relative location which depends on its own frame of reference.

Categorizing indoor positioning Systems can be based on the technology options as well as on the positioning algorithms used for. From positioning algorithms point of view there are mainly three types [11]:

- Conventional triangulation,
- Scene analysis,
- Proximity positioning algorithms.

Based on these fundamental technologies and algorithms, research centers and universities try to find out new IP Systems by taking into account the advantages of one of the three positioning technologies or by combining, in a relevant way, some of them. The capability of positioning a device can be done for instance for wireless technology, through four steps, as shown in Figure 1-2.

- Detect the signals coming from fixed access points within particular vicinity,
- Calculate the propagation times,
- Estimate the position with respect to these access points,
- Use positioning information for every context aware application (shopping mall, hospital, marketing…etc.

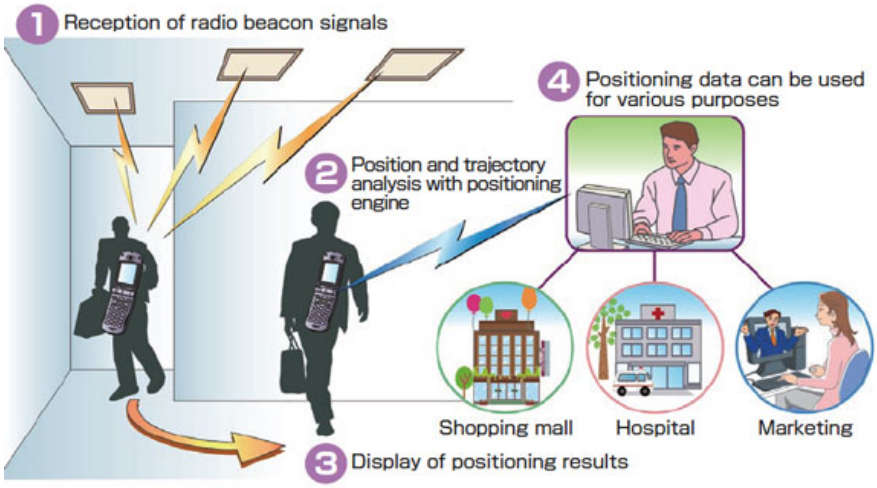

Figure 1-2: Understanding Indoor Positioning System.

1.3 Indoor Positioning Systems

In this section, we introduce a short review about a variety of IP Systems. These IP Systems will be explained according to the criteria and requirements specified in the previous section which focuses on the user needs in Personal Networks. Thus we can know the advantages and limitations of these IP Systems from the user point of view.

1.3.1 Infrared (IR) Positioning Systems

Infrared (IR) positioning systems [12], [13], [14] use IR technology to perform localization as shown in Figure 1-3. There are three main systems IR uses: Active Badge, Firefly, and OPTOTRAK PRO series.

The simplicity of the systems architecture, the accurate positioning and the ability to be carried by a person, are the common advantages of these systems. On the other hand, the main disadvantages are that IR positioning systems are limited within a room and need high directional line-of-sight communication between transmitters and receivers without interference from strong light sources.

Some limitations for sensing the location in terms of security, privacy, cost, and finally the IR wave cannot penetrate opaque materials, and many tags has to be installed on the localized object, which adds more complexity for implementation.

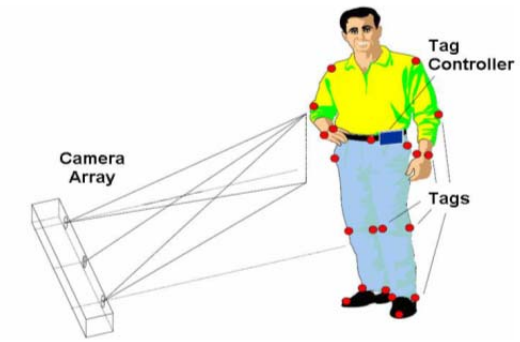

Figure 1-3: Example of IR Positioning system: The Firefly motion tracking architecture.

1.3.2 Ultra-sound Positioning Systems

Another way to perform object positioning is to use ultrasound signal. With this kind of inexpensive positioning solutions, ultrasonic technology and triangulation technique are

used to estimate the location of a target installed on a person. Usually, a combination of the ultrasound signals and Radiofrequency signals are used to perform synchronization and coordination in the system [15], [16]. This increases the system coverage area.

There are three Ultrasound positioning systems: Active Bat [17], Cricke [18] and, Sonitor [19]. All of them suffer from reflected ultrasound signals, noise, and have lower measurement accuracy (several centimeters) than IR-based systems (several millimeters).

1.3.3 Radio Frequency (RF) Positioning Systems

Today the main solutions for localization use RF wireless techniques that are reported in a huge amount of publications and which can be summarized in a comprehensive survey assessed in 2001, by Hightower & Borriello [20]. As mentioned previously, the taxonomy of localization mechanisms shows that there are mainly four ways to perform localization. The first one includes active localization where the beacon sends signals to localize target and acts as RP or radar. The second one deal with cooperative localization, i.e. the target cooperates with the system, and acts as RP or SP. The third way concerns passive localization where the system deduces location from observation of opportunistic signals, acting as SP, and finally the last way is blind localization where the system deduces location of object without *a priori* knowledge of its characteristics, and hence acts as RP.

Radiofrequency (RF) technologies are used in IP Systems to provide larger coverage area. In addition, they need less hardware comparing to other systems because of their capability to travel through walls and human bodies.

The main techniques used by RF-based positioning systems are triangulation and fingerprinting techniques. Fingerprinting gives a good estimation performance in complicated indoor environments, where it depends on location related characteristics to calculate the location of a user or a device. Here are some introductions to different types of RF positioning system.

1.3.3.1 **Radio Frequency Identification (RFID)**

The radio frequency identification (RFID) is commonly used in complex indoor environments such as office, hospital, etc. it can be used to stores and retrieves data through electromagnetic transmission, also it enables flexible and cheap identification of an individual

person or device. There are two kinds of RFID technologies, passive RFID and active RFID [21]. We could distinguish between the two kinds by specifying where the target is, if it is at the receiver side then the technology is passive RFID, otherwise it is active RFID. The targets with passive RFID are small and inexpensive but their coverage range is short. Conversely, in Active RFID, cost of targets is higher and their coverage area is larger. As an example, RadarGolf sells a golf ball that helps golf player to locate his golf ball quickly over a range of some 10 to 30 meters. The system uses received signal strength or imaging techniques to locate the ball.

1.3.3.2 **Wireless local area network (WLAN)**

Many of the public areas such as train stations, universities, and many else have used WLAN technology to implement their networks. So the existing WLAN infrastructures in indoor environments have been reused by WLAN-based positioning systems, which reduce drastically the cost of indoor positioning. The WLAN-based positioning systems can also reuse PADs, laptops, and mobile phones as tracked targets to locate persons, hence this WLAN technology is already integrated into these wireless devices.

Companies such as AeroScout, Ekahau, PanGo, and WherNet provide Wi-Fi tags able to track locations of notebook PC and persons. However, there are many problems, dealing with the channel effects, that affect the accuracy of location estimation.

1.3.3.3 **Bluetooth, the IEEE 802.15.1 standard**

Bluetooth replaces the IR ports mounted on mobile devices because it enables a longer range of few tens of meters (Bluetooth 2.0 Standards). Bluetooth chipsets are low cost, it results in low price tracked targets which are used in the positioning systems. In general, the infrastructures in Bluetooth-based positioning systems [22] consist of various Bluetooth clusters. In each cluster, the other mobile terminals locate, using fingerprinting technique, the position of a Bluetooth mobile device. However, accuracy from 2m to 3m and delay of about 20s is only what can Bluetooth-based positioning system provides, as it suffers from the drawbacks of RF positioning technique in the complex and changing indoor situations.

1.3.3.4 **Sensor Networks**

Here, the sensors simply detect any specific changes in a physical or an environmental condition, for example, sound, pressure, temperature, light, etc., and produce relative outputs.

Sensor based IP Systems use a number of known sensors in a fixed position and locates the position of an object from the measurements taken from these sensors. Due to the decreasing price and size of sensors, IP Systems sensor based [23], [24] provides a cost-effective and convenient way of locating persons. Compared with the mobile phone, cheap and small sensors have limited processing capability and low battery power. The drawbacks could be summarized as less accurate, low autonomy, low computational ability…. So, more efforts are needed to offer precise and flexible indoor positioning services.

1.3.3.5 **The ultra-wide band UWB**

Short duration of the ultra-wideband (UWB) [25] pulses helps to filter the multipath, and hence offers theoretically higher accuracy. So UWB technology has gained popularity in positioning systems. In addition, UWB technology offers various advantages over other positioning technologies used in the IP Systems such less interference, high penetration ability…. Furthermore, the positioning system is a cost-effective solution, because the UWB sensors are cheap. In addition, UWB based positioning system is scalable due to larger coverage range of each sensor.

Companies such as Ubisense or Be Spoon, defined an UWB platform devoted to industrial users such as warehouse, or propose a UWB chip able to perform a 1D localization with a few centimeters accuracy using time delay measurement.

1.3.4 **Alternative systems**

One of the oldest and classical position estimation ways is to use magnetic signals [26]. It gives a high accuracy and does not suffer from non-line of sight, where also the magnetic sensors are small in size, robust and cheap, but with a limited coverage range. This solution belongs to Dead Reckoning (DR) systems that are inertial based relative positioning system. They rely on sensing the component of MU's acceleration or velocity and then after integration of these components, one can access the track of the MU. However odometer, gyroscope, compass and accelerometer, which are the main devices of DR, are subject to drift error and may be updated regularly.

Vision-based positioning can easily provide some location-based information, using low price camera to cover a large specified area, it can track the locations and identify persons or devices in a complex indoor environment [27]. The tracked person does not need carrying

or wearing any device. But it has some drawbacks dealing with privacy and reliability. It is also influenced by many interference sources such as weather, light, motion, etc., and requires higher computational ability.

Audible sound is a possible technology for indoor positioning [28]. Since everyone has his own mobile unit such as mobile phone, PDA, etc., each MU has audible sound service. Then these devices can be reused by the audible sound-based positioning system for IP, and the users can use their personal devices in an audible sound positioning system to get their positions. Audible sound properties have some limitation, like the interference with sound noises and low penetration ability, therefore, the scope of an infrastructure component is within a single room.

We summarize in the following table the comparison between these solutions

Table 1-1 Comparison between Indoor Positioning Technologies.

Technology	Positioning technique	Advantages	Disadvantages
RFID	Proximity, RSS	Penetrate solid, non-metal objects; does not require LOS between RF transmitters and receivers.	The antenna affects the RF signal, the positioning coverage is small, the role of proximity lacks communications capabilities, cannot be integrated easily with other systems [29], RF is not inherently secure.
WLAN	RSS	Cover more than one building due to use existing communication networks; WLANs exist approximately in the majority of buildings; LOS is not required [30].	A major drawback of WLAN fingerprinting systems is the recalculation of the predefined signal strength map in case of changes in the environment [30]
Bluetooth	Proximity, RSSI	Does not require LOS between communicating devices; a lighter standard and highly ubiquitous; it is also built into most smartphones, personal digital assistants, *etc*. [31].	The greater number of cells, the smaller size of each cell and hence better accuracy, but more cells increase the cost; requires some relatively expensive receiving cells; requires a host computer to locate the Bluetooth radio.
Sensor Networks	Pattern recognition	They are relatively cheap compared with other, such as ultrasound and ultra-wideband technologies [32].	Requires LOS, coverage is limited [30].
UWB	TDOA/TOA	High accuracy positioning, even in the presence of severe multipath, may passes through walls, equipment, and any other obstacles; UWB will not interfere with existing RF systems if properly designed.	High cost of UWB equipment [30]; although UWB is less susceptible to interference relative to other technologies, it is still subject to interference caused by metallic materials [31].

1.4 Measuring Principles

The generic flow chart of the major process in the indoor self-positioning system is described in Figure 1-4. The first step is to detect the signal travelling from RU to MU or from MU to RU. Then apply the chosen metric depending on the application. Third chose the well suited algorithm and finally give the location information.

Figure 1-4: Flow Chart of general Indoor positioning system.

For RF systems, there are mainly three metrics used by several algorithms in positioning systems to localize a MU. Triangulation, scene analysis, and proximity are often used and each of them has advantages and disadvantages. Combining two of positioning metrics could lead to get better performance.

1.4.1 RF Metrics for Wireless Localization

To perform localization, engineers and researchers use the well-known triangulation method. There are two main derivations to estimate the target location based on the geometric properties of triangles: lateration and angulation.

Lateration, which is a range-based method, uses multiple RU to position a MU. Instead of measuring its distances, it measures received signal strengths (RSS), time of arrival (TOA) or time difference of arrival (TDOA). Some systems use Roundtrip Time of Flight (RTOF) or received signal phase method, which can be considered as a narrow band version of TDOA.

In the same way, angulation uses also at least two RU but it is not a range-based method as it computes the angles of the MU seen by the different RU. The Fingerprint and image recognition are other non-range based methods that can allow positioning.

1.4.1.1 **Time of arrival (TOA)**

In free space scenario, the signal propagation time is directly proportional to the distance between the MU and the RU using the velocity law. Once the time is measured and the speed of light is already known ($3.1 * 10^8$m/s), the distance can be determined. Therefore, as shown in Figure 1-5, TOA is the absolute arrival time of each copy of the signal at the MU, and at least three RU are used to enable 2-D positioning.

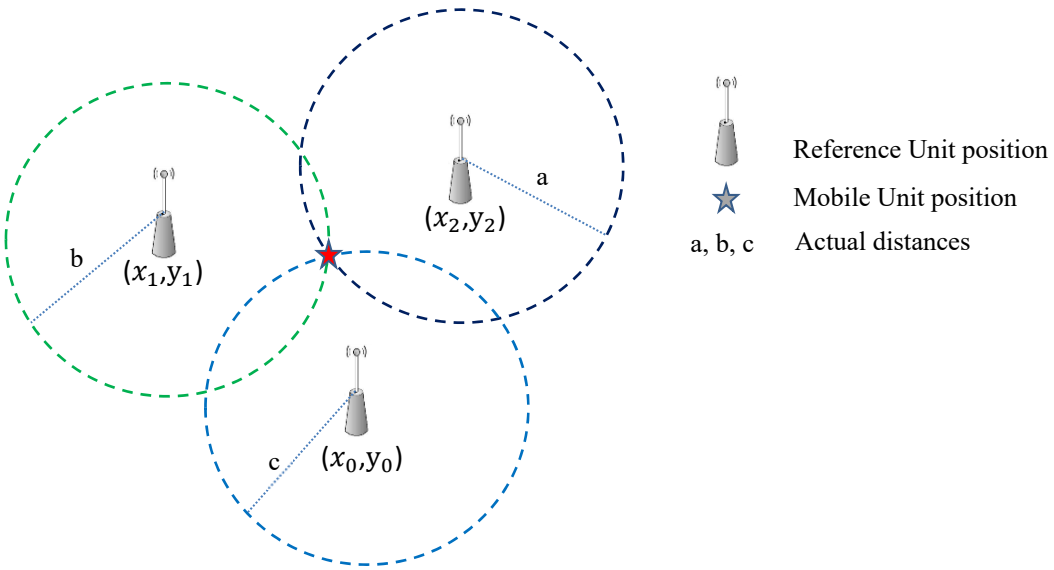

Figure 1-5: Time of arrival (ToA)-based approach.

In general, there are two main problems in using TOA. First, precise temporal synchronization is necessary between the MU and all RU; thus, while the synchronization is quite accurate, it is not always practical (atomic clock is required for GPS). Second, each received signal has to be labeled, to give the MU the ability to distinguish which signal is coming from which RU.

There are many algorithms for TOA-based indoor location system like closest-neighbor (CN) and residual weighting (RWGH) [33], and straightforward approach. In CN algorithm, the location of the MU is simply the location of the nearest RU to it. The RWGH algorithm uses a form of a weighted least-squares algorithm, it is suitable for Line of Site (LOS), non-LOS (NLOS) and mixed LOS/NLOS channel conditions. In straightforward approach, the position of the MU uses a geometric method to compute the intersection points of the circles of TOA as in Figure 1-5.

Another approach is to locate the target using TOA by minimizing the sum of squares of a nonlinear cost function, i.e., least-squares algorithm [34]. By assuming the location of the mobile terminal at (x_0,y_0), and it transmits a signal at time t_0, to the N base stations located at (x_1, y_1), $(x_2, , y_2)$..., (x_N, y_N) that receive the signal at time t_1, t_2, t_N. The cost function can be formed by:

$$\boldsymbol{F}(\boldsymbol{r}) = \sum_{i=1}^{N} \alpha_i^2 \ f_i^2(\boldsymbol{r}) \tag{1}$$

Where α_i can be chosen to reflect the reliability of the received signal at the measuring unit i, and $f_i(r)$ is given as follows:

$$f_i(r) = c(t_i - t) - \sqrt{(x_i - x)^2 + (y_i - y)^2} \tag{2}$$

Where c is the speed of light, and $\boldsymbol{r} = (x, y, t)^T$. This function is formed for each measuring unit, $i = 1, 2, \dots, N$ and $f_i(r)$ could be made zero with the proper choice of $x, y, and\ t$. The location estimate is determined by minimizing the cost function $\boldsymbol{F}(\boldsymbol{r})$.

1.4.1.2 **Time difference of arrival (TDOA)**

Unlike the TOA, TDOA is the difference between two TOA, and needs to solve a set of nonlinear equations to estimate the MU location. This approach does not need synchronization between the MU and RU, but it only does between the receivers. This leads us to take into account the distances between the RUs. If they are large, the synchronization will be practically hard, and if they are small, we have to deal with collocated RUs scenario which our estimation is focused on.

Each TDOA produced has a hyperboloid related to two measuring units where the transmitter must lie on it as in Figure 1-6.

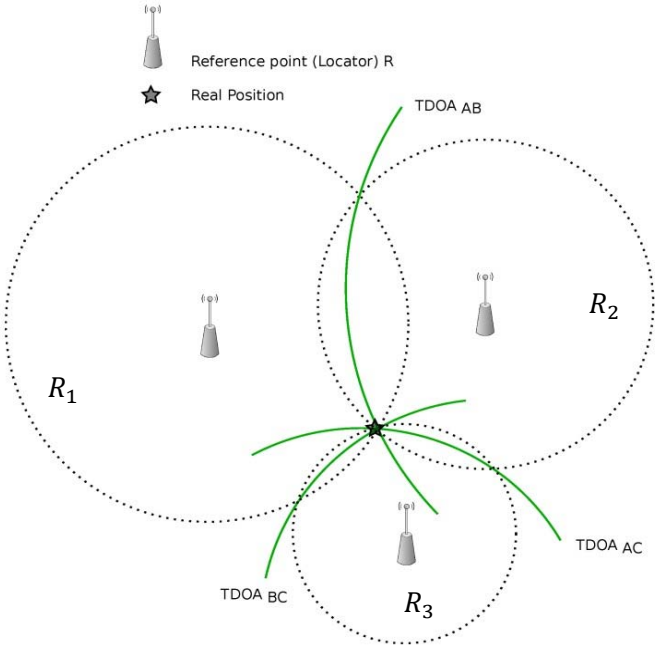

Figure 1-6 Time difference of arrival (TDOA)-based approach.

The equation of the hyperboloid is given by:

$$R_{i,j} = \sqrt{(x_i - x)^2 + (y_i - y)^2 + (z_i - z)^2} - \sqrt{\left(x_j - x\right)^2 + \left(y_j - y\right)^2 + \left(z_j - z\right)^2} \quad (3)$$

Where (x_i, y_i, z_i) and (x_j, y_j, z_i) represent the fixed receivers *i* and *j*; and *(x, y, z)* represent the coordinate of the location. The easier solution for the hyperbolic TDOA equation shown in (3) is to linearize the equations through the use of a Taylor-series expansion and create an iterative algorithm [35]. To estimate a 2-D location of the location as shown in Figure 1-6, two hyperbolas are formed from TDOA measurements at three fixed measuring units $(R_1, R_2, and\ R_3)$.

1.4.1.3 **Phase Of Arrival (POA)**

The phase of arrival (POA) [36] has the same concept than the TDOA, except that it depends on the phase carrier (or phase difference) to estimate the range in the narrowband signal. To explain the concept of POA let us see Figure 1-7. Two RUs 1 and 2 are placed at particular locations. The MU emit sinusoidal signal with frequency *f*, in order to determine the phases of the signal received at each RU. The transmitted signal reaches each RU after a TDOA τ, which leads to a POA $\varphi_i = 2\pi f\tau$. Then the POA based positioning system is able

to adopt the algorithms using TDOA measurement to locate the MU. However POA needs unwrapping solutions to solve the ambiguity problem.

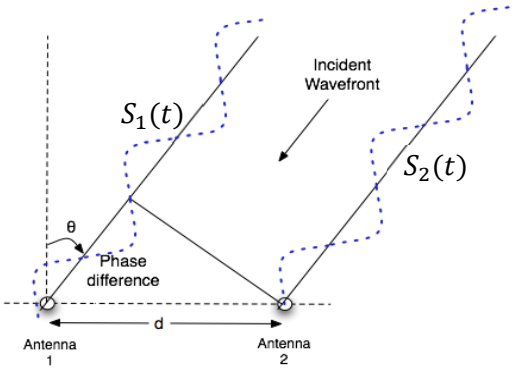

Figure 1-7: Principle of carrier phase interferometry.

1.4.1.4 **Round Trip of flight (RTOF)**

The main concept of this method is to use common radar approach. Several RUs acting as transponders respond to the interrogating signal sent by the MU, which measures the roundtrip propagation time as illustrated in Figure 1-8. Notice that its range measurement mechanism is similar to TOA, except that RTOF performs easily the above synchronization since the MU acts as a collocated transmitter and receiver.

The difficulty is to know what is the exact delay/processing time caused by the RUs. It could be ignored in long-range or medium-range systems, where it has to be taken into account for short-range systems. An algorithm to measure RTOF of wireless LAN packets is presented in [37] with the result of measurement error of few meters.

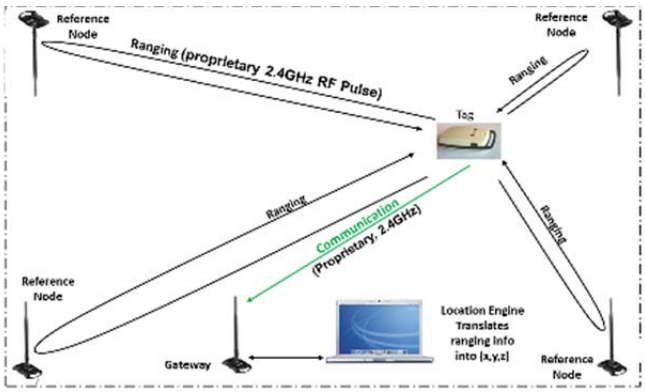

Figure 1-8: Example of RTOF system : Essensium Positioning System.

1.4.1.5 **Received signal strength (RSS)**

By measuring the attenuation of emitted signal strength, it could be possible to estimate the distance of the MU from some set of RUs, where signal attenuation has a relationship with the path loss. Comparing between the transmitted signal strength and the received signal strength, results into a range estimate for free space scenario. Multipath fading and shadowing has an effect on this method, so it can be improved by utilizing the premeasured RSS contours centered at the receiver [38] or multiple measurements at several base stations.

1.4.1.6 **Angle of arrival (AOA)**

Also called the Direction of Arrival (DOA) is commonly referred to as Direction Finding (DF). In this method, each RU is a center of a circle where the MU lies. Two RUs form pairs of angle direction lines, and then the location of the MU can be found in the intersection of these lines, as shown in Figure 1-9.

For 3-D location, AOA methods use at least three known RUs (A, B, C), and three measured angles a, b, c to derive the position of the MU. A big advantage of AOA is that no times synchronization between MU and RUs are required.

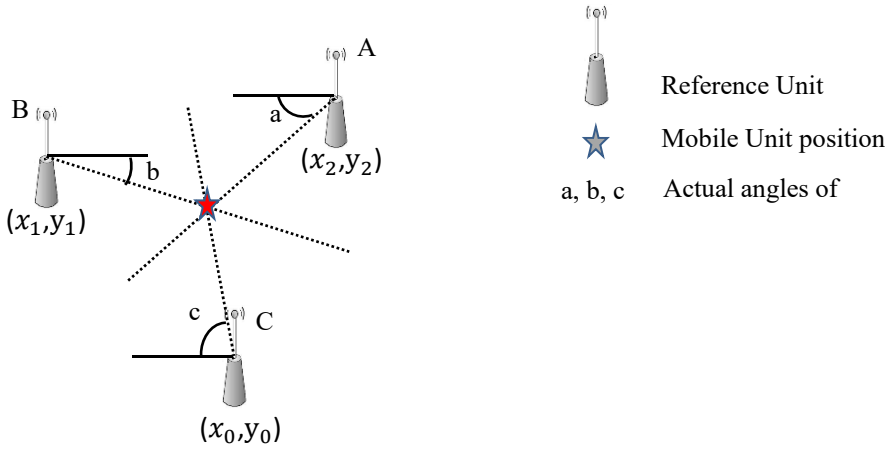

Figure 1-9: Basic AOA positioning.

The drawback of AOA measurements is that the quality of the final position estimate degrades rapidly as the MU moves away from the RU, and needs relatively large antennas or antenna arrays. More detailed discussions on AOA estimation algorithms and their properties are provided in [39].

We summarize in Table 1-1 the comparison of these metrics :

Table 1-2 Comparison of RF metrics.

Criteria	AOA	TOA	TDOA	RSS
Position Estimation	The intersection of several pairs of angle direction lines	The distance is directly proportional to time taken by the signal to go from the target to references.	Multiple intersected hyperbolas related to the delta in time between the signal's arrivals at multiple references.	The distance is inversely proportional to received signals strength from several references at the target.
2D space	At least two reference nodes			
3D space	At least three reference nodes		At least four reference nodes	
Synchronization	Lower requirement in terms of clock precision	All nods have to be precisely synchronized	Only the reference nodes need to be synchronized	Not required
Issues	Small errors in angle measurement egatively impact accuracy [40].	Relative clock drift between sender and receiver.	Lower accuracy than TOA with the same system geometry.	Sensitive to channel inconsistency, Require short distances between nodes.
Advantages	the receiver does not need to maintain phase coherence with the time source [41].	It is the most accurate technique, if precise synchronization achieved [42] [40].	It needs only to synchronize the base stations participating in the positioning [40] [43].	It is simple to deploy, there is no need for specialized hardware at the mobile station [44].
Disadvantages	Require costly and large dimensions of antenna arrays. As the distance from the source increases, the position accuracy decreases [45].	It is complex to implement [10], it requires precise time synchronization of all the devices which is high cost [40] [43].	It needs some prior knowledge to eliminate the position ambiguity [40], it is affected by multipath of signals [40].	The establishment of accurate indoor propagation model is very difficult. [43], and affected by environmental dynamics [46].

1.4.2 Scene Analysis

Scene analysis based on RF signal is done by collecting features (fingerprints) of a scene, then matching them with one taken before. RSS-based location fingerprinting is commonly used in scene analysis.

Location fingerprinting consists of two stages: offline stage and online stage. In offline stage collecting signal strengths from nearby base stations/measuring units are done. During the online stage, the currently observed signal strengths and previously collected information are used by a location positioning technique.

We mention four location fingerprinting-based positioning algorithms using pattern recognition technique: K-nearest-neighbor (KNN) [47], neural networks [48], support vector machine (SVM) [49] - [50], and smallest M-vertex polygon (SMP) [51].

1.4.3 Proximity

This technique is one of the simplest algorithms to implement and is already in use today. Locate a MU is done with respect to a well-known dense grid of antennas. A MU is considered to be at the same place as the antenna that receives the strongest signal from it.

One of the most particular examples is the Cell Identification (Cell-ID) or Cell Of Origin (COO) method. The systems using IR and RFID are also often based on this method. In RFID systems, RFID scanners are installed to cover all the area, the presence of the object in a one scanner area is used to determine the location of the object.

1.4.4 Conclusion

Whatever the considered metric and the proposed commercially available system, all these kinds of solutions, methods, and systems are well performing but not in dense multipath environments such as indoor scenarios. Hence it is very important to imagine alternative solutions that can work seamlessly either for outdoor or indoor applications. To attain this ultimate goal called *"continuity of localization"*, important research must be directed toward multiple ways dealing mainly with accuracy and precision but also with granularity and scale, relative or absolute positioning, mobile or fixed objects, infrastructure and cost, co-existence with communication systems.

1.5 Objectives

The presented brief overview shows a clear advantage for RF solutions due to their properties of propagation. It also points out that location estimation is more robust and more precise if the metric used is based on time measurement.

Based on these facts, we develop original research to improve the time delay measurement techniques. In order to release the constraints due to accurate synchronization between RU and MU, we do not consider TOA but TDOA. Which doing so, one should however observe accurate synchronization between the different RUs. This can be made easily if we consider that all the RUs are close to each other, in the way that they can be connected wired. We call this scenario collocated RUs.

We also mention that the proposed solution, which requires wideband signals, should be performed without demanding new infrastructures and may use the already existing popular communication signals and standards. Doing so, one can claim a dedicated infrastructure free solution based on multicarrier communication and especially on Orthogonal Frequency Division Multiplexing (OFDM) signal. The following block diagram shown in Figure 1-10, summarizes the considered scenario.

Figure 1-10: General block diagram the proposed method.

The main objective of this thesis is therefore to extract, for self-positioning purpose and from channel estimation, very small TDOA, compared to the bandwidth of interest. Indeed the proposed approach attempts to minimize the amount of bandwidth for the considered TDOA of interest.

Starting with the communication part, we develop a good knowledge of the communication relevant parameters dealing with – for example – SNR, multicarrier implementation, roll off factor, accepted BER, type of modulation…etc, and then we formulate the problem based on the estimation of channel state information (CSI) to allow simultaneously the localization, by means of TDOA estimation, and the communication.

The performance of the proposed TDOA estimator is evaluated by both numerical simulations and experimental results. They will be illustrated in the following chapters which give high precision compared with the classical methods.

1.6 Conclusion

Personal Networks require various types of context aware communications to offer flexible and adaptive services. It provides, into one single network, a private and user-centric solution by combining all users' personal devices at various places in different types of networks. One of the important information, in this context, is location, which enables, tracking, navigation, monitoring, and other location-aware services to make everyday life smart and more secure.

We presented in this chapter, the system architectures and working principles of different existing IP Systems that have been classified into four categories. We gave their performance and suggested to target dedicated infrastructure free IP solutions based on TDOA and able to provide at short-term accurate location.

Bibliography

[1] https://uk.nec.com/en_GB/emea/about/neclab_eu/projects/magnet.html

[2] M. Vossiek, L. Wiebking, P. Gulden, J. Wieghardt, C. Hoffmann and P. Heide, "Wireless Local Positioning," *IEEE Microwave magazine,* vol. 4, no. 4, pp. 77-86, 2003.

[3] K. K. Muthukrishnan, M. Lijding and P. J. Havinga, "Towards Smart Surroundings: Enabling Techniques and Technologies for Localization," *International Symposium on Location- and Context-Awareness,* pp. 350-362, 2005.

[4] I. G. Niemegeers and S. M. H. d. Groot, "Research issues in adhoc distributed personal networking," *Wireless Personal Communications,* vol. 26, no. 2-3, pp. 149-167, 2003.

[5] M. Dru and S. Saada, "Location-based mobile services: The essentials," *Alcatel Telecommunications Review,* pp. 71-76, 2001.

[6] S. Bush, "A Simple Metric for Ad Hoc Network Adaptation," *IEEE Journal on Selected Areas in Communications,* vol. 23, no. 12, pp. 2272 - 2287, 2005.

[7] E. Yanmaz and O. K. Tonguz, "Location Dependent Dynamic Load balancing," *GLOBECOM '05. IEEE Global Telecommunications Conference,* p. 5, 2005.

[8] H. Tannous, D. Istrate, A. Benlarbi-Delai, J. Sarrazin, M. Idriss, M.-C. H. B. Tho and T. T. Dao, "Exploring various orientation measurement approaches applied to a serious game system for functional rehabilitation," *Engineering in Medicine and Biology Society (EMBC), 2016 IEEE 38th Annual International Conference of the,* 2016.

[9] B. Hofmann-Wellenho, H. Lichtenegger and J. Collins, "Global Positioning System Theory and Practice," 2001.

[10] H. Liu, H. Darabi, P. Banerjee and J. Liu, "Survey of wireless indoor positioning techniques and systems," *IEEE Transactions on Systems, Man, and Cybernetics, Part C (Applications and Reviews),* vol. 37, no. 6, pp. 1067-1080, 2007.

[11] X. Fernando, S. Krishnan, H. Sun and K. Kazemi-Moud, "Adaptive denoising at Infrared wireless receivers",," *Proc. SPIE,* vol. 5074, 2003.

[12] R. Want, A. Hopper, V. Falcao and J. Gibbons, "The Active Badge LocationSystem," *ACM Trans. Information Systems,* vol. 10, no. 1, pp. 91-102, 1992.

[13] R. States and E. Pappas, "Precision and repeatability of the Optotrak 3020 motion measurement system," *J. Medical Engineering and Technology,* vol. 30, no. 1, pp. 1-16, 2006.

[14] N. Priyantha, A. Chakraborty and H. Balakrishnan, "The cricket location- support system," *Proc. ACM Conference on Mobile Computing and Networking,* 2000.

[15] E. Aitenbichler and M. Mhlhuser, "An IR Local Positioning System for Smart Items and Devices," *Proc. 23rd IEEE International Conference on Distributed Computing Systems Workshops (IWSAWC03),* 2003.

[16] A. Ward, A. Jones and A. Hopper, "A New Location Technique for the Active Office," *IEEE Personal Communications,* vol. 4, no. 5, pp. 42-47, 1997.

[17] N. Priyantha, A. Chakraborty and H. Balakrishnan, "The cricket location- support system," *Proc. ACM Conference on Mobile Computing and Networking,* 2000.

[18] "Sonitor System Website, 2008, http://www.sonitor.com/".

[19] J. Hightower and G. Borriello, "A Survey and Taxonomy of Location Systems for Ubiquitous Computing," *Technical Report UW-CSE 01-08-03,* 2001.

[20] H. D. Chon, S. Jun, H. Jung and S. W. An, "Using RFID for Accurate Positioning," *Proc. International Symposium on GNSS,* 2004.

[21] S. Thongthammacharl and H. Olesen, "Bluetooth Enables In-door Mobile Location Services," *Proc. Vehicular Technology Conference,* vol. 3, pp. 2023-2027, 2003.

[22] J. C. F. Michel, M. Christmann, M. Fiegert, P. Gulden and M. Vossiek, "Multisensor Based Indoor Vehicle Localization System for Production and Logistic," *Proc. IEEE Intl Conference on Multisensor Fusion and Integration for Intelligent Systems,* pp. 553-558, 2003.

[23] D. Niculescu and R. University, "Positioning in Ad Hoc Sensor Networks," *IEEE Network Magazine,* vol. 18, no. 4, pp. 24 - 29, 2004.

[24] S. J. Ingram, D. Harmer and M. Quinlan, "UltraWideBand Indoor Positioning Systems and their Use in Emergencies," *Proc. IEEE Conference on Position Location and Navigation Symposium,* pp. 706-715, 2004.

[25] E. B. B. T. O. S. F. Raab and H. R. Jones, "Magnetic Position and Orientation Tracking System," *IEEE Trans. Aerospace and Electronic systems,* Vols. AES-15, no. 5, pp. 709-718, 1979.

[26] S. H. B. M. B. B. M. H. a. S. S. J. Krumm, "Multi-Camera Multi-Person Tracking for Easy Living," *Third IEEE International Workshop on Visual Surveillance,* 2000.

[27] D. S. A. Madhavapeddy and R. Sharp, "Context-Aware Computing with Sound," *Proc. 5th Intl Conference on Ubiquitous Computing,* 2003.

[28] S. Z., J. G. and H. C, "Theoretical and Mathematical Foundations of Computer Science," *A Survey on Indoor Positioning Technologies,* p. 198–206, 2011.

[29] M. R., "Indoor Positioning Technologies," *Ph.D. Thesis.Institute of Geodesy and Photogrammetry,ETH Zurich,* 2012.

[30] H. J. and B. G., "Location systems for ubiquitous computing," *IEEE Comput.,* vol. 34, pp. 57-66, 2001.

[31] L. J., S. D. and L. K., "Indoor navigation system based on omni-directional corridorguidelines," *Proceedings of the 2008 International Conference on Machine Learning and Cybernetics,* pp. 1271-1276, 2008.

[32] M. Kanaan and K. Pahlavan, "A comparison of wireless geolocation algorithms in the indoor environment," *Proc. IEEE Wireless Commun.Netw. Conf,* vol. 1, pp. 177-182, 2004.

[33] B. Fang, "Simple solutions for hyperbolic and related position fixes," *IEEE Transactions on Aerospace and Electronic Systems,* vol. 26, no. 5, pp. 748-753, 1990.

[34] C. Drane, M. Macnaughtan and C. Scott, "Positioning GSM telephones," *IEEE Communications Magazine,* vol. 36, no. 4, pp. 46-54, 1998.

[35] K. Pahlavan, X. Li and J. Makela, "Indoor geolocation science and technology," *IEEE Commun. Mag.,* vol. 40, no. 2, pp. 112-118, 2002.

[36] A. Teuber, B. Eissfeller and T. Pany, "A Two-Stage Fuzzy Logic Approach for Wireless LAN Indoor Positioning," *Position, Location, And Navigation Symposium, 2006 IEEE/ION,* 2006.

[37] D. J. Torrieri, "Statistical theory of passive location systems," *IEEE Transactions on Aerospace and Electronic Systems,* Vols. AES-20, no. 2, pp. 183-198, 1984.

[38] B. V. Veen and K. Buckley, "Beamforming: A versatile approach to spatial filtering," *IEEE ASSP Magazine,* vol. 5, no. 2, pp. 4-24, 1988.

[39] Z. Farid, R. Nordin and M. Ismail, "Recent advances in wireless indoor localization techniques and system," *Journal of Computer Networks and Communications,* 2013.

[40] J. Friedman, A. Davitian, D. Torres, D. Cabric and a. M. Srivastava, "Angle-of-arrival-assisted relative interferometric localization using software defined radios," *In Military Communications Conference,,* pp. 1-8, 2009.

[41] Y. Gu, A. Lo and I. Niemegeers, "survey of indoor positioning systems for wireless personal networks," *Communications Surveys & Tutorials,* vol. 11, no. 1, pp. 13-32, 2009.

[42] Z. Song, G. Jiang and C. Huang, "A survey on indoor positioning technologies.," *In Theoretical and Mathematical Foundations of Computer Science,* pp. 198-206, 2011.

[43] K. Kaemarungsi and P. Krishnamurthy, "Properties of indoor received signal strength for wlan location fingerprinting," *In Mobile and Ubiquitous Systems: Networking and Services,* pp. 14-23, 2004.

[44] C. N. Reddy and M. B. Sujatha, "Tdoa computation using multicarrier modulation for sensor networks," *International Journal of Computer Science & Communication Networks,* vol. 1, no. 1,

2011.

[45] C. Wu, Z. Yang, Y. Liu and W. Xi, "Will: Wireless indoor localization without site survey," *Parallel and Distributed Systems IEEE Transactions,* vol. 24, no. 4, pp. 839-848, 2013.

[46] P. Bahl and V. N. Padmanabhan, "RADAR: An in-building RF-based user," *Proc. IEEE INFOCOM,* vol. 2, pp. 775-784, 2000.

[47] S. Saha, K. Chaudhuri, D. Sanghi and P. Bhagwat, "Location determination of a mobile device using IEEE 802.11b access point signals," *Proc. IEEE Wireless Commun. Netw. Conf,* vol. 3, pp. 1987-1992, 2003.

[48] B. Ottersten, M. Viberg, P. Stoica and A. Nehorai, "Exact and large sample ML techniques for parameter estimation and detection in array processing," *Radar Array Processing pp 99-151.*

[49] N. Cristianini and J. Shawe-Taylor, "An Introduction to Support Vector Machines," 2000.

[50] J. M.I., N. Robert and S. Bernhard, "The Nature of Statistical Learning Theory," 2000.

Chapter 2: Multi carrier communication signals

2.1 Introduction

This chapter is the first main part of our work in the sense that, first we develop here the whole Multicarrier (MC) OFDM communication bench, leading later to TDOA measurement, and then discuss the impacting parameters such as SNR, rolling factor, pilots...

Previously and in order to position our work relatively to other multi carrier techniques leading to positioning, we give first a brief overview of those specific positioning methods. We then develop the mathematical derivation and describe the well-known features dealing with digital modulation and coding by considering transmitter and receiver parts. We also give the main technique already used to compensate multipath effects and to evaluate SNR. Let's precise, that the most used processes here have been performed using MATLAB. We expect that the results obtained can provide a useful reference material for future measurements provided in chapter 4.

2.2 General principle of MC based TDOA estimation

The general communication block diagram dealing with TDOA estimation process is illustrated in the Figure 2-1.

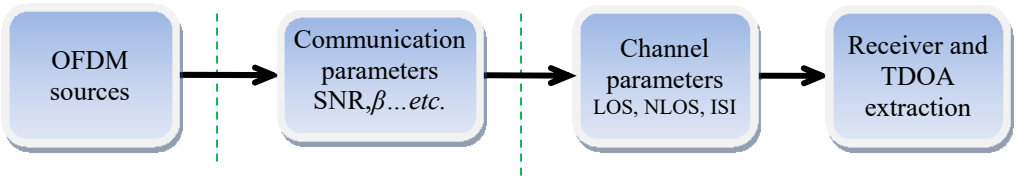

Figure 2-1: The block diagram of TDOA estimation

Multiple OFDM signals travel through the channel toward the receiver. Once the main communication parameters (SNR, Roll of factor etc.) properly defined and evaluated, one can perform, at the receiving part, energy detection or channel estimation to extract the useful TDOA, i.e., time difference of arrival, between the receiver and the OFDM sources.

As it will be demonstrated in chapter III, received power and the channel behavior are directly impacted by TDOA, and of course by the other communication environmental factors. So some practical solutions will be suggested to reinforce the effect of useful TDOA

and to reduce the negative effects of the communication environmental factors. So each part and process of the multicarrier communication system has to be studied clearly to find out whether its influence on the precision of the proposed method is good or not.

2.3 Multi carrier based positioning systems and OFDM solutions

For communications issues, and due to evident reasons linked to redundancy principle, the structure of the multicarrier systems is more powerful, against the multipath channel, than any single carrier schemes. It also seems, due to the relative bandwidth, well suited for the time delay based location device. The following sections present a short overview of multicarrier based positioning solutions.

2.3.1 Blind solution

Many references cited in [1] underline the fact that, in a given network, each sensor independently can identify boundaries in a received MC signal, by looking for the repetition of a given sequence in this signal. Then it can calculate some statistical features (e.g., the sample mean or variance) of each sequence, and transmit, for positioning purpose, the sequence repetition times and the associated feature values to another sensor. This approach, which does not require any knowledge of the transmitted signal, is defined as blind, and is well suited for OFDM based communication. Indeed, in OFDM format, the insertion of a cyclic prefix (CP) before each sequence of data makes the beginning and the end of each sequence identical, leading to the notion of repeated sequence and hence can allow, as mentioned former, the blind identification. Let's note that for our purpose, CP leads also to the concept of circular convolution, which is of great interest to handle, in an easy way, OFDM signal both in the time domain and in the frequency domain.

2.3.2 Training solution

At the opposite side, there are several other papers in the literature that perform positioning by using a specially designed training MC signal. For example, the work reported in [2], based on the Schmidl–Cox [3] and Minn [4] synchronization algorithms, uses such a cooperative scheme, and with the same concept, the authors in [5] uses, for accurate positioning, cooperative transmitters and receivers in an indoor positioning system. With using of a known transmitted signal, the authors in [6] look for time delay induced by phase

rotations across subcarriers at the receiver. With the same way in IEEE 802.11a wireless LANs, the authors in [7] and [8] correlate the received signals with a training sequence.

2.3.3 Alternative solution

Two other positioning methods are tangentially relevant since they involve multi carrier signals. First in [9], the authors combine the standard TDOA positioning with Cell ID positioning. Recall that the Cell ID method works only if the received power levels indicate that the mobile is within the base station scope of coverage. Second in [10], the extraction of both time of arrival and direction of arrival information is done using several receivers; each of them has an antenna array. All the measurements from all antennas of all receivers are available, at all times, in a central station. Moreover, training data is assumed to be available and will help to solve location problem.

2.3.4 OFDM based positioning

Generally, the positioning methods using OFDM signals in the existing literature are divided into two categories. The first category locates the boundaries of OFDM signals by using the traditional or improved timing synchronization algorithms [11], [12] [13]. The idea behind those methods is to deal with timing synchronization as with the TDOA estimation. Essentially, timing synchronization and TDOA estimation are the same tasks for the receiver. However, the sampling rate limits the accuracy of such methods, and generally, an error of several meters is expected. The second category uses modern spectral estimation techniques [14], [15], [16] and deals with the high-resolution algorithms such as multiple signal classification MUSIC, ESPRIT. These algorithms are applied to the frequency-domain channel estimation to extract a more accurate estimate of the first path in the time domain. Again, the sampling rate limits these mathematical methods that are, by the way, too sensitive to the model. However their accuracy is much better than that of the first category.

2.3.5 Conclusion

To conclude this very brief overview, positioning systems using the multicarrier techniques are mainly based on locating the boundaries of each received signal. The idea behind that is to find the time delay of each received signal, then collecting all the data in a centralized unit. In our knowledge, none of them exploits CSI. As mentioned, several limits and problems need to be solved prior to any deployment. It then seems clear that a deep study

and understanding of how building up the multicarrier signal, for location or time delay issues, have to be done. So the next sections are focused on the main steps of multicarrier digital signal implementation and the effects of the main communication parameter on its performance regarding the TDOA purpose.

2.4 Data modulation

One of the basic elements in the communication system is the symbol, which we need to transmit and receive correctly. The environment of the communication system affects the symbol, leading to channel effect. Therefore, the most active way to find the communication system behavior is to observe the change over this symbol. There are many ways to construct the symbol, which is known as modulation process. Among all of modulation methods, we chose QPSK modulation. In fact, for our purpose, there is no difference to choose any other modulation method.

2.4.1 QPSK Based Communication System

Let us take data-In as a train of N symbols $\big(s(0),\dots,s(N-1)\big)$, where each symbol $s(i)$ is represented by one of $M = 2^K$ possible sequences bits. Therefore the equivalent expression for $s(k)$ is:

$$s(i) = A\left(cos\left(\frac{(2k+1)\pi}{M}\right) + j\,sin\left(\frac{(2k+1)\pi}{M}\right)\right) = A\,(I_i - j\,Q_i) \qquad (4)$$

A is the amplitude. In QPSK modulator, $K = 2$ bits leading to represent $s(i)$ in one of the following set (00, 01, 11, 10) for each k = 0,1,2,3 respectively.

We summarize in Table 2-1 the four symbol mapping definitions for QPSK, the expression of $s(i)$ and the amplitude of I-Q signals.

Table 2-1 QPSK symbol mapping definition

Symbol	Bits	s(t)	Phase (Deg.)	*I*	*Q*
S_0	00	$1/\sqrt{2}e^{j\pi/4}$	45	$1/\sqrt{2}$	$1/\sqrt{2}$
S_1	01	$1/\sqrt{2}e^{j3\pi/4}$	135	$-1/\sqrt{2}$	$1/\sqrt{2}$
S_2	11	$1/\sqrt{2}e^{-j3\pi/4}$	225	$-1/\sqrt{2}$	$-1/\sqrt{2}$
S_3	10	$1/\sqrt{2}e^{-j\pi/4}$	310	$1/\sqrt{2}$	$-1/\sqrt{2}$

The constellation points of $s(i)$, represented by one of $M = 4$ basis functions every T_d second with a bandwidth of $f_d = 1/T_d$, is given in Figure 2-2 for transmitting part and receiving part as well.

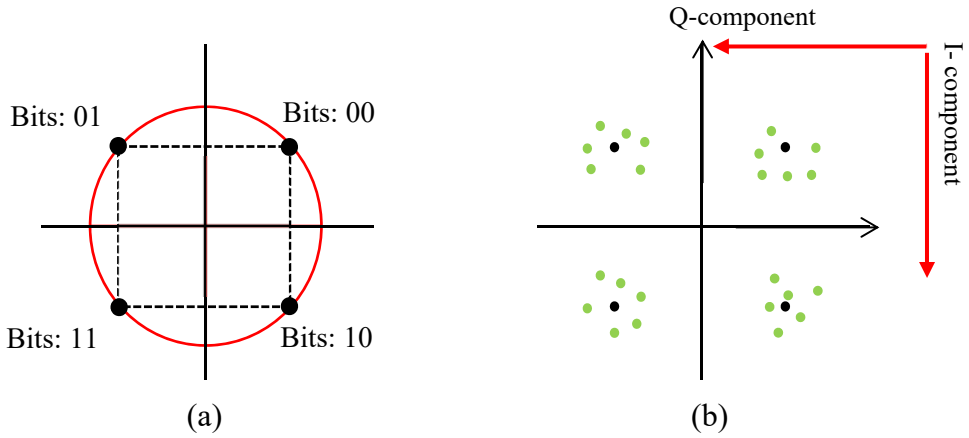

Figure 2-2: Constellation diagram of QPSK, (a) transmitting side, (b) receiving side

At the transmitter, the constellation is obviously shown with perfect square. At the receiver, the channel affects the quality of signal and is then helpful for observing the level of system distortion for performance subjects. Usually to measure the communication system efficiency, the bit error rate (BER), which is a unit less performance measure, is plotted in function of Signal-to-Noise Ratio (SNR).

We give in next section, the mathematical derivation leading to SNR calculation, which is an important parameter for performance assessment of TDOA estimation.

2.4.2 SNR calculation

To test the performance of TDOA estimation method and communication system quality, we have to calculate SNR. Indeed SNR affects the accuracy of estimation, since data is passed through several functions such as filtering, amplifier, digital to analog and analog-to-digital converters and others. So SNR measurement is required to find out the best estimation of the channel.

On the other hand, SNR information is widely used in the implementation of many techniques and components measurement in digital communications. For example, knowledge of SNR is required in power control [17], as well as in rate adaptation [18].

We present in the following section two methods leading to SNR determination. One is mathematically based, and the second is experimentally based.

2.4.2.1 **Mathematical driven solution**

There are many ways to perform SNR estimation. Among the four SNR absolute estimators discussed in [19], there is one that has both the smallest bias and smallest mean-square-error (MSE). It is simply based on receiver statistics inversely related to SNR. Moreover, it has good performance for SNR $\geq$ 5dB, making it useful for practical applications. In this paper, the SNR is defined, for QPSK modulation, as:

$$SNR = L \cdot \left(\sum_{i=1}^{L} \frac{\left(|\hat{I}_i| - |\hat{Q}_i| \right)^2}{\hat{I}_i^2 - \hat{Q}_i^2} \right)^{-1} \tag{5}$$

where

$$\hat{I}_i = I_i + n_{Ii} \; ; \; \hat{Q}_i = Q_i + n_{Qi} \tag{6}$$

$\hat{I}_i \; and \; \hat{Q}_i$ denote the in-phase component and the quadrature component of the total received signal-plus-noise of the i_{th} received symbol, respectively,. I_i, Q_i, n_{Ii}, and n_{Qi}, $i \in \{1 \,..\, L\}$, denote the in-phase signal component, the quadrature signal component, the in-phase noise component and the quadrature noise component, of L symbols of a received signal, respectively.

We systematically compare this mathematical expression to experimental SNR that is obtained as explained hereafter.

2.4.2.2 **Practical driven approach**

From practical point of view, there is another simple way to determine the SNR from the power spectrum of the signal. As we know, the mean power P of a discrete signal can be calculated using the following equation:

$$P = \frac{1}{N} \sum_{n=0}^{N-1} x^2[n] \tag{7}$$

where, $x[n]$ denotes discrete samples with N points.

In frequency domain, equation (7) leads, through Parseval theorem, to the power spectral density (PSD). So, as we show in Figure 2-3, by integrating each point of the PSD over the resolution bandwidth centered on the carrier frequency (here f_c=3 Ghz), we compute the total power spectrum, including noise power.

To measure the noise power only, we perform the integration of the PSD over the same bandwidth centered on frequency f_c' far away enough from the previous carrier frequency (here $f_c' = 2{,}8GHz$).

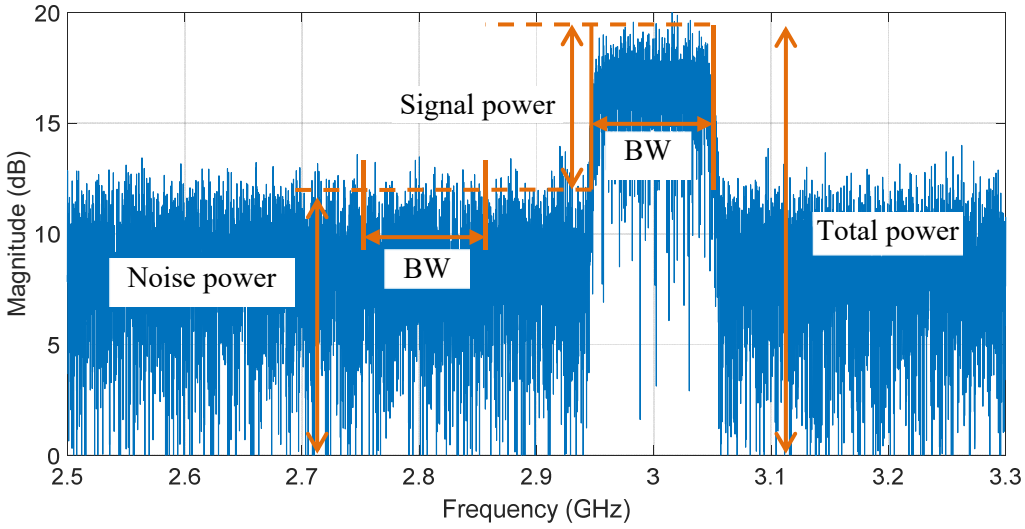

Figure 2-3: Example of the spectrum of the received signal

Now the SNR simply could be calculated as:

$$SNR = \frac{Power\ of\ the\ received\ signal\ around\ f_c}{Power\ of\ the\ received\ signal\ away\ from\ f_c} - 1$$

It's obvious that this practical solution woks under the assumption that there is no parasitic signal in the considered spectrum. The simulation results will be presented in the next section.

2.4.3 **Simulation results**

The block diagram for implementing the QPSK modulation and demodulation are shown in Figure 2-4.

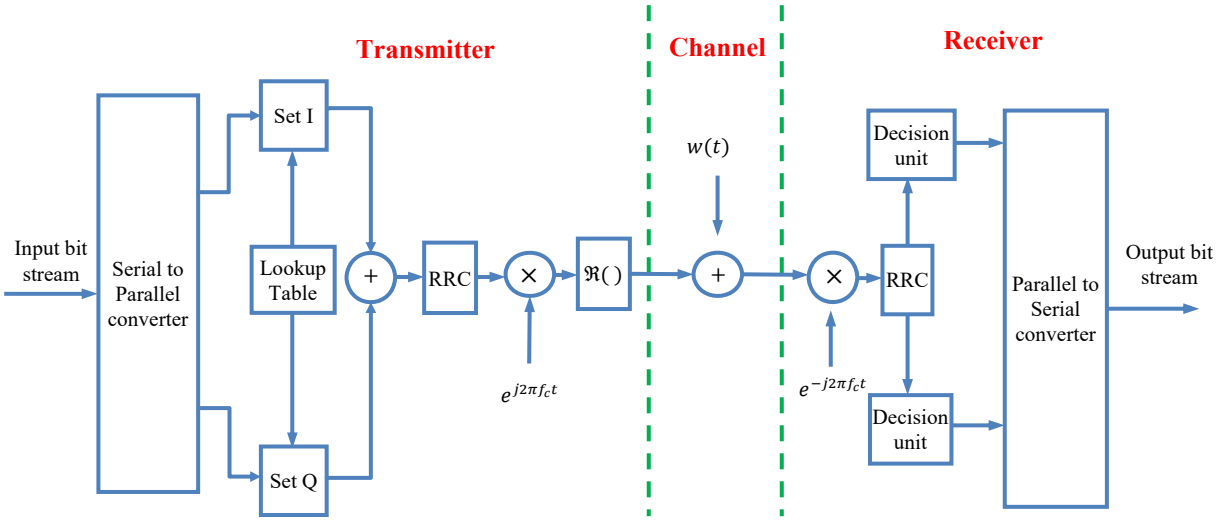

Figure 2-4: QPSK Modulator/ Demodulator Block diagram

The serial to parallel converter takes the bits stream coming in at a bit rate of R_d and splits into two streams, each of half bit rates. Depending on the dual pattern coming in, I and Q amplitudes are set from a lookup table function Table 2-1. Both of them up converted to higher frequency band centered at f_c after being shaped by a root raised cosine (RRC) filter. Then AWGN channel is added to the transmitting signal for testing the simulation code.

At the receiver, the signal is down-converted to the baseband signal, and then passed through the RRC filter for retransforming it to bits by the code decision block. The code is executed under the following parameters:

Table 2-2 Parameters of QPSK simulation

Parameter name	Parameter value
Number of bits to process	1024 Kb
Bandwidth (f_d)	100 MHz
Sampling Frequency (f_s)	10 GHz
Carrier Frequency (f_c)	3 GHz
Filter Type	RRC
Roll off *(β)*	0.15
Channel Model	AWGN
SNR range	[0 : 14]dB
Method of SNR calculation	Practical, Mathematical

Figure 2-5 shows the plot of BER versus SNR for the QPSK system using the two SNR estimators. The black curve is the theoretical BER and the red and blue curves are the obtained BER as function of SNR estimated from practical and mathematical estimators. For SNR > 8dB, the mathematical estimator is close to actual one, where the practical estimator is fits with the actual for all represented SNR. However this verifies the functionality of the QPSK implementation.

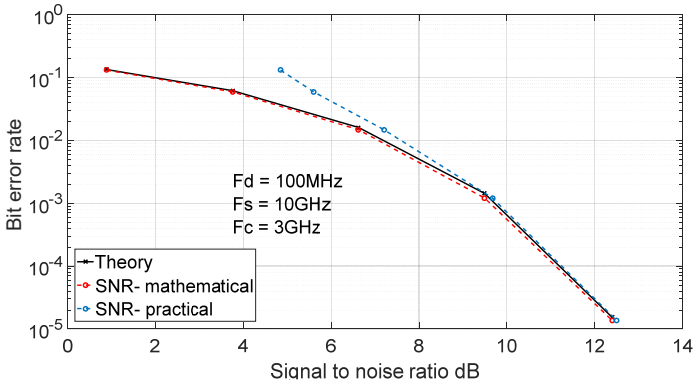

Figure 2-5: BER verses SNR – Performance curve for QPSK Modulation

The constellation diagrams at the receiver along with the constellation diagram at the transmitter are shown in Figure 2-6, for different values of SNR, leading to the definition of the minimum SNR required for ensuring good quality of communication.

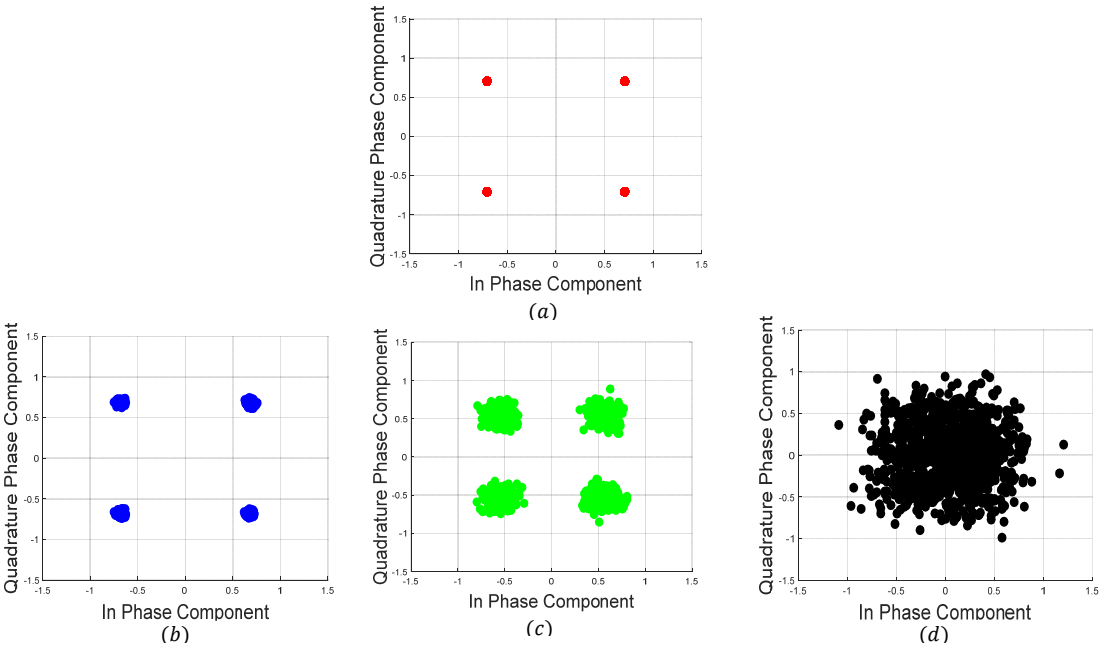

Figure 2-6: Constellation diagram: (a) at the transmitter, (b) at the receiver for SNR = 30 dB, (c) for SNR = 15 dB, (d) for SNR = 1 dB

At this point we established the first step in building up the communication system which deals with basic modulation of the message but still deals with free space channel and one carrier waveform. In the next section, we implement the multicarrier signal using QPSK modulation to study realistic multipath channel.

2.5 OFDM communication system

OFDM is a well popular multicarrier technique that offers many advantages to perform high quality and high data rate communication in complex channels. This section presents the different steps required for implementing OFDM modulation technique needed for channel estimation and leading further to TDOA extraction.

2.5.1 Transmitter/Receiver module

We first pass the QPSK complex symbols stream with length N: $(X[0], \ldots, X[N-1])$ through a serial-to-parallel converter, whose output is a set of N_c rate subcarriers (the length of IFFT). In order to generate the OFDM time sample $x[n]$, an IFFT is applied on OFDM frequency complex components $X[k]$ leading to the following relationship:

$$x[n] = \frac{1}{\sqrt{N_c}} \sum_{k=-\frac{N_c}{2}}^{\frac{N_c}{2}-1} X[k]\, e^{j\left(\frac{2\pi kn}{N_c}\right)} \qquad for \quad n = -\frac{N_c}{2}, \ldots, 0, \ldots, \frac{N_c}{2} - 1. \tag{8}$$

Therefore the OFDM symbol consists of linearly modulated sub channels. So increasing the number of subcarriers makes the signal more robust against frequency selective channel effects [20], and helps effectively to estimate the channel response.

$$x(t) = \frac{1}{T_{sub}} \int_{-0.5}^{+0.5} X(f) e^{j(2\pi ft)} df\,, \qquad 0 \le t < T_{sub} \tag{9}$$

An OFDM signal is formed by summing all the N_c modulated orthogonal subcarriers with equal frequency spacing $\Delta f = 1/T_{sub}$. At the receiver, for free space non-noisy channel, $y(t) = x(t)$. So the received signal in the continuous frequency domain, after the FFT is:

$$Y(f) = \frac{1}{T_{sub}} \int_{0}^{T_{sub}} x(t) e^{-j2\pi ft} dt \tag{10}$$

In the discrete frequency domain representation, the signal is written as:

$$Y[k] = \frac{1}{\sqrt{N_{sc}}} \sum_{n=-\frac{N_c}{2}}^{\frac{N_c}{2}-1} x[n] e^{-j2\pi kn/N_c} = X[k] \quad for \quad n = 0,1,\dots,N_c - 1. \tag{8}$$

We have to mention that the OFDM symbol corresponds to a composite signal of N_c symbols in a parallel form and has duration of T_{sym} where the original symbol $X[k]$ length, due to transmitting N_c symbols in parallel form, has been extended from T_d to $T_{sym} = N_c \cdot T_d$. The block diagram in Figure 2-7 illustrates the conventional OFDM modulation and demodulation process, respectively.

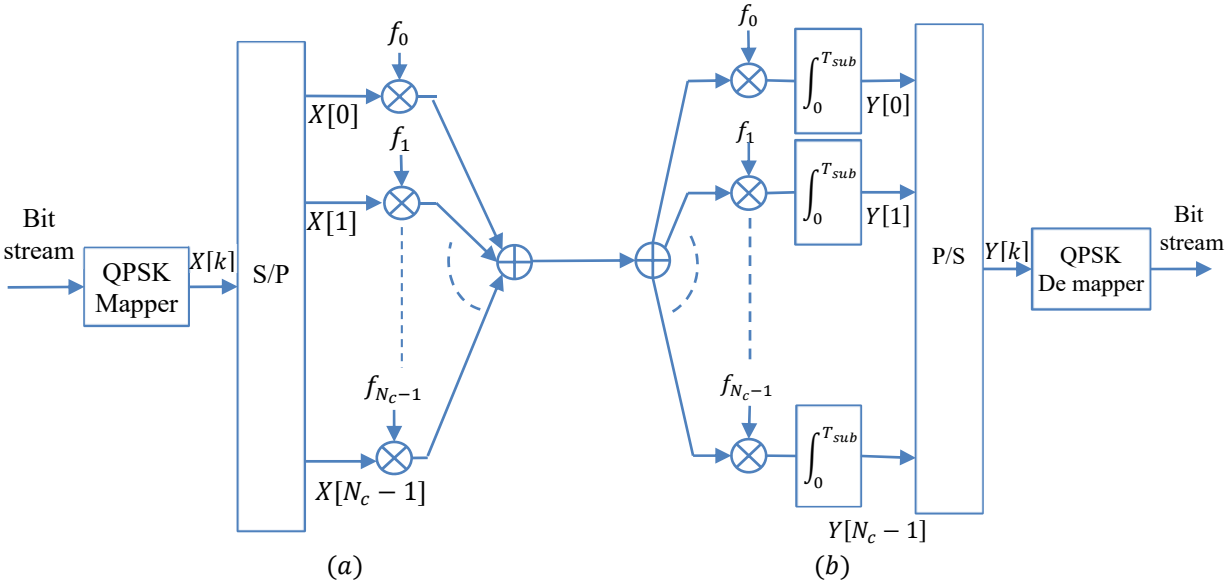

Figure 2-7: OFDM implementation (a) modulation (b) demodulation

2.5.2 Guard Interval

Until now, all what have been done is only for implementing the communication system. To achieve robust communication system targeting TDOA estimation, we have to explore deeply the effect of the channel.

The way how OFDM technique deals with the channel is the key solution for achieving our target. So as it will be seen in chapter 3, we deal with multipath as a negative phenomenon for positioning issue and at the same time as a positive one for communication performance in terms of SNR improvement. Let's now see the impact of the channel.

2.5.2.1 **Channel Effects on OFDM Symbols**

The effect of the channel, with an impulse response $h(t)$, on the received OFDM symbol $x(t)$ is given as:

$$y(t) = x(t) * h(t) + w(t) = \int_0^{\infty} h(\tau)\, x(t-\tau)\, dt + w(t) \quad (9)$$

where (*) stands for convolution product and $w(t)$ is the Additive White Gaussian Noise (AWGN).

By discretizing the equation (9) at $nT_d = nT_{sym}/N_{sc}$, it can be rewritten as follows:

$$y[n] = x[n] * h[n] + w[n] = \sum_{m=0}^{\infty} h[m]x[n-m]\, dt + w[n] \quad (10)$$

where $x[n] = x(nT_d), y[n] = y(nT_d), h[n] = h(nT_d)$, and $w[n] = w(nT_d)$.

As discussed in the previous section, OFDM solves the effect of the channel fading problem by modulating the data in the frequency domain over N_c narrow bands and hence OFDM sub-symbols length is longer than the delay spread of the channel.

However, as a result of multipath, inter symbol interference (ISI) effect still remains as a harmful factor that may break the orthogonality among the subcarriers in the OFDM scheme. For improving the OFDM signal performance to deal with the ISI effect, it is essential to insert a guard interval between two consecutive OFDM symbols called Cyclic Prefix of appropriate length to avoid this effect.

2.5.2.2 **Cyclic Prefix (CP)**

The OFDM guard interval is inserted by the cyclic extension of the OFDM symbol (for some continuity) with CP (cyclic prefix) or CS (cyclic suffix). We use CP to extend the OFDM symbol by copying the last samples of the OFDM symbol into its front. As $f_d = 1/T_d$ then $\Delta f = f_d/N_c = 1/(N_c T_d)$ and $T_{sub} = N_c T_d = 1/\Delta f$, where Δf is the subcarrier space and T_{sub} denotes the duration of the effective OFDM symbol without guard interval.

The net OFDM symbol duration is T_{sub} and by adding the CP of length T_G in terms of samples, the extended OFDM symbols will be $T_{sym} = T_{sub} + T_G$. To illustrate the concept, an

OFDM symbols, which has the CP of length T_G is shown in Figure 2-8(a). It is obvious from the Figure 2-8(b) that if the minimum length of the guard interval (CP) is equal to or longer than the maximum delay of a multipath channel, ISI will not affect the FFT of the next OFDM symbol, and its negative effects are confined within the guard interval. This implies to maintain the orthogonality among each delayed subcarrier with all other subcarriers is maintained over T_{sub}.

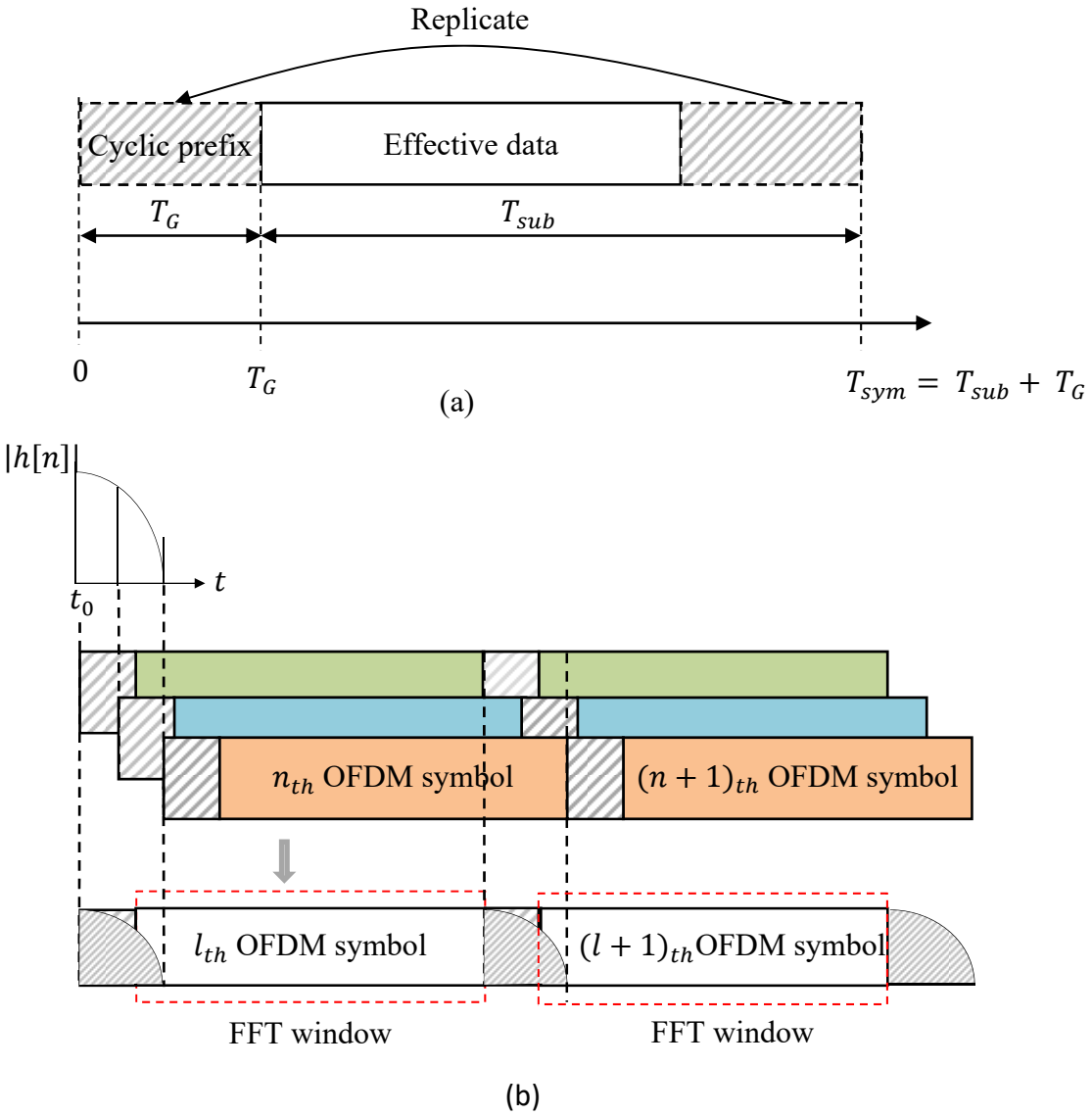

Figure 2-8: Effect of a multipath channel on the received signal with CP: (a) OFDM symbols with CP (b) ISI effect of a multipath channel on OFDM symbols with CP length shorter than the maximum delay of the channel.

Mathematically, we assume the length of the CP is longer than the maximum delay of the channel; subsequently, the OFDM receiver takes the FFT of the received samples to yield:

$$Y[k] = \sum_{n=-\frac{N_c}{2}}^{\frac{N_c}{2}-1} y[n]e^{-j2\pi kn/N_c}$$

$$= \sum_{n=-\frac{N_c}{2}}^{\frac{N_c}{2}-1} \left\{ \sum_{m=0}^{\infty} h[m]x[n-m] + w[n] \right\} e^{-j2\pi kn/N_c}$$

$$= H[k]X[k] + W[k] \tag{11}$$

where $X[k]$, $Y[k]$, $H[k]$, and $W[k]$ denote the k_{th} subcarrier frequency components of the transmitted symbol, received symbol, channel frequency response, and noise respectively. The last identity in Equation (11) implies that the OFDM system can be simply thought as multiplying the input symbol by the channel frequency response in the frequency domain.

It can be equivalently represented as in Figure 2-9.

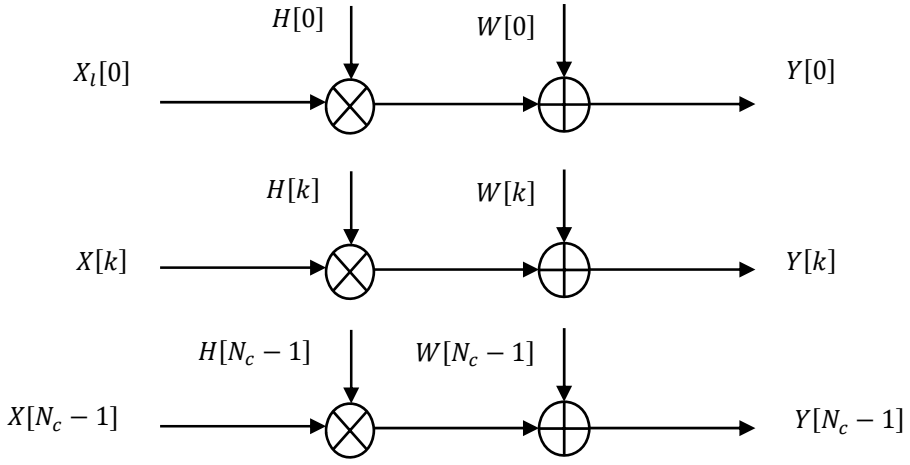

Figure 2-9: Frequency-domain equivalent model of OFDM system

Meanwhile, as cyclic prefix gives the ability, due to the concept of circular convolution, to estimates the channel simply by dividing, in the frequency domain, the transmitting signal over the received signal, the channel estimation is one-step process, which simply performs $H[k] = Y[k]/X[k]$.

From this point we can start the TDOA estimation simply by exploring the channel frequency response (CFR).

2.5.3 **Guard Band and roll of factor**

Symbols shaped with the squared pulses are hard to create and require a lot of bandwidth. So to make them practical to send, we use shaped pulses that convey the same information but use smaller bandwidths and have other nice properties such as inter-symbol interference rejection. We use RRC filter, which is one of the most common pulse shaping. The main factor of RRC is β which controls the shape and the bandwidth of the signal. The passband and baseband signals for the OFDM symbol, shaped by an RRC window $h_{RC}(t)$ with a roll-off factor β, can be written respectively as follows:

$$x(t) = Re\left\{ h_{RC}(t - T_{sym}) \sum_{k=\frac{-N_c}{2}}^{\frac{N_c}{2}-1} X_k \, \Psi_k(t) \right\} \tag{12}$$

and

$$x^{rc}(t) = h_{RC}(t - T_{sym}) \sum_{k=\frac{-N_c}{2}}^{\frac{N_c}{2}-1} X_k \, e^{j2\pi k\Delta f(\, t - T_{sym})} \tag{13}$$

where

$$\Psi_k(t) = \begin{cases} e^{j2\pi f_k(\, t - lT_{sym})}, & for \;\; -(T_G + T_W/2) \le t \le (T_{sub} + T_W/2) \\ 0, & otherwise \end{cases} \tag{14}$$

and

$$h_{RC}(t) = \begin{cases} 0.5 + 0.5\, cos\left(\pi(t + \beta T_{sym} + T_G)/\beta T_{sym}\right) & for - (T_G + \beta T_{sym}/2) \le t < -(T_G - \beta T_{sym}/2) \\ 1.0 & for \; -(T_G + \beta T_{sym}/2) \le t < (T_{sub} - \beta T_{sym}/2) \\ 0.5 + 0.5\, cos\left(\pi(t - T_{sub} + \beta T_{sym})/\beta T_{sym}\right) & for \;\; (T_{sub} - \beta T_{sym}/2) \le t \le (T_{sub} + \beta T_{sym}/2) \end{cases} \tag{15}$$

Figure 2-10 shows the raised cosine window that is used to shape OFDM symbols for reducing their out-of-band powers.

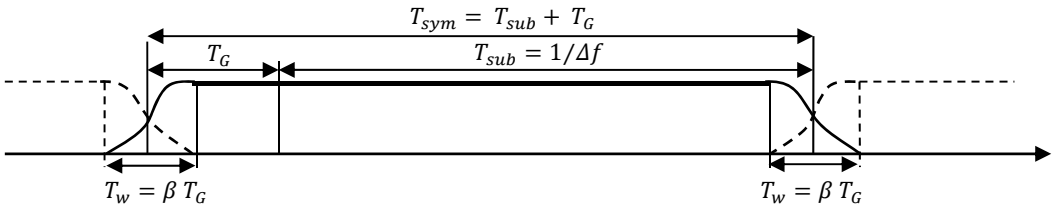

Figure 2-10 Raised cosine window for OFDM symbol

As the roll-off factor β increases, the transition part of the RC window becomes smoother, but the useful data will be lost, thus decreasing the accuracy of TDOA estimation. However this will be explained in more details in chapter 3.

2.6 MATLAB implementation

2.6.1 Transmission part

We describe in this section the main steps required to an up converted transmitting signal. The specific numerical values used in the Matlab code are given in Table 2-3.

Table 2-3 Numerical values for the OFDM parameters

Parameter name	Parameter value
Number of sub-carriers k	1024
Value of carrier number k_{min}	0
Value of carrier number k_{max}	1023
Duration T_{sym}	10.24 µs
guard interval T_g	0.1 µs
Sub-carrier spacing Δf	9.766 kHz
Overall bandwidth	100 MHz

A block diagram of the generation of OFDM signal is shown in Figure 2-11, with underling the main nodes (A), (B), and (C).

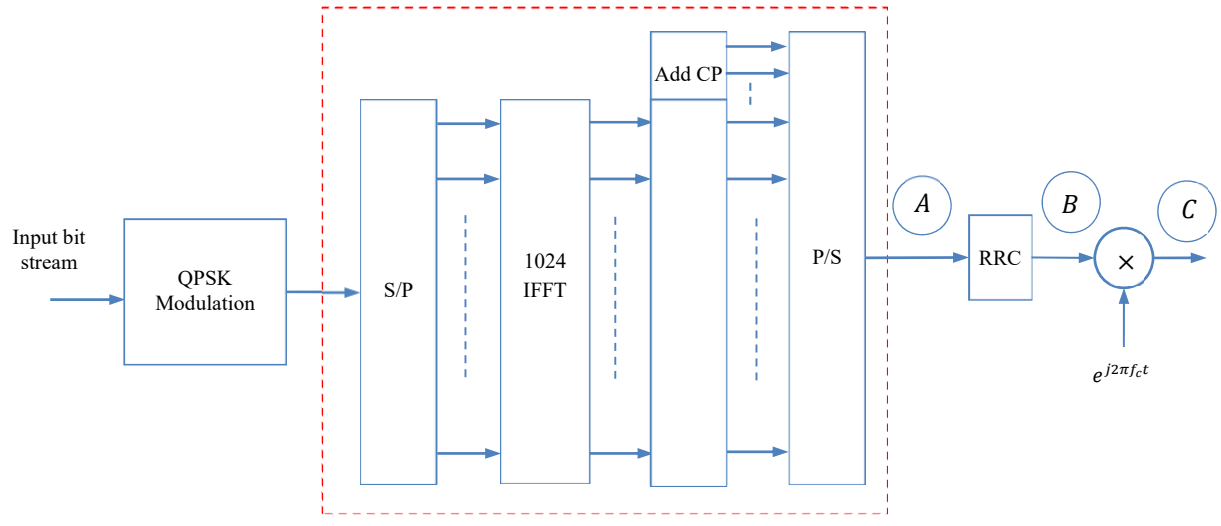

Figure 2-11: OFDM symbol generation

As derived in section 2.5.1, we build up the OFDM signal at (A). The signal carrier uses T_{sym} as its time period. At (B) the signal is filtered and up sampled to meet Shannon criteria related to carrier frequency f_c . The next step is to perform the quadrature multiplex

double-sideband amplitude modulation. At (C) the time response is shown in Figure 2-12(a), and the frequency responses of the direct simulation using two different Matlab functions PSD and FFT, are shown in Figure 2-12(b).

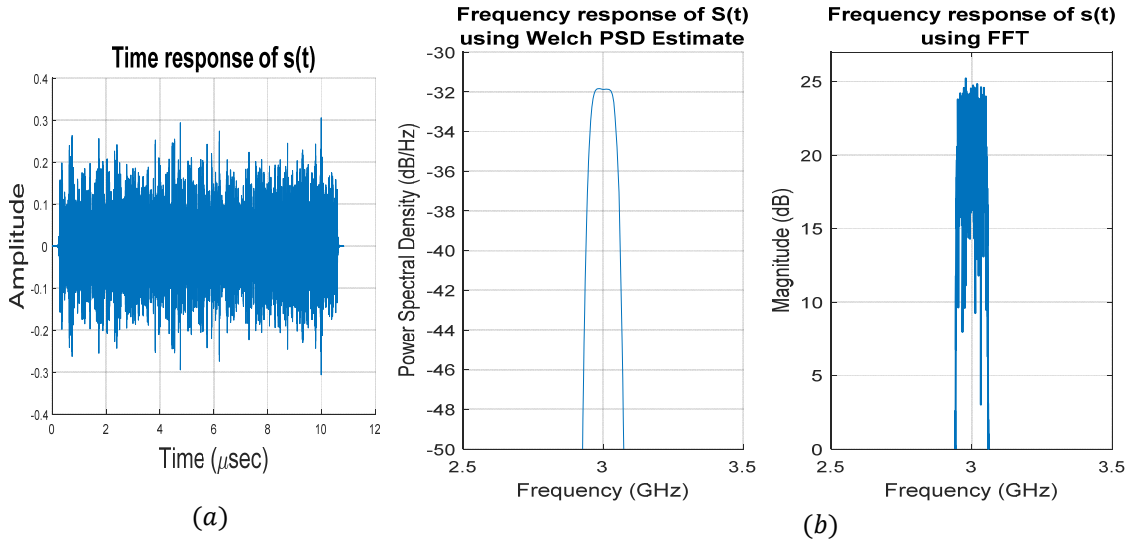

(a) (b)

Figure 2-12: Time and Frequency responses of transmitted signal $s(t)$ using a central frequency $f_c = 3\ GHz$

2.6.2 **Reception part**

As in the transmission case, we specified the names of the simulation variables and the output processes in the reception description of Figure 2-13. At $\grave{A}$ we get a down converted signal and at $\grave{B}$ the baseband one. The results of this simulation are shown in Figure 2-14 and Figure 2-15.

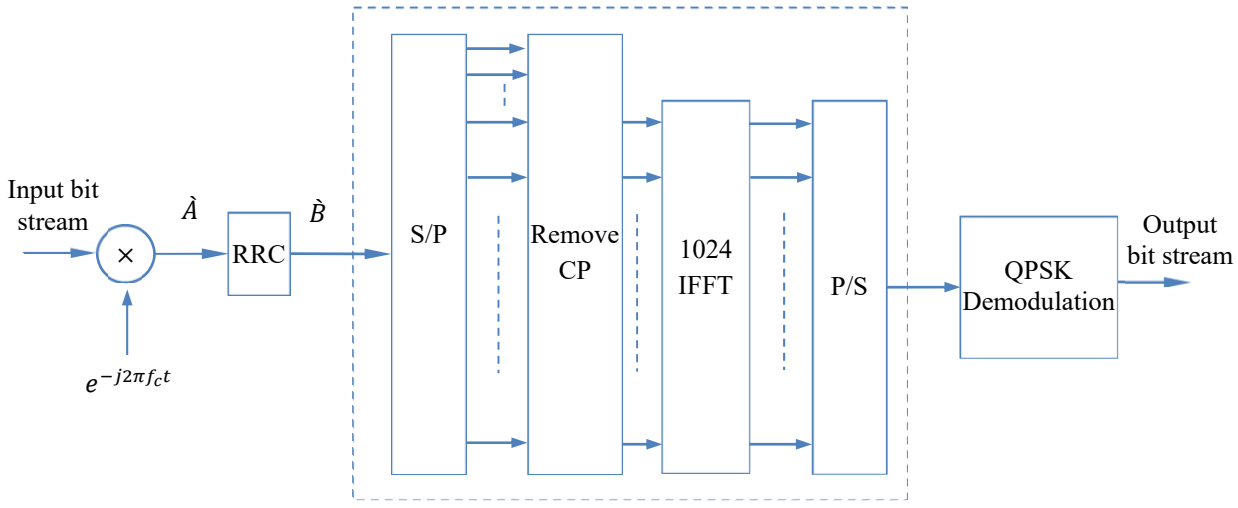

Figure 2-13: OFDM symbol reception.

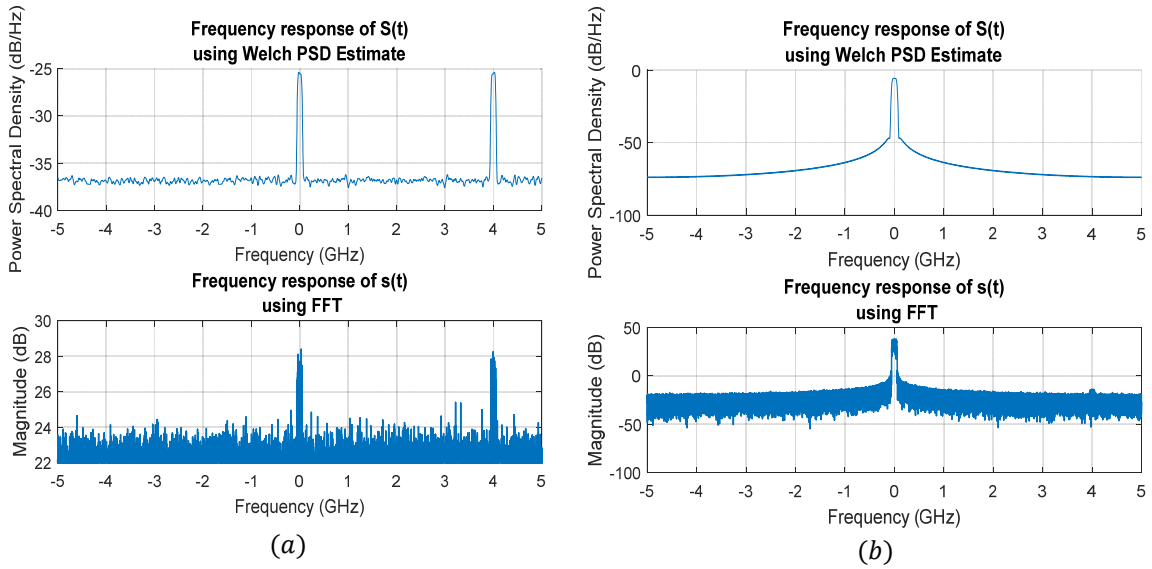

Figure 2-14: Frequency responses of received signal (t) : (a) at À, and b) at Ò

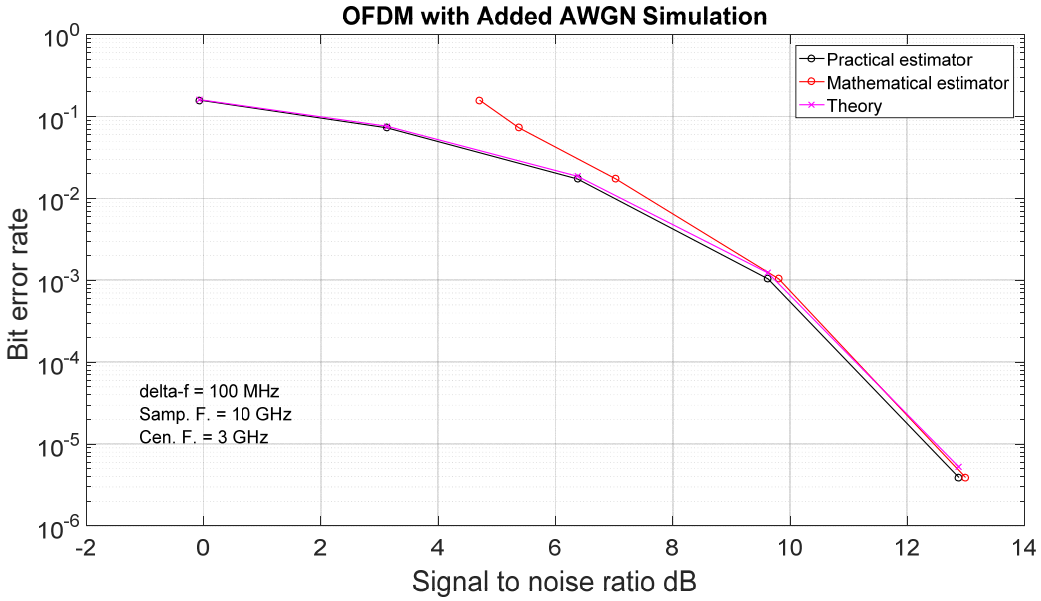

Figure 2-15: BER vs. SNR – Performance curve for OFDM

2.7 Channel Estimation

There are several reasons that make the channel estimation a challenging problem. Due to mobility of transmitter and receiver or scattering object, the radio channel is highly dynamic. So the transmitted signals are typically reflected and scattered before arriving at receivers along multiple paths. Due to multipath propagation, mobility, and local scattering the resulting signal is spread in frequency, time, and angle.

As mentioned many times before, for TDOA estimation we have to find out how channel is estimated in OFDM technique. In free space channel, the more accurate the channel estimation, the more accurate the TDOA extraction. This will give the general formula for the information related to TDOA. Note that all the processes of channel estimation are done within the used bandwidth, which limits, by means of Rayleigh criteria, the TDOA resolution.

Generally, in wireless systems, transmitted information passes through a radio channel, which directly affects it. To recover this information from the distorted signal, the effect of the channel must be estimated in conventional coherent receivers. In other words, as long as the receiver accurately estimates how the channel modifies the transmitted signal, it can recover the transmitted information. Let's note that OFDM naturally exploits channel estimation to achieve equalization. So in principle, it should not be difficult to deal with channel estimation in OFDM system.

In literature, different techniques are proposed to estimate the channel such as Blind and non-blind which are the two main categories of channel estimation techniques for OFDM based systems. The blind channel estimation methods exploit the statistical behavior of the received signals and require a large amount of data [21]. Hence, they suffer severe performance degradation in fast fading channels [22]. On the other hand, in the non-blind channel estimation methods, there are two main groups: decision directed channel estimation (DDCE) and data-aided. The first one uses information of previous channel estimation, the other one uses incomplete OFDM symbol or a portion of the transmitted signal, called pilot, at the receiver. The non-blind channel estimation technique provides a good performance and depends on the arrangement of the pilots (blocks type, comb type, and lattice type).

2.7.1 **Pilot block**

As will be shown in chapter 3, we use pilot for TDOA extraction from channel estimation. Figure 2-16 shows the arrangements of pilot of blocks type.

Using this type, OFDM symbols with pilots at all subcarriers (referred to as pilot symbols herein) are transmitted periodically for channel estimation. Then a time-domain interpolation is performed to estimate the channel along the time axis using those pilots.

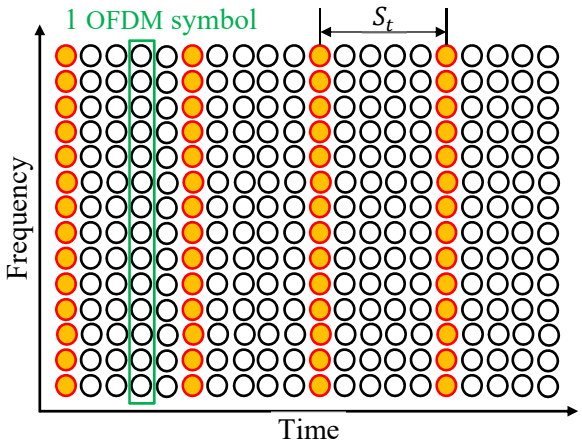

Figure 2-16: Block-type pilot arrangement

In order to keep track of the time-varying channel characteristics, the pilot symbols must be placed as frequently as the channel coherence time t_{coh}. Let S_t denote the period of pilot symbols in time, then it must satisfy the following inequality:

$$S_t \leq \frac{1}{f_{Doppler}} = t_{coh} \tag{16}$$

Since pilot tones are inserted into all subcarriers, the block-type pilot arrangement is suitable for frequency-selective channels.

2.7.2 **Mathematical derivation**

The following equations discuss the estimation of the channel for the block type pilot arrangement based on Least Square (LS) Estimator [23], where due to its simplicity it has been widely used for channel estimation.

We assume that there is no inter carrier interference. So the training transmitted symbols for N_c subcarriers can be represented by the following diagonal matrix:

$$\boldsymbol{X} = \begin{bmatrix} X[0] & 0 & \cdots & 0 \\ 0 & X[1] & & 0 \\ \vdots & & \ddots & \vdots \\ 0 & \cdots & 0 & X[N_c - 1] \end{bmatrix}$$

where $X[k]$ denotes a pilot tone at the kth subcarrier, with $E\{X[k]\} = 0$ and $Var\{X[k]\} = \sigma_x^2$, for $k = 0, 1, 2, \cdots, N_c - 1$.

Taking the channel as $\boldsymbol{H} = \left[H[0], H[1], \cdots, H[N_{sc}-1]\right]^T$, where $H[k]$ is the channel gain for each subcarrier k, the received training signal $Y[k]$ can be represented as:

$$\boldsymbol{Y} \triangleq \begin{bmatrix} Y[0] \\ Y[1] \\ \vdots \\ Y[N_c-1] \end{bmatrix} = \begin{bmatrix} X[0] & 0 & \cdots & 0 \\ 0 & X[1] & \cdots & 0 \\ \vdots & \vdots & \ddots & \vdots \\ 0 & \cdots & 0 & X[N_c-1] \end{bmatrix} \begin{bmatrix} H[0] \\ H[1] \\ \vdots \\ H[N_c-1] \end{bmatrix} + \begin{bmatrix} W[0] \\ W[1] \\ \vdots \\ W[N_c-1] \end{bmatrix}$$
$$= \boldsymbol{XH} + \boldsymbol{W} \tag{17}$$

where $\boldsymbol{W}$ is a noise vector given as $\boldsymbol{W} = \left[W[0], W[1], \cdots, W[N_{sc}-1]\right]^T$ with $E\{W[k]\} = 0$ and $Var\{W[k]\} = \sigma_W^2$, $k = 0, 1, 2, \cdots, N_c - 1$. In the following discussion, let $\widehat{\boldsymbol{H}}_{\boldsymbol{LS}}$ denote the estimate of channel $\boldsymbol{H}$. The LS channel estimation method minimizes the following cost function:

$$J\left(\widehat{\boldsymbol{H}}_{LS}\right) = \left(\boldsymbol{Y} - \boldsymbol{X}\widehat{\boldsymbol{H}}_{LS}\right)^H \left(\boldsymbol{Y} - \boldsymbol{X}\widehat{\boldsymbol{H}}_{LS}\right) \tag{18}$$

where $(*)^H$ means the conjugate transpose operation. By setting the derivative of the function with respect to $\widehat{\boldsymbol{H}}_{LS}$ to zero:

$$\frac{\partial\left(\widehat{\boldsymbol{H}}_{LS}\right)}{\partial\widehat{\boldsymbol{H}}_{LS}} = -2(\boldsymbol{X}^H\boldsymbol{Y})^* + 2\left(\boldsymbol{X}^H\boldsymbol{X}\widehat{\boldsymbol{H}}_{LS}\right)^* = 0 \tag{19}$$

we have $\boldsymbol{X}^*\boldsymbol{X}\widehat{\boldsymbol{H}} = \boldsymbol{X}^*\boldsymbol{Y}$, which gives the solution to the LS channel estimation for each subcarrier k.

$$\widehat{\boldsymbol{H}}_{LS} = \boldsymbol{X}^{-1}\boldsymbol{Y} \tag{20}$$

Let us denote each component of the LS channel estimate $\widehat{\boldsymbol{H}}_{LS}$ by $\widehat{H}_{LS}[k]$ then:

$$\widehat{H}_{LS}[k] = \frac{Y[k]}{X[k]}, \qquad k = 0, 1, 2, \cdots, N_c - 1 \tag{21}$$

The mean-square error (MSE) of this LS channel estimate is given as:

$$MSE_{LS} = E\left\{\left(\boldsymbol{H} - \widehat{\boldsymbol{H}}_{LS}\right)^H \left(H - \widehat{\boldsymbol{H}}_{LS}\right)\right\} = \sigma_w^2/\sigma_x^2 \tag{22}$$

The MSE_{LS} in Equation (22) is inversely proportional to the SNR, which implies that it may be subject to noise enhancement.

2.7.3 **Channel estimation testing**

This section discusses the results of the simulation that were performed based on the information and mathematics discussed in the Section 2.7. The communication system for pilot-based block type channel estimation is shown in Figure 2-17.

We use the blocks of QPSK and OFDM as illustrated in the previous sections. Then the pilots are inserted by choosing specified indexes which will be use also by the receiver. At the receiver the channel estimation is done simply by dividing the received pilots over the transmitted ones in frequency domain. In order to get the channel, a liner interpolation is applied. Finally the equalizer compensate the received data to get the estimated.

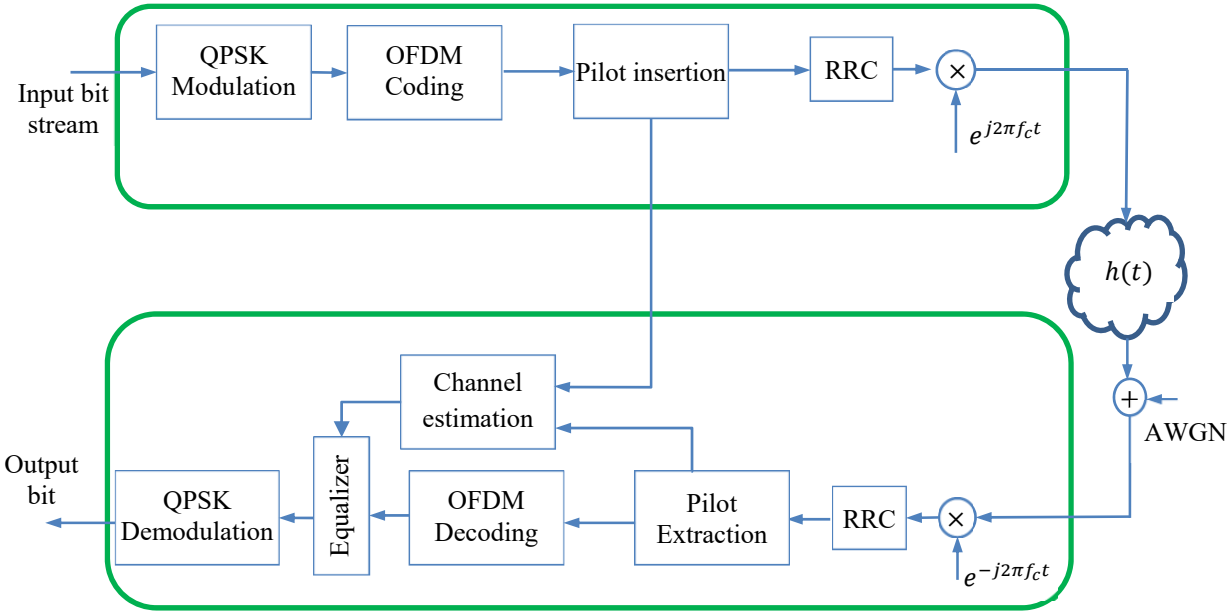

Figure 2-17: Communication block diagram and channel estimation subsystem

Using parameters in Table 2-4,

Figure 2-18 shows the comparison of BER with different SNR's on QPSK constellation using OFDM in 2 different channel models.

Table 2-4 Simulation Parameters

Parameter name	Parameter value
No of used Subcarriers	1024
Pilot number	1000
Constellation	QPSK
Channel Model	AWGN + Multipath

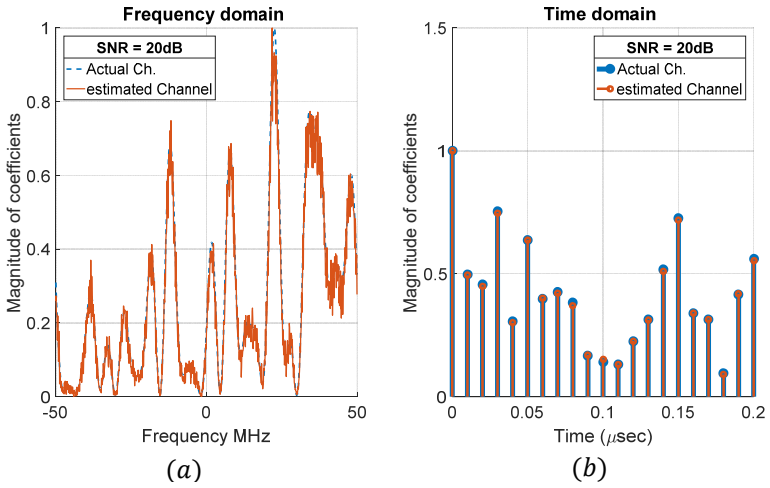

Figure 2-18: Channel responses with multipath: (a) frequency domain (b) time domain

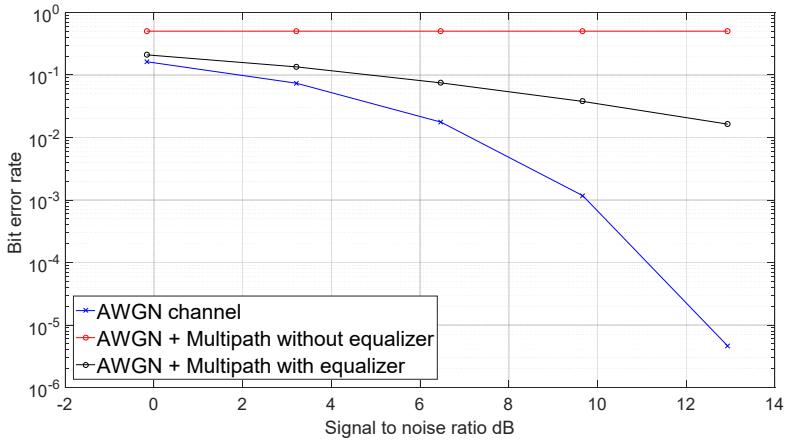

Figure 2-19 BER verses SNR – Performance curve with channel effect

As seen, for small SNR values the calculated BER is quite large due to relative high power of noise. As SNR is increased the BER decreases as shown.

2.8 Conclusion

In this section the mathematical derivation of the whole communication system is presented with some preliminary comments on how each step could affect the measurements of TDOA. The simulation code is implemented using Matlab programming language to implement the OFDM signals. All the illustrated parameters have been simulated with different values and shown the effect on the overall communication system. This study gives us now the possibility to propose many original solutions dealing with the extraction, from the well-known communication features, the time delay information which plays a central role in the wireless location process.

Bibliography

[1] S. Wu and Y. Bar-N, "OFDM Channel Estimation in the Presence of Frequency Offset and Phase Noise," *Proc. IEEE,* vol. 5, pp. 3366-70, Int'l. Conf. Commun.,.

[2] C. Mensing, S. Plass and A. Dammann, "“Synchronization algorithms for positioning with OFDM communications signals," *in Proc. 4th Workshop Positioning, Navigation, Communication,* pp. 205-210, 2004.

[3] T. M. Schmidl and D. C. Cox, "Robust frequency and timing synchronization chronization for OFDM," *IEEE Trans. Commun.,* vol. 45, no. 12, pp. 1613-1621, 1997.

[4] H. Minn, V. K. Bhargava and K. B. Letaief, "A robust timing and frequency synchronization for OFDM systems," *IEEE Trans. Wireless Commun,* vol. 2, no. 4, pp. 822-839, 2003.

[5] I. F. Progri and W. R. Michalson, "An investigation of a DSSS-OFDMCDMA-FDMA indoor geolocation system," *in Proc. Position Location Navigation Symp,* pp. 662-670, 2004.

[6] P. J. Voltz and D. Hernandez, "Maximum likelihood time of arrival estimation for real-time physical location tracking of 802.11a/g mobile stations in indoor environments," *Proc. Position Location Navigation Symp,* pp. 585-591, 2004.

[7] H. Reddy, M. G. Chandra, P. Balamuralidhar, S. G. Harihara, K. Bhattacharya and E. Joseph, "An improved time-of-arrival estimation for WLAN-based local positioning," *Proc. 2nd Int. Conf. Comm. Systems Software Middleware,* 2007.

[8] F. Winkler, E. Fischer, E. Grass and G. Fischer, "A 60 GHz OFDM indoor localization system based on DTDOA," *presented at the 14th IST Mobile & Wireless Comm.,* 2005.

[9] S. H. Yoo, C. Yoo, S. Lee, S. Y. Kim and a. S. Yoon, "A novel scheme for positioning error mitigation in OFDM-based on wireless location systems," *Proc. 9th Intl. Conf. Advanced Comm. Technology,* vol. 2, pp. 1267-1370, 2007.

[10] O. Bar-Shalom and A. J. Weiss, "Direct position determination of OFDM signals," *the IEEE 8th Workshop Signal Processing Advances in Wireless Comm,* 2007.

[11] O. Bar-Shalom and A. Weiss, "Efficient direct position determination of orthogonal frequency division multiplexing signals," *IET Radar Sonar and Navigation,* vol. 3, no. 2, pp. 101-111, 2009.

[12] S. P. a. A. D. C. Mensing, "Synchronization Algorithms for Positioning with OFDM Communications Signals," *in Proc. 4th Workshop on Positioning Navigation and Communication,* pp. 205-210, 2007.

[13] "Bounds on Distributed TDOA-Based Localization of OFDM Sources," *Proc. IEEE International Conference on Acoustics, Speech and Signal Processing (ICASSP'09),,* pp. 2289-2292, 2009.

[14] X. Li and K. Pahlavan, "“Super-resolution TOA Estimation with Diversity for Indoor Geolocation,"

IEEE Trans. Wireless Commun., vol. 3, no. 1, pp. 224-234, 2004.

[15] P. J. Voltz and D. Hernandez, "Maximum likelihood time of arrival estimation for real-time physical location tracking of 802.11a/g mobile stations in indoor environments," *Proc. IEEE Position Location and Navigation Symposium (PLANS'04),* pp. 585-591, 2004.

[16] T. J. S. Khanzada, A. R. Ali and A. S. Omar, "Time Difference of Arrival Estimation using Super Resolution Algorithms to Minimize Distance Measurement Error for Indoor Positioning Systems," *Proc. IEEE International Conference on Multitopic Conference (INMIC'08),* pp. 443-447, 2008.

[17] J. Zander, "Performance of optimum transmitter power control in cellular radio systems," *IEEE Trans. Veh. Technol.,,* vol. 41, pp. 57-62, 1992.

[18] K. Balachandran, S. R. Kadaba and S. Nanda, "Channel quality estimation and rate adaptation for cellular mobile radio," *IEEE J. Sel. Areas Commun.,* vol. 17, pp. 244-1256, 1999.

[19] N. C. Beaulieu, A. S. Toms and D. R. P. Modulations, "Comparison of Four SNR Estimators for QPSK," *IEEE COMMUNICATIONS LETTERS,* vol. 42, pp. 43-45, 2000.

[20] Y. S. Cho, J. Kim, W. Y. Yang and C. G. Kang, "MIMO-OFDM WIRELESS COMMUNICATIONS WITH MATLAB," *Wiley-IEEE Press eBook Chapters,* 2010.

[21] S. Wu and Y. Bar-Ness, "OFDM Channel Estimation in the Presence of Frequency Offset and Phase Noise," *Proc. IEEE Int'l. Conf. Commun.,* vol. 5, p. 3366–3370, 2003.

[22] B. Han, X. Gao and X. You, "An iterative joint channel estimation and symbol detection algorithm applied in OFDM system with high data to pilot power ratio," *Communications, 2003. ICC '03. IEEE International Conference on,* pp. 2076-2080, 2003.

[23] J.-H. Lee, Y.-H. Kim and S.-C. Kim, "Pilot symbol initiated iterative channel estimation and decoding for QAM modulated OFDM signals," *Vehicular Technology Conference, 2003. VTC 2003-Spring. The 57th IEEE Semiannual,* pp. 1322-1326, 2003.

Chapter 3: OFDM based TDOA estimation

3.1 Introduction

This chapter is the core of our work. It starts with a brief state of the art of TDOA positioning systems. Then we explain, through mathematical derivation, first the direct model leading to express the channel function as function of the TDOA, and second the inverse problem that allows TDOA extraction from channel estimation. After performing many simulations, either in free space channel or in noisy and multipath channels, we asset the performance of such a TDOA estimation, and prepare the materials for upcoming experimental validation dealt with in chapter 4.

3.2 Algorithms for TDOA-based positioning

The TDOA technique as its name indicates, endeavors to measure the difference of time delay of the source signals received by a number of spatially separated antennas, and solve a set of nonlinear equations to estimate the source location.

Over the past few decades, localization problem have been investigated based on TDOA measurements as time delay estimation (TDE) problem. The classical TDE techniques are based on correlations [1]. One of the various traditional synchrony measures, Cross-Correlation Computation (CCC) [2] is the most direct and earliest developed TDE algorithm, which is formulated based on Single-Input-Multiple-Output (SIMO) configuration where the single-path propagation with two receivers. Let's note that, due to the reciprocity principle, SIMO configuration can sometime turn to MISO configuration, hence the roles of transmitters and receivers are swapped.

To improve the CCC method, the generalized cross-correlation (GCC) algorithm [3] unifies various correlation-based algorithms into one general framework, and it also provides a mechanism to incorporate knowledge to enhance the performance of TDE. However, Cross-Correlation is computationally expensive, depending on the used bandwidth and on the Rayleigh criterion, and has limited time resolution, which degrades its performance significantly when the signal components are closely spaced.

Many high resolution TDOA algorithms have been proposed recently to deal with the scenario where signals from different paths have close delays [4]. Mainly, these algorithms split into two branches where they have been studied in the temporal domain.

One is the optimal maximal likelihood (ML) time delay estimators using techniques like expectation maximization (EM) [5], importance sampling [6], [7], and formulating the time delay as a least squares (LS) fitting problem [8] [9]. But, these algorithms often converge to local optima. So to solve this problem, two time delay estimators using weighted-Fourier-transform-based relaxation (WRELAX) are proposed in [10]. Unfortunately, large numbers of data samples are required to achieve accurate time delay estimation.

Another branch is based on the subspace methods that can explicitly cope with the multisource correlation matrix such as MUSIC [11], [12] and ESPRIT [13]. By observing the Eigen structure of the sensor correlation matrix, the signal subspace can be extracted and the position of several sources can be estimated. These subspace methods do not account for a realistic reverberant signal propagation model.

Except for those main branches, some delay estimation techniques can also be adapted to TDOA estimation. They have the ability to deal with the multipath environment, such as Hou and Wu proposed in [14]. Starting with a model-based sinusoidal estimation method, they converted time delay estimation problem into a sinusoidal parameter estimation problem. Several other model-based sinusoidal estimation methods are also presented in [15]. These methods often involve a spectral division operation and did not touch with the scenario where different paths have close delays.

3.3 Definition of the direct model

The scenario considered in the present work is described in Figure 3-1. It supports OFDM communication, already presented in chapter 2.

As seen a Multiple-Input Single-Output (MISO) configuration is used and composed of a single RU with two collocated transmitting antennas A_1 and A_2 separated by a baseline ($B \ll d_1, d_2$), and a MU with a single receiving antenna A_R. Distances d_1 and d_2 are defined between A_R and A_1 and between A_R and A_2 respectively.

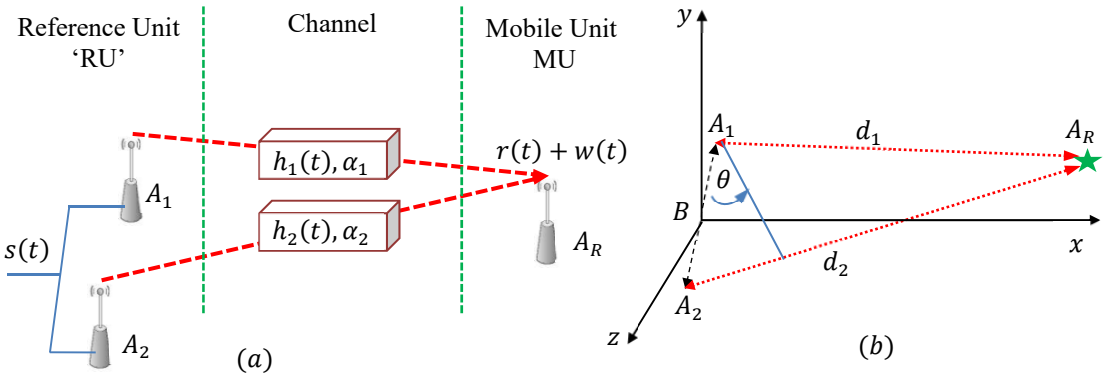

Figure 3-1: MISO acquisition (a) and associated geometry (b)

Based on the geometry of acquisition in Figure 3-1 (b), the actual TDOA "τ", is expressed as follows: $\tau = \frac{d_1 - d_2}{c} = \frac{Bsin(\theta)}{c}$, where c is the speed of light. So one can conclude that the values of τ are bounded by $\frac{B}{c}$ and hence verify:

$$-B/c \leq \tau \leq B/c \tag{23}$$

The geometrical limitation shown in equation (23) will be further discussed in chapter 4. We define hereafter the frequency limitation of TDOA.

3.3.1 Frequency limitation

The time difference of arrival is naturally linked to the available bandwidth f_d which normally conditions the minimum measurable TDOA, in the sense of Rayleigh or Fourier resolution. As we target TDOA estimation, one can expect overpass this physical limitation and may link the minimum TDOA to the sampling frequency f_s. In theory, this limitation stands for the resolution of the considered estimator and the following relationship:

$$\tau_{min} = \frac{1}{f_s} \tag{24}$$

Since $\tau \geq \frac{1}{f_d}$ is solvable, one can define the maximum TDOA, we target, should verify

$$\tau_{max} = \frac{1}{f_d} \tag{25}$$

So all the TDOA we consider belongs to the following set $\left[\frac{1}{f_s}, \frac{1}{f_d}\right]$.

3.3.2 **Signal model**

Using free space channel configuration, the RU periodically sends, simultaneously through antennas A_1 and A_2, a signal toward MU. In the following, we state the main steps leading to express the received signal as a function of the TDOA. Let us consider the transmitted signal $s(t)$ as:

$$s(t) = x(t)e^{j2\pi f_c t} \tag{26}$$

where the data signal $x(t)$ has expression given in equation (6) in chapter 2 and having a mean power P. It behaves like an equivalent low pass signal of $s(t)$ occupying a bandwidth f_d, centered at a carrier frequency f_c .

At the receiver, the signal $r(t)$, affected by the AWGN $\mathcal{N}(0, \sigma^2)$, whose power density is noted $N_0/2$, is expressed as follow:

$$r(t) = h_1(t) * s(t) + h_2(t) * s(t) + w(t) = h(t) * s(t) + w(t) \tag{27}$$

where (*) stands for convolution product.

Considering a free space scenario $h_1(t) = \alpha_1\delta(t - t_1)$, and $h_2(t) = \alpha_2\delta(t - t_2)$, with $h(t) = \ h_1(t) + \ h_2(t)$. Therefore in the baseband, the received signal, noted $y(t)$, can be written as:

$$y(t) = \ h_1(t) * x(t) + h_2(t) * x(t) + w(t) = h(t) * x(t) + w(t) \tag{28}$$

and in the frequency domain, considering the circular convolution provided by CP, it can be expressed as follow:

$$Y(f) = \ H_1(f) \cdot X(f) + H_2(f) \ \cdot X(f) + W(f) = H(f) \cdot X(f) + W(f) \tag{29}$$

where $H_1(f) = \alpha_1 e^{-i2\pi f t_1}$, and $H_2(f) = \alpha_2 e^{-i2\pi f t_2}$, $H(f) = \ H_1(f) + \ H_2(f)$.

Once these preliminary expressions stated, one can derive the direct model using three different approaches. The first deals with energy detection and the two others are related to the CSI.

3.3.3 **Energy based approach**

Defining a direct model consists in formulating the relationship between a measurable quantity and the parameter of interest; here the TDOA. First, one can simply associate the TDOA to the energy detected at the MU. For this purpose we need to integrate over an observation time T_{obs} the following quantity:

$$y(t)\,.\,y(t)^{*} = \alpha_1^2 x_1^2 + \alpha_2^2 x_2^2 + \alpha_1\alpha_2 x_1 x_2^{*} + \alpha_1\alpha_2 x_1^{*} x_2 + \sigma^2 \tag{30}$$

where $x_1 = \delta(t - t_1) * x(t)$, and $x_2 = \delta(t - t_2) * x(t)$, and σ^2 is noise power. With respect to the formula of $x(t)$ in chapter 2, the detected energy, for each frequency f, and for a given TDOA τ, takes the following form:

$$E(f,\tau) = T_{obs} \cdot P \cdot (\alpha_1^2 + \alpha_2^2 + 2\alpha_1\alpha_2 \cos(2\pi f\tau)\,) + N_0 \tag{31}$$

This expression is the first tentative to address the direct model. It gives a univocal relationship between $E(f,\tau)$ and TDOA but supposes the perfect knowledge of the transmitted power P. Due to channel effects, this constraint is not well suited for accurate TDOA estimation, and a simple normalization cannot help. We do prefer to link the TDOA to quantity that is not depending on P. The only way of avoiding this constraint is to work with channel estimation, which is already built information in OFDM communication standards.

3.3.4 **Channel based approach**

It is well-known that any effect of the channel observed around f_c, could be reproduced in the baseband representation, so the effect of TDOA can hence be reproduced either around the carrier frequency f_c or in the baseband domain. So one can obtain from equation (29), that the frequency response of the channel $H(f,\tau)$ is affected by TDOA. In the next two sections we will investigate, by recalling the well-known two paths channel, how TDOA could affect the channel. We first explore the square of magnitude of the frequency response channel, and then we work on complex quantity of this response.

3.3.4.1 **Square of magnitude of the channel transfer function**

In order to show TDOA τ in the transfer function $H(f,\tau)$, we write from equation (29):

$$H(f,\tau) = e^{-i2\pi f t_1}\left(\alpha_1 + \alpha_2 e^{-i2\pi f \tau}\right) \tag{32}$$

where $= t_2 - t_1$. So squaring (10) gives:

$$H \cdot H^* = \alpha_1^2 + \alpha_2^2 + 2\alpha_1\alpha_2 \cos(2\pi f \tau) \tag{33}$$

This second tentative of defining a direct model, exhibits, as expected, a sinusoidal shape depending on TDOA, and solves the problem encountered in energy detection. However, as it will be seen in the following, another difficulty may occur. To emulate the effect of the TDOA on the channel magnitude, we build up a Single-Input-Single Output (SISO) system as depicted in Figure 3-2.

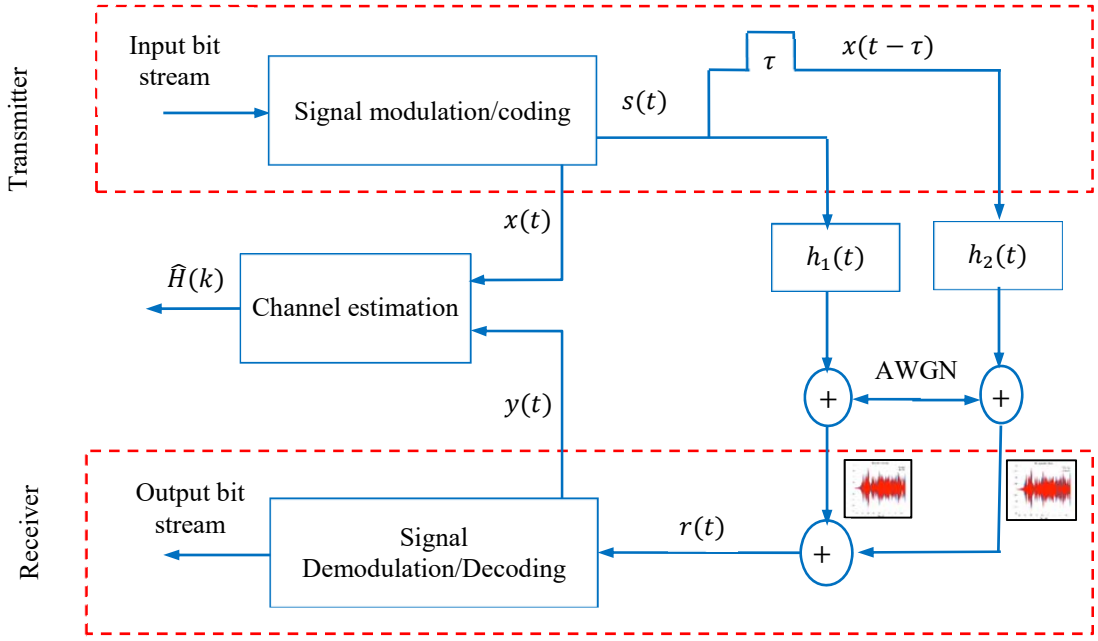

Figure 3-2: Simulation block diagram of an OFDM based SISO communication emulating a MISO scenario

This system acts as a MISO configuration but without needing to take into account the baseline *B*. Considering an input bit stream, the transmitted data is a random sequence using QPSK-OFDM modulation. It is first split into two branches, and a controllable time delay τ, playing the role of TDOA, is inserted in one branch. In each branch "*i*", modeled by its transfer function $H_i(f) = \alpha_i$, an AWGN is added. The combination of these two branches leads to the useful OFDM signal from which the channel estimation is performed at the receiving part.

The test conditions, for this simulation, are listed in Table 3-1.

Table 3-1 Test parameters

Parameter name	Parameter value
f_s	10 GS/s
f_c	3 GHz
f_d	100 MHz
No of used Subcarriers	1024
Channel Model	Free space +AWGN
Roll of factor	0.35

We present in Figure 3-3, for different TDOA, the square of magnitude of the channel transfer function emulating the MISO configuration given in Figure 3-1. Each curve is fitted by a function extracted from the direct model (black line) given in equation (33).

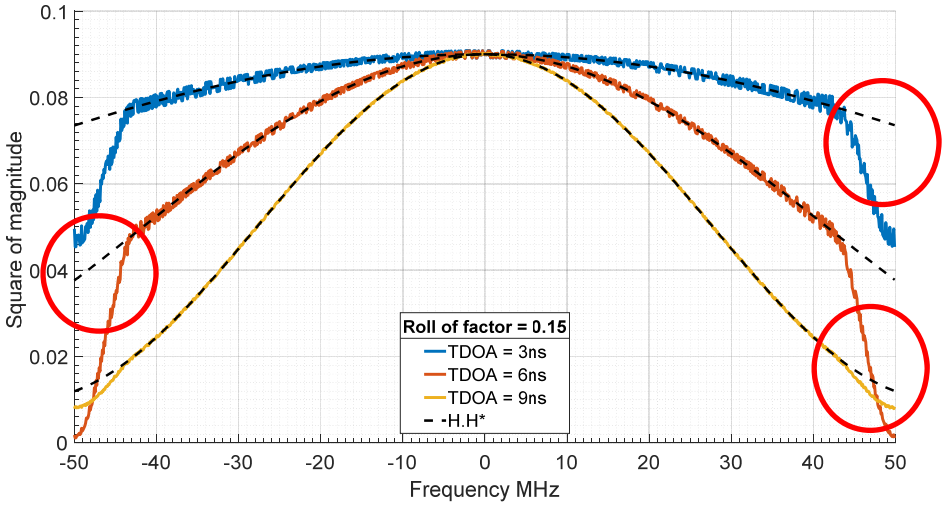

Figure 3-3: Examples of squared magnitude of the channel transfer function without noise.

As expected, the simulated curves have almost the shape announced by the direct model, and show a sinusoidal amplitude modulation of the spectrum, whose frequency period δF is, in principle, only conditioned by TDOA.

However, we note that (cf. red circles) there are some defects on the edges of the bandwidth. The only parameter in the fixed communication system that affects the bandwidth is the roll of factor β, which conditions the shape to the RRC filter.

To demonstrate this effect, we plot in Figure 3-4 the square of magnitude of the frequency response channel considering a fixed value of TDOA set to 0.6 ns, and several values of $\beta = [0.15, 0.55, 0.95]$.

As clearly seen and well expected the roll of factor impacts negatively the shape of the magnitude of $H(f,\tau)$. This problem, which is normally enhanced by the squaring operation, needs to be solved prior to any TDOA estimation.

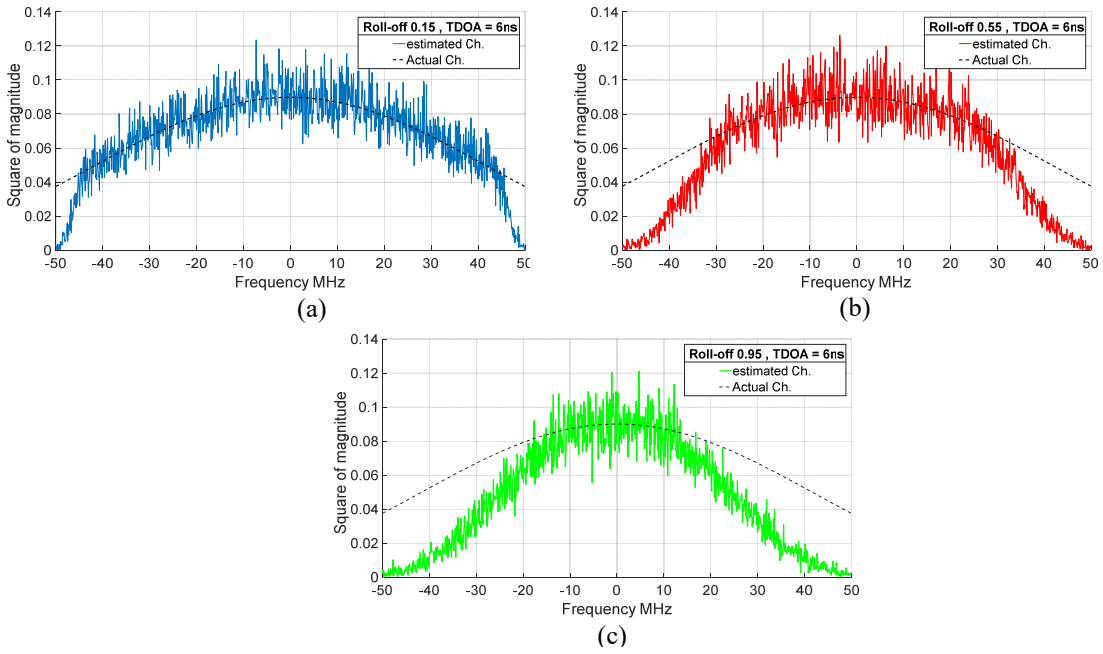

Figure 3-4: Roll of factor effect on the square of magnitude of the transfer function. Test parameters are reported in Table 3.1 and SNR = 20 dB

$$a)\ \beta = 0{,}15, b)\ \beta = 0{,}55, and\ c)\beta = 0{,}95$$

3.3.4.2 **Complex frequency response of the channel**

Instead of working with quadratic approach, which increases the effects of the roll off factor, one can work on complex value of $H(f)$. From relation (11), we can extract equation (34) for the real part and the imaginary part of $H(f)$ and suggest estimating the TDOA using such direct model.

$$\Re[H(f)] = \alpha_1 + \alpha_2\, cos(2\pi f\tau)\,, \qquad \Im[H(f)] = \alpha_2\, sin(2\pi f\tau) \tag{34}$$

Indeed, for both real part and imaginary parts, a sinusoidal variation depending on TDOA occurs. To see the effect of the TDOA on equation (34), we rerun, under the same parameters in Table 3-1, the simulation block diagram illustrated in Figure 3-2.

After plotting the real and imaginary parts of the channel estimation in Figure 3-5 (a) and Figure 3-5 (b) respectively, we see the same defect, mentioned in the previous section, on the imaginary part, but the real part seems less affected. This is due to the fact that, for certain

TDOAs, that make the real part maximum around the carrier frequency, the shape of the real part of $H(f)$ in baseband is naturally similar to the shape of the RRC.

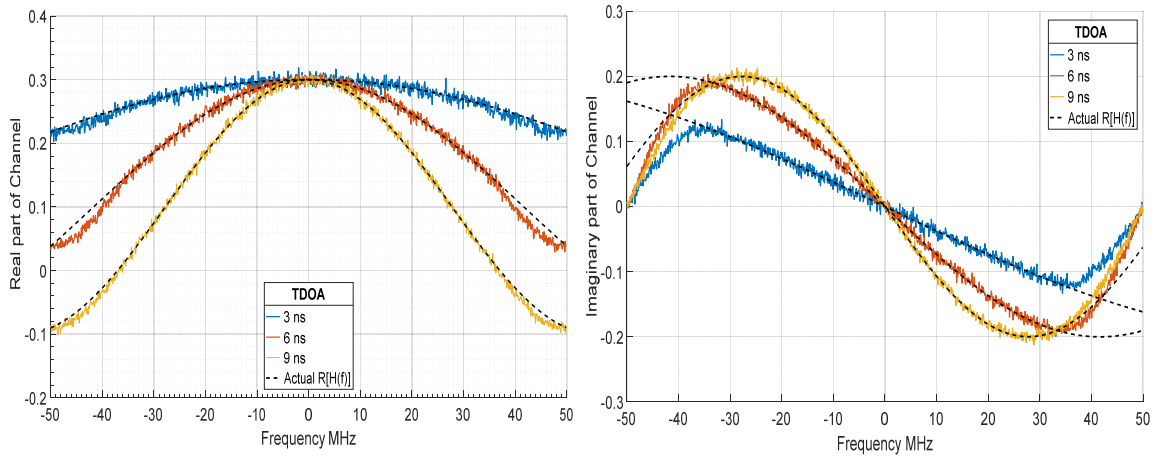

(a) (b)

Figure 3-5: Channel estimation components for 3 different TDOA with β=0.15: a) Real part, b) Imaginary part

Obviously for other TDOAs that do not exhibit a such maximum, the behavior of the complex frequency response changes and may lead to the following complementary figures.

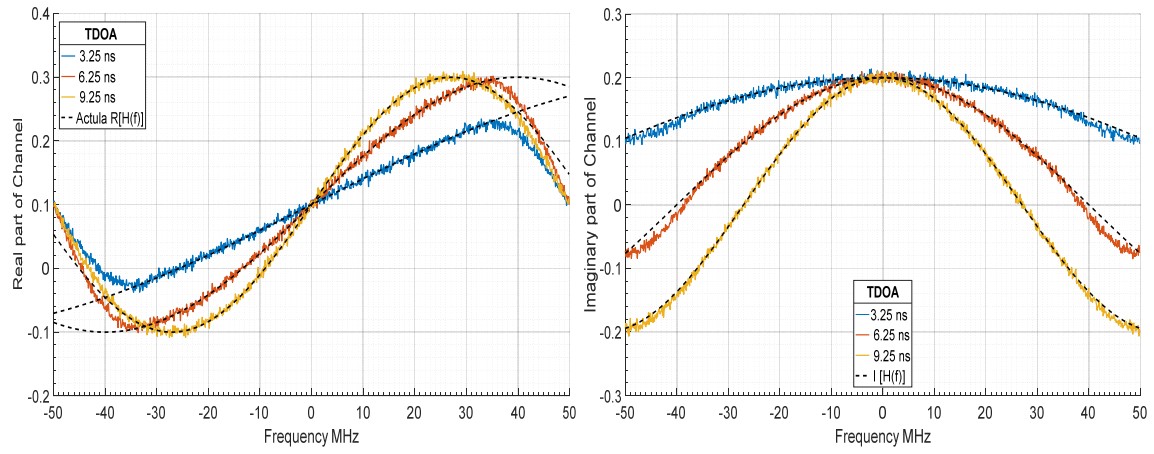

(a) (b)

Figure 3-6: Channel estimation components for 3 different TDOA with β=0.15:

This observation leads us to consider, for inverse problem, both real and imaginary part of $H(f,\tau)$, and hence to imagine new solutions to estimate the TDOA in a proper way. It is the content of the next section.

3.4 Inverse problem: TDOA extraction

As previously explained, the TDOA of interest lies in both the real and imaginary parts of the channel frequency response in baseband representation. So once the channel is estimated (chapter 2 section 2.7), it is easy to isolate the TDOA dependent terms ($\cos(2\pi f\tau)$ or $\sin(2\pi f\tau)$) and then to extract TDOA by a well appropriate way. Indeed, to cope with all the values of TDOA belonging to $[\frac{1}{f_s}, \frac{1}{f_d}]$, we introduce more suited metrics called Useful Information and noted $US(\tau, f)$ that should be able to give more possibilities for extracting TDOA even if it is too small. Therefore we distinguish three classes of TDOA compared to the useful bandwidth f_d: large TDOA, small TDOA, and very small TDOA.

3.4.1 Large TDOA

Large TDOA is defined as TDOA that is superior to $1/f_d$. It occurs when the baseline B is large, compared to c/f_d, and when the MU is set at grazing angle regarding the line of baseline ($\theta = \frac{\pi}{2}$ in Figure 3-1(b)). So if TDOA is large enough, $H(f)$ exhibits many periods δF. This converts the TDOA estimation into a sinusoidal parameter estimation problem, i.e., estimating "τ" in $\cos(2\pi f\tau)$. So one can exploit the frequency period δF expressed as follow:

$$\delta F = \frac{1}{\tau} \tag{35}$$

In free space channel, the frequency period δF is exactly equal to the inverse of "τ". According to this equation; it clearly appears that δF could never exceed a maximum value $\delta F_{max} = \frac{c}{B}$. This analysis shows that if the useful bandwidth f_d is chosen as a multiple value of δF_{max},($i.e., f_d = n.\delta F_{max}$), then the received spectrum will exhibit a maximum of n frequency periods δF_{max}.

If we assume that at least one period is totally described over the whole bandwidth f_d, then by using the Fourier decomposition, it can be possible to access to a kind of “spoof” channel impulsive response, which is directly expressed in the domain of TDOA. The first non-zero line in this spectral analysis is normally the TDOA of interest [16].

To simulate this approach, we use the set-up defined in Figure 3-2 and the test conditions in Table 3-1, and we set the useful TDOA at 40ns. At the receiver, the periodicity in the channel estimation appears as depicted in Figure 3-7 (a), and a simple FFT algorithm may exhibit two lines (Figure 3-6 (b)), one at zero and the second at the TDOA of interest.

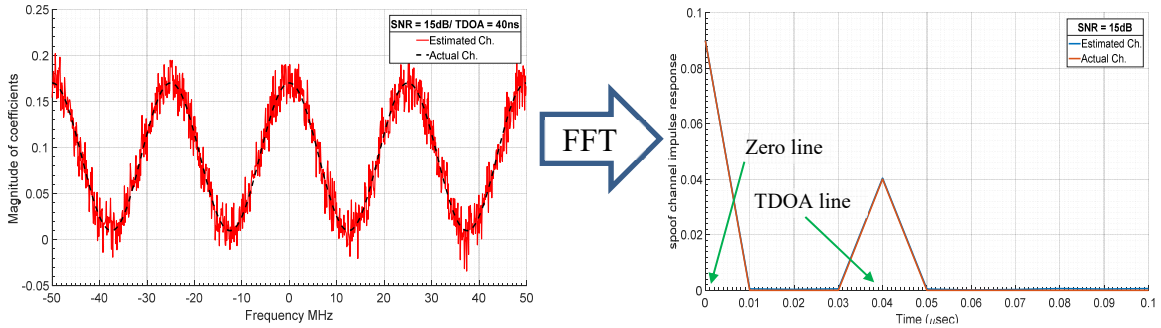

(a) (b)

Figure 3-7: Two kinds of representation of the channel transfer function a) in the frequency domain, b) in the time difference of arrival domain.

This conventional approach provides also the possibility to discriminate useful TDOA bounded by $1/f_d$, from the unbounded TDOAs that could be produced by multipath, but it is no longer valid if targeted TDOAs, with regard to the bandwidth, are small. This leads us to the next section.

3.4.2 Small TDOA

Small TDOA is defined as TDOA that is less than $1/f_d$, but remains greater than $1/f_s$. Within this situation, none periodicity in the receiving spectrum can occur, and Fourier analysis could no longer be performed. So we need to imagine alternative solutions to resolve small TDOA without requiring more bandwidth f_d. We will present in the next section how to process the useful information to extract TDOA of interest.

3.4.2.1 Useful information using square of magnitude of $H(f,\tau)$

Useful Information is defined as a function that depends only on the frequency and on the TDOA of interest. As seen in the direct model with the square of magnitude of $H(f,\tau)$, the useful information $US_{SM}(\tau,f)$ is defined as:

$$US_{SM}(\tau,f) = \frac{H \cdot H^* - \alpha_1^2 - \alpha_2^2}{2\alpha_1\alpha_2} = \cos(2\pi f\tau) \tag{36}$$

The unknown coefficients (α_1, α_2) dealing with the amplitude of $H_1(f)$ and $H_2(f)$ can be measured by exploiting the received signal in a single-input- single-output SISO configuration. Actually, if only the antenna A_1 sends a message to the receiving antenna A_R, the channel spectrum leads directly to α_1. Similarly, if only the antenna A_2 sends a message to the receiving antenna A_R, the channel spectrum leads directly to α_2. It is clear that during the measurement of α_1, and α_2 the channel is assumed to be stationary.

As we already know the type of the useful information function, we propose, for extracting τ, to generate several vector of $cos(2\pi f\boldsymbol{\tau})$ where $\boldsymbol{\tau}$ is vector of N_τ points. Then by matching these vectors with the useful information vector, $\hat{\tau}$ satisfies the estimated TDOA:

$$\tilde{\tau} = argmin\left(\sum\left(US_M - cos(2\pi f\boldsymbol{\tau})\right)^2\right) \tag{37}$$

However, before testing this approach we need to solve the problem of roll of factor effect, which impacts the edges of the bandwidth, by eliminating edge sub carriers. Indeed, as well known, the RRC filter expands the null-to-null bandwidth according to the following equation:

$$F_{effective} = f_d(1+\beta) \tag{38}$$

So if we consider N_c subcarriers, one should remove from each edge $\frac{N_c*\beta}{2}$ subcarriers to cancel or reduce the roll off factor effect. The resulting channel transfer function, leading to the concept of "edged" channel, corresponding to β=0.15 and N_c=1024, is shown Figure 3-8, where 153 subcarriers were removed.

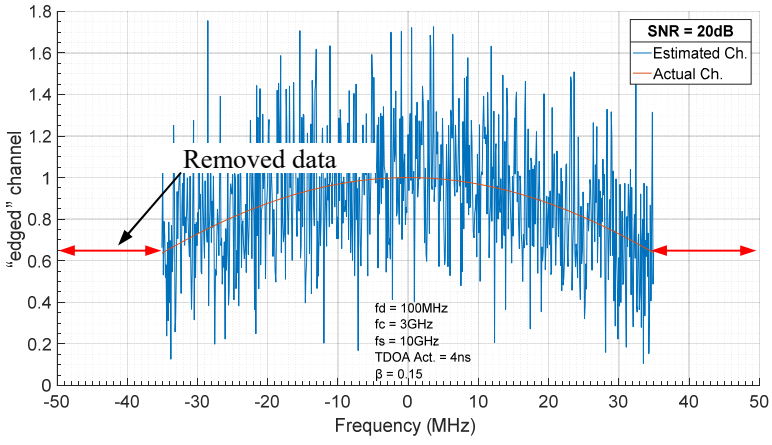

Figure 3-8 : Square of magnitude of "edged" channel

To verify this approach, we built up a simulation program which its block diagrams is shown in Figure 3-9 below.

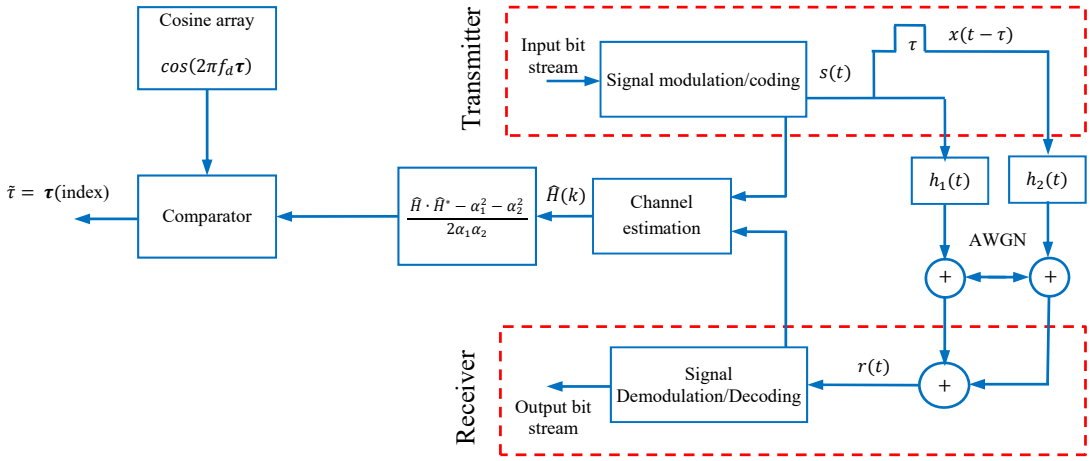

Figure 3-9: Block diagram of TDOA estimation using $US_{SM}(f,\tau)$

At the transmitter, the signal, which is composed of the original signal and its delayed copy with TDOA of interest, is passed through a free space channel. Then the resulting signal is added to a noise. At the receiver, the estimation of "$\tilde{\tau}$" is done by applying equation (37) on the useful information calculated from estimated channel, where $\boldsymbol{\tau}$ is a generated vector which contains values with maximum value $\tau_{max} = 1/f_d$.

The simulation is applied under the parameters listed in Table 3-2. This table will be used for all the upcoming simulation processes.

Table 3-2 Test parameters

Parameter name	Parameter value
f_s	10 GHz
f_c	3 GHz
f_d	100 MHz
No of used Subcarriers	1024
Channel Model	Free space +AWGN
SNR	[3:7.5:10] dB
τ	$[0: 1/f_d]$

The Figure 3-10 shows that, by shortening the length of data with respect to the roll off factor, it is possible to estimate the TDOA with values less than the inverse of the used bandwidth.

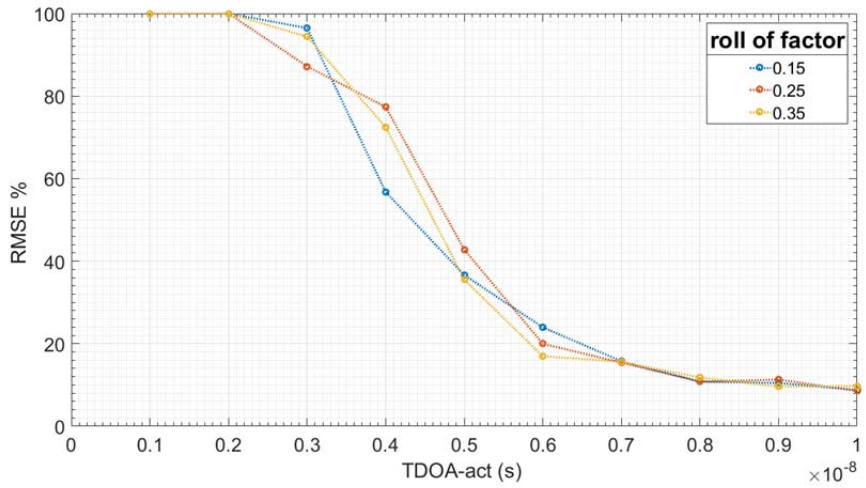

Figure 3-10 : $US_{SM}(f,\tau)$ estimator performance with SNR=10dB

As seen the effect of the roll of factor is almost neglected, as the estimator behaves similar in all the values of the roll of factor. However, due to the reduction of the processed data, the accuracy of the estimator may decrease leading us to propose alternative solutions that avoid cutting edge of the spectrum. This will be presented in the next section.

3.4.2.2 **Useful information from real and imaginary parts of $\boldsymbol{H(f,\tau)}$**

Once the transfer function of the channel is established, one can isolate, with respect to equation (32), the cosine and sine parts and define the Useful Information, which resides in the two functions:

$$US_I(\tau,f)=\frac{\Re[H(f)]-\alpha_1}{\alpha_2}=\cos(2\pi f\tau)\ ;\ US_Q(\tau,f)=\frac{\Im[H(f)]}{\alpha_2}=\sin(2\pi f\tau) \qquad (39)$$

We generate, via MATLAB, series of cosine and sine functions with different values of "τ", and then compare them with the measured $US_I(\tau,f)$and $US_Q(\tau,f)$. By using a least square criterion, the two estimated TDOA $(\tilde{\tau}_I,\tilde{\tau}_Q)$ extracted from $US_I(\tau,f)$and $US_Q(\tau,f)$ and the true estimated TDOA $\tilde{\tau}$ satisfy respectively :

$$\tilde{\tau}_I=argmin\left[\sum(US_I-\cos(2\pi f\boldsymbol{\tau}))^2\right]$$

$$\tilde{\tau}_Q=argmin\left[\sum\left(US_Q-\sin(2\pi f\boldsymbol{\tau})\right)^2\right]$$

$$\tilde{\tau}=argmin\left[Err(\tilde{\tau}_I),Err\left(\tilde{\tau}_Q\right)\right] \qquad (40)$$

where $\boldsymbol{\tau}$ is a vector of N_τ points between $[1/f_s, 1/f_d]$, and $Err(\tilde{\tau}_I), Err(\tilde{\tau}_Q)$ are the minimum least square error, from which $(\tilde{\tau}_I, \tilde{\tau}_Q)$ are taken. To validate this proposed approach, we build up the simulation diagram as shown in Figure 3-11.

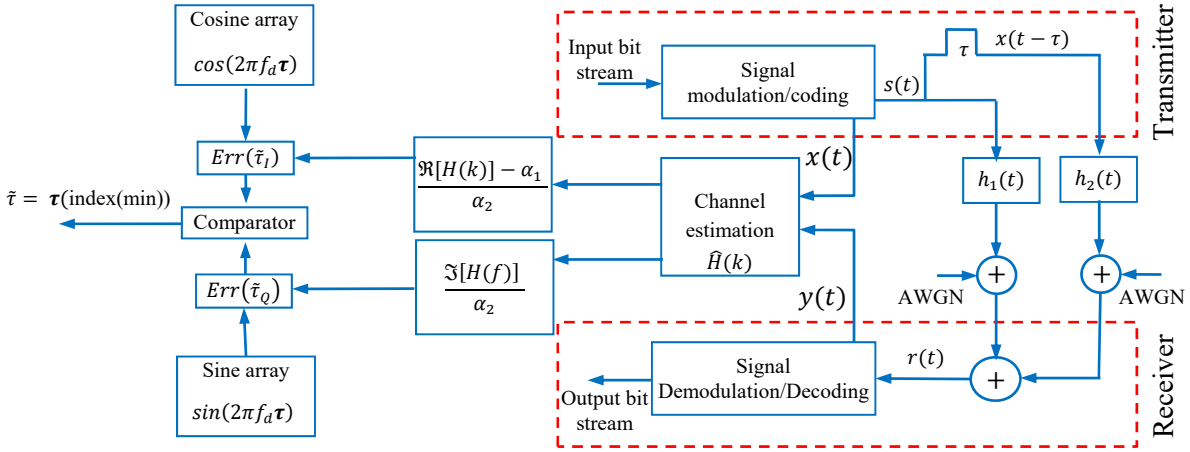

Figure 3-11: Block diagram of TDOA estimation using $US_I(f,\tau)$ and $US_Q(f,\tau)$

At the transmitter, the signal, which is composed of the original signal and its delayed copy with TDOA of interest, is passed through a free space channel. Then the resulting signal is added to a noise. At the receiver, the estimation of "$\tilde{\tau}$" is done by applying equation (40) on the useful information calculated from estimated channel, where $\boldsymbol{\tau}$ is a generated vector which contains values with maximum value $\tau_{max} = 1/f_d$. The simulation is applied under the same parameters listed in Table 3-2 with β =0.35. The Figure 3-12 shows that hoping between $US_I(f,\tau)$ and $US_Q(f,\tau)$ and choosing the best estimation, naturally reduces the RMSE on TDOA, as the black dots point out.

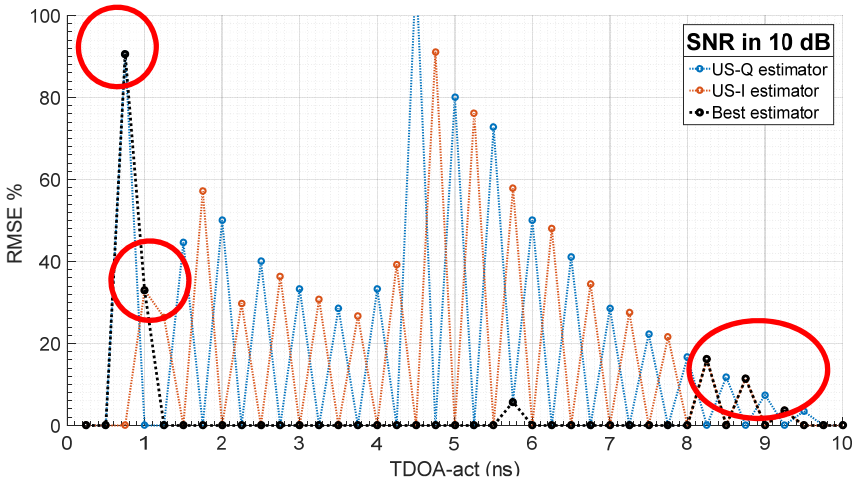

Figure 3-12 : $US_I(f,\tau)$ and $US_Q(f,\tau)$ estimators performance with SNR=10dB

However, for some TDOAs (red circles), the estimation is not well done. This means that even if we get the lower error in estimation process, it does not match necessary the actual value. This is happened because this estimator does not compare the error of the same function, as one comparator is for sine fitting and the other is for cosine fitting. So this forces us to find another way to unify this comparison. It's what we suggest in the following section.

3.4.2.2.1 Useful information using $sinc$ function

The sine-cosine functions tested former can be advantageously replaced by another Useful Information noted $US_J(\tau)$ made with integration over the considered bandwidth of both real and imaginary parts of $H(f,\tau)$. This leads to the following result for the real part:

$$\frac{1}{f_d}\int_{f_c-\frac{f_d}{2}}^{f_c+\frac{f_d}{2}} \Re[H(f)]\, df = \alpha_1 + \alpha_2 sinc(\pi\tau f_d)\cos(2\pi f_c\, \tau) \tag{41}$$

and for the imaginary part :

$$\frac{1}{f_d}\int_{f_c-\frac{f_d}{2}}^{f_c+\frac{f_d}{2}} \Im[H(f)]\, df = \alpha_2 sinc(\pi\tau f_d)\sin(2\pi f_c\, \tau) \tag{42}$$

and hence to define the new Useful Information $US_{JI}(\tau,f)\ and\ US_{JQ}(\tau,f)$, which resides in the $sinc$ function, we consider only the peak values of the previous relationships. This gives:

$$\begin{aligned} US_{JI}(\tau) &= \frac{Peak(abs(\frac{1}{f_d}\int_{f_c-\frac{f_d}{2}}^{f_c+\frac{f_d}{2}} \Re[H(f)]\, df)) - \alpha_1}{\alpha_2} \\ US_{JQ}(\tau) &= \frac{Peak(abs(\frac{1}{f_d}\int_{f_c-\frac{f_d}{2}}^{f_c+\frac{f_d}{2}} \Im[H(f)]\, df))}{\alpha_2} \end{aligned} \tag{43}$$

This exhibits to use (21) to show that the TDOA of interest verify:

$$\begin{aligned} \tilde{\tau}_{JI} &= argmin\left[US_{JI}(\tau) - sinc(\pi\boldsymbol{\tau} f_d)\right] \\ \tilde{\tau}_{JQ} &= argmin\left[US_{JQ}(\tau) - sinc(\pi\boldsymbol{\tau} f_d)\right] \\ \tilde{\tau} &= argmin\left[Err(\tilde{\tau}_{JI}), Err(\tilde{\tau}_{JQ})\right] \end{aligned} \tag{44}$$

where "$\boldsymbol{\tau}$" is a vector of N_τ points between $[1/f_s, 1/f_d]$. $Err(\tilde{\tau}_{JI}), Err(\tilde{\tau}_{JQ})$ are the minimum error, from which $\tilde{\tau}_{JI}, \tilde{\tau}_{JQ}$ are taken. In addition to that, the presence of the sinc function gives this solution an advantage that lies in the fact that TDOA "τ" is unambiguously found in the interval $[1/f_s : 1/f_d]$, and due to integration, may reduce both the effect of multipath as well as noise. To validate this approach simulation diagram in Figure 3-13 is modified by adding the integration part and new comparator with $sinc$ function generated with 41 TDOA values within the range $[1/f_s : 1/f_d]$. With the same parameters of Table 3-2 and $\beta = 0.35$

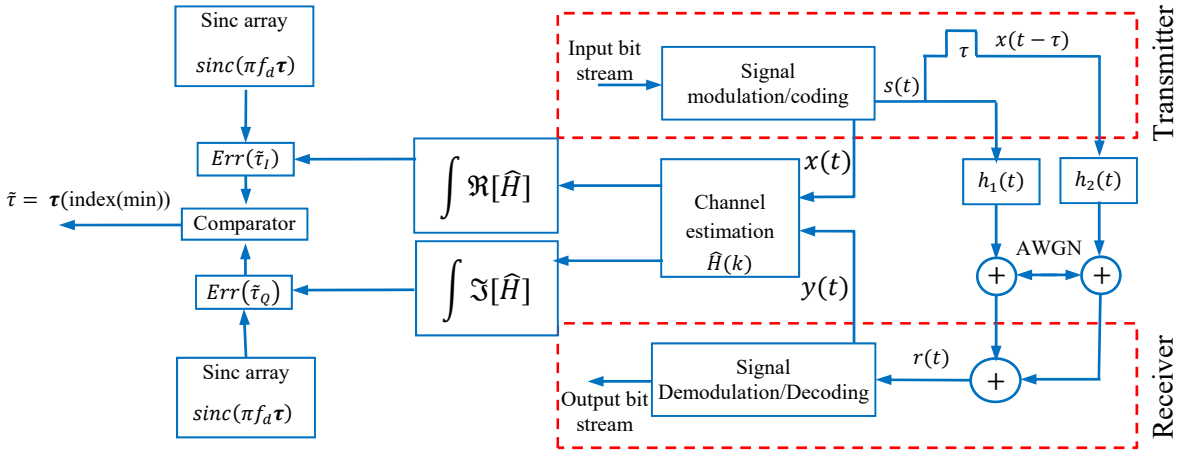

Figure 3-13: Block diagram of TDOA estimation using $US_J(f,\tau)$ function

The Figure 3-14 below shows that this method is valid for TDOA estimation, since all the most of τ actual values are estimated without adding any complexity to the system. The performances are better than those obtained with $US_{JI}(f,\tau)$ and $US_{JQ}(f,\tau)$.

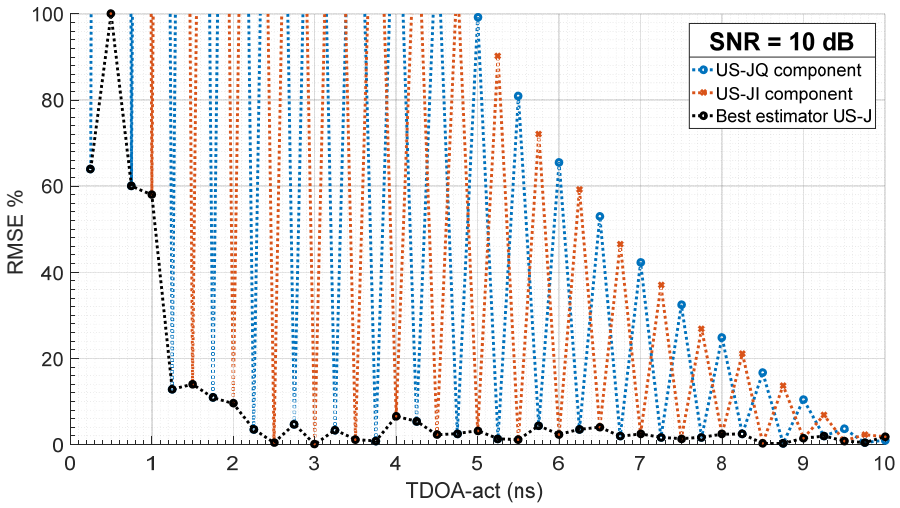

Figure 3-14: $US_J(f,\tau)$ estimator performance

We run this estimator by varying SNR and obtained the Figure 3-15 below.

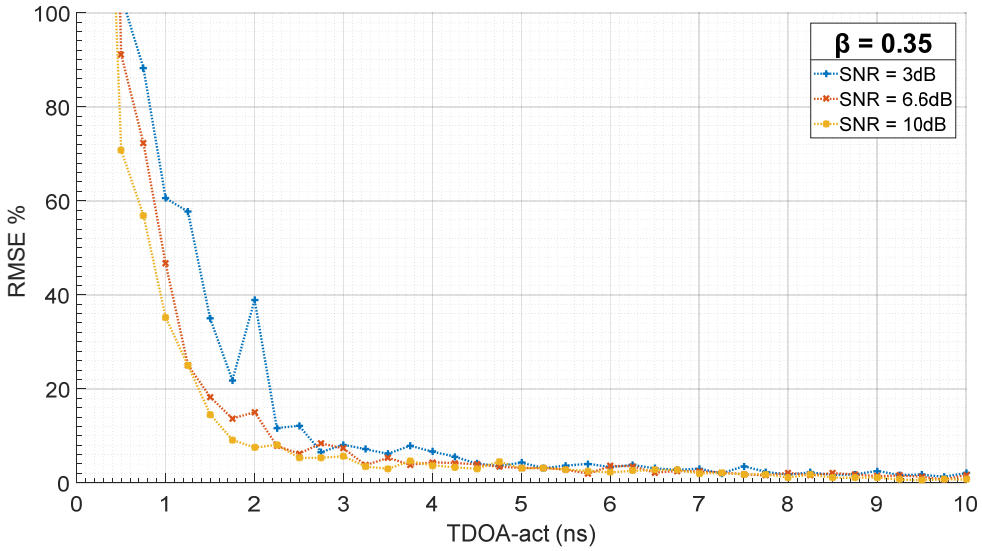

Figure 3-15 : $US_J(f,\tau)$ estimator performance with different SNR

this Figure 3-15 shows that despite a null-to-null bandwidth of 100 MHz, it can be seen that, in free space channel, the TDOA can be estimated with an error less than 10%, up to 1.75 ns with SNR less than 10dB.

As the temporal resolution is no longer proportional to the inverse of the bandwidth, and is better than what obtained in the classical spectral methods, one can talk about high-resolution approach. But we have to mention that until now we do not take into account the effect of the multipath, which will be treated in a separated section.

3.4.3 **Very small TDOA**

All the previous simulation considers the range of TDOA between $[1/f_s : 1/f_d]$ without taking into account the hypothesis of very small value due to very small B or to paraxial position ($d_1 \approx d_2$). This region of very small TDOA, critical for TDOA estimation, is set to $[1/f_s : 1/(10 * f_d)]$.

To solve this problem, we have to find where the *sinc* function based estimator has a best performance along over all the range $[1/f_s : 1/f_d]$. By determination of the optimal region, one can add an ad hoc time delay, in one arm of the MISO system, to shift the critical estimation region to optimal one Figure 3-16.

In *sinc* fitting, the best estimation region will be around the inflexion point. where a maximum of sensitivity is obtained. τ_{opt} satisfies:

$$\left[\frac{d^2}{d\tau^2} sinc(\pi f_d \tau_{opt})\right] = 0 \tag{45}$$

If we insert in one arm of the splitter an additional delay line set to τ_{opt}, it will act as an optimal operating point to acquire high precision in the measurement of "τ".

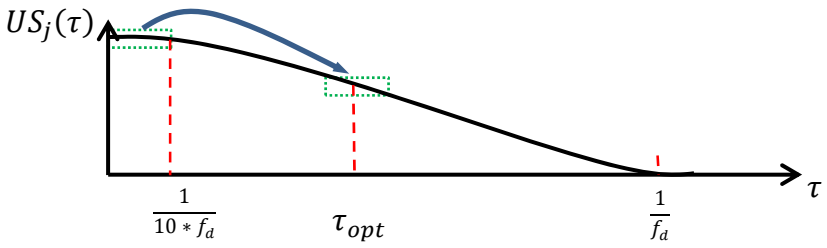

Figure 3-16: Definition of the optimal added time delay around the inflexion point

To verify this idea, we modify the previous simulation diagram as depicted in Figure 3-17 and repeat all the previous simulation for maximum of TDOA equal to $1ns$. The simulation will run under the same parameters listed in Table 3-2. The test first is done under several values of SNR chosen in the following set [10, 15, 20] dB to find out the best possible performance of the estimator. Then the simulation will run under several values of roll of factor which is the most important factor affecting the estimator. As discussed before we shift all the TDOA range to the inflexion point which is $\tau_{opt} = 4.5\ ns$.

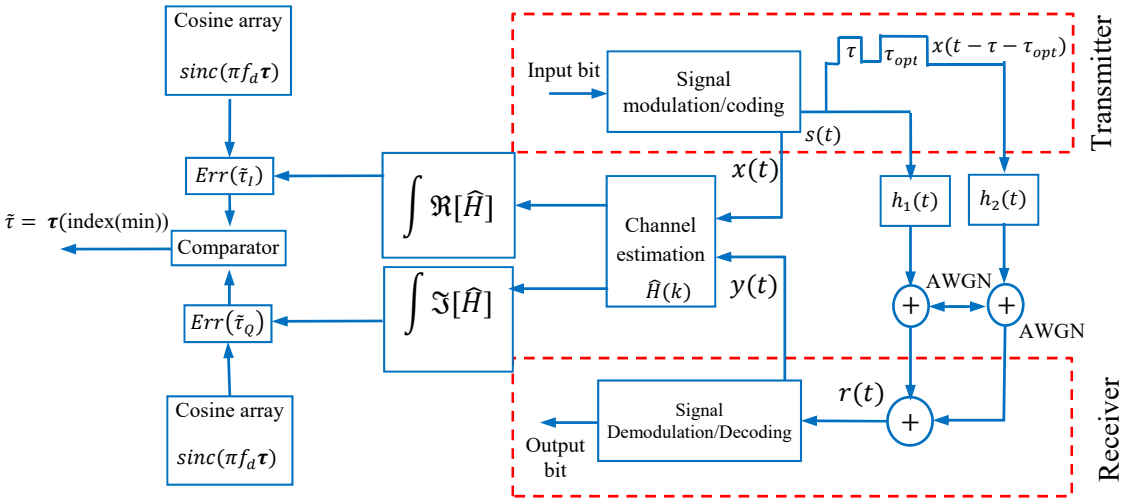

Figure 3-17: Block diagram of TDOA estimation with τ_{opt}= 4.5 ns

The Figure 3-18 shows that the method is still valid since the most of "τ" actual values are estimated within the used bandwidth.

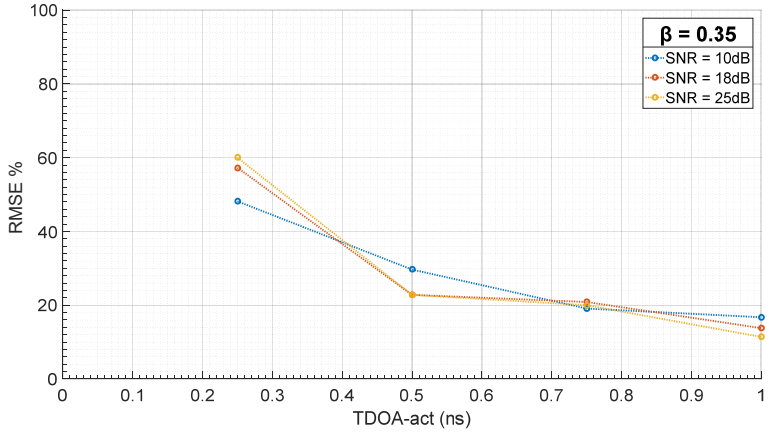

Figure 3-18: $US_J(f,\tau)$ estimator performance with τ_{opt}= 4.5ns: The RMSE in % versus the actual TDOA.

It seems that the noise power does not affect significantly the estimator performance, thanks to the integration, which is included in the estimator. Now the second test is to varying the roll of factor value between [0.15, 0.2, 0.25].

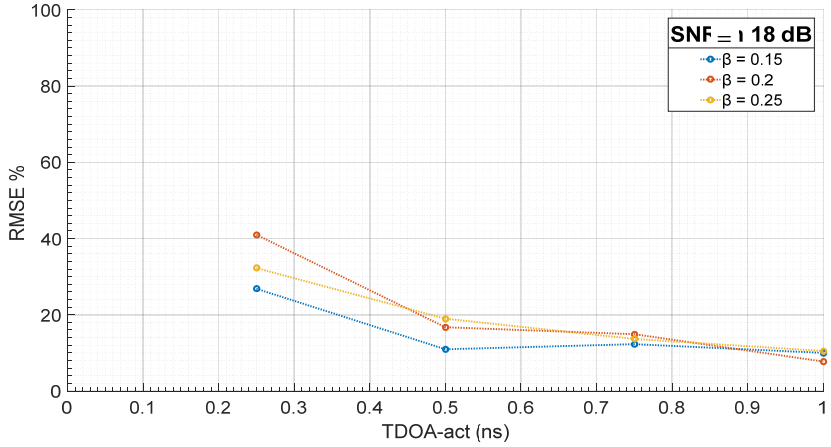

Figure 3-19 : Estimator performance with τ_{opt}= 4.5ns: the RMSE in % versus the actual TDOA.

The Figure 3-19 shows that despite a null-to-null bandwidth of 100 MHz, it can be seen that, for SNR superior to 10 dB in free space channel, TDOA greater than 0.5 ns can be estimated with an error less than 15%, , which five times the inverse of sampling frequency. The gain brought by the proposed method is 20 times compared to conventional Fourier based estimator leading to super-resolution concept.

3.4.4 **Cramer Rao Bound Limit**

In this study, we work on the Cramer-Rao bound (CRB) as a well-known performance metric that will express the lower bound on the variance of the unbiased estimator of TDOA. This bound noted σ_{CR}, is extracted from Fisher information, and can be expressed, for TDOA estimation, as follow [17]:

$$\sigma_{CR} = \frac{1}{\beta}\frac{1}{\sqrt{\Delta F_N T_{obs} SNR_{IN}}} \tag{46}$$

where SNR_{IN} is the effective input signal to noise ratio, ΔF_N is the noise bandwidth at the MU, and $\beta = 2\pi\sqrt{\frac{\int_{-\infty}^{+\infty} f^2 W_s(f)df}{\int_{-\infty}^{+\infty} W_s(f)df}}$ is by definition the root mean square radian frequency in the received spectrum, with $W_s(f)$ the signal power density spectrum, as shaped by the MU. If this shape is rectangular, β is reduced to $\frac{\pi}{\sqrt{3}} f_d$. Using this hypothesis and considering $\Delta F_N = f_d$, the Cramer-Rao bound is approximated by:

$$\sigma_{CR} = \frac{0.55}{f_d}\frac{1}{\sqrt{f_d T_{obs} SNR_{IN}}} \tag{47}$$

If SNR_{IN} = 0dB, T_{obs}=10.24 μs and f_d=100MHz then $\sigma_{CR} = 0.17\, ns$. To test our approach accuracy with respect to the CRBL, we perform the simulation under the test condition listed in Table 3-3.

Table 3-3 Simulation parameters for CRBL

Parameter name	Parameter value
Observation Time	$[10.24; 20.4; 30.72; 40.96]\ \mu s$
Number of iteration	100
Noise range	[0, 10]dB
Bandwidth (f_d)	100 MHz
Sampling Frequency (f_s)	10 GHz
Carrier Frequency (f_c)	3 GHz
Channel Model	AWGN

Taking a fixed value of TDOA equal to 0.7 ns, 100 simulations have been performed with several time observation values under several SNR values. As seen in Figure 3-20 the

estimator performance is, for low observation time, is twice the CRLB, but treads to it if observation time is increased.

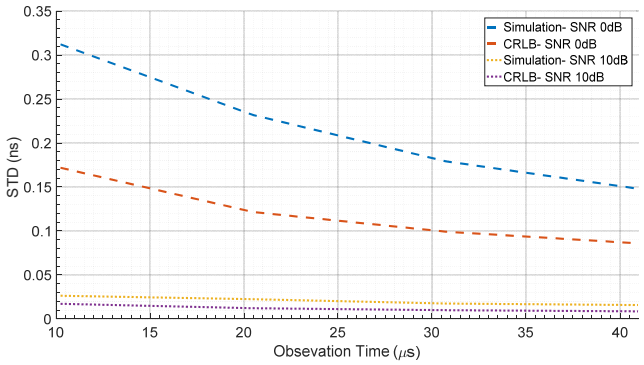

Figure 3-20: CRBL Theory and simulation results comparison for $US_J(f,\tau)$ based estimator

To test our approach under several situation and environment of communication system, the next two major sections will present the performance of our estimator by changing the parameters related to the communication system and by adding the multipath effects.

3.5 Communication parameters effect

In this section we test the effect of the parameters related to the communication system by simulating the estimation of the coefficients $\alpha_1$and , α_2, and by considering the effect of the number of pilots required for channel estimation.

3.5.1 Estimation of the coefficients α_1, α_2

Bad estimation of the coefficients α_1 and α_2 may naturally lead to big error in channel estimation. To improve the extraction of the useful information $US_{JI}(\tau,f)$ or $US_{JQ}(\tau,f)$ we can take advantage of the new added delay called τ_p, verifying $\tau_p \geq 1/f_d$, in one branch of the transmitter. This allows having periodicity in the channel, and hence by performing phase demodulation of the transfer function, we can extract useful information without requiring the prior knowledge of α_1.

Indeed, after adding the delay τ_p, the equation (34), can be written as:

$$\Re[H(f)] = \alpha_1 + \alpha_2\, cos\left(2\pi f\left(\tau+\tau_p\right)\right), \Im[H(f)] = \alpha_2\, sin\left(2\pi f\left(\tau+\tau_p\right)\right) \qquad (48)$$

Let's now, as for phase demodulation, multiply $\Re\{H(f)\}$ by $cos(\pi f \tau_p)$ then:

$$\begin{aligned}\Re\{\cdot\} * cos(2\pi f\tau_p) &= \alpha_1 cos(2\pi f\tau_p) + \frac{\alpha_2}{2} cos\left(2\pi f(\tau + 2\tau_p)\right) + \frac{\alpha_2}{2} cos(2\pi f\tau) \\ \Im\{\cdot\} * cos(2\pi f\tau_p) &= \frac{\alpha_2}{2} sin\left(2\pi f(\tau + 2\tau_p)\right) + \frac{\alpha_2}{2} sin(2\pi f\tau)\end{aligned} \quad (49)$$

which by appropriated pass band filtering eliminates the coefficient α_1 and leads, after normalization by $\alpha_2/2$, to a new useful information noted $US_{J\ delay}(\tau, f)$ expressed as:

$$\begin{aligned}US_{JI\ delay}(\tau, f) &= \frac{2 \cdot \int_{f_c - \frac{f_d}{2}}^{f_c + \frac{f_d}{2}} \left(\Re\{H(f)\}.cos(2\pi f\tau_p)\right)}{\alpha_2} \\ US_{JQ\ delay}(\tau, f) &= \frac{2 \cdot \int_{f_c - \frac{f_d}{2}}^{f_c + \frac{f_d}{2}} \left(\Im\{H(f)\}.cos(2\pi f\tau_p)\right)}{\alpha_2}\end{aligned} \quad (50)$$

The use of this derivation will be used in the experimental part, where the improvement is clearly observed.

3.5.2 **Number of pilots**

The pilot is used for the channel estimation process. The pilot frequency in the OFDM frame is the ratio between the number of carriers for data to the number of carriers for pilots. We will test our estimation with several values of the pilot frequency. Figure 3-21 shows that decreasing the pilot frequency leads to increase the accuracy of TDOA estimation.

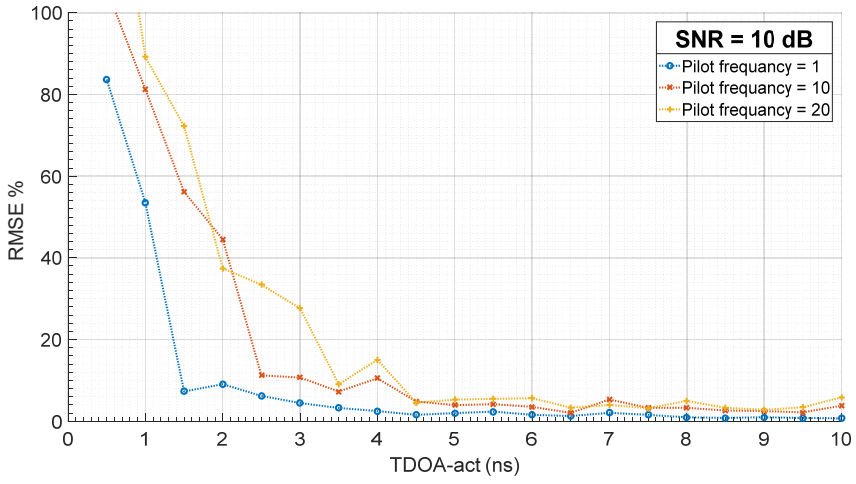

Figure 3-21: Estimator performance: The RMSE in % versus the actual TDOA

3.6 Communication environment effect

Communication environment effects deal mainly with the channel and antennas. We focus here on the channel and mainly on the multipath effects.

The sources of the multipath (MP) are diverse; they depend on several situations such as scattering, reflecting.... To combat MP effects, OFDM techniques supporting ad hoc cyclic prefixes perform well to ensure a robust communication.

In our proposed MISO configuration, MP has harmful effect on TDOA estimation since it is not easy to extract the useful TDOA from all the other TDOAs generated by the MP especially those happened within the region less than B/c. So to reduce such effects tailored solutions need to be deployed.

This section will begin be modeling the effect of multipath, then a complemented proposed solution to our approach is presented. At the end, we test our approach under the effect of such parameter related to the communication environment.

3.6.1 Multipath modeling

To model MP, we consider the MISO scenario depicted in Figure 3-22.

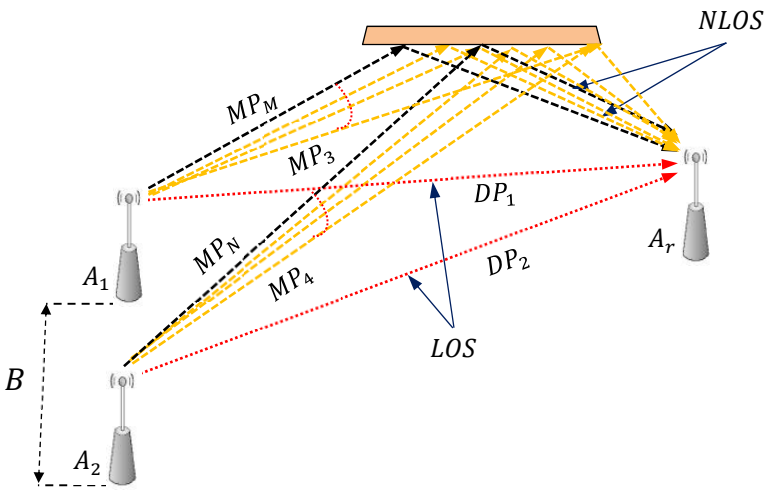

Figure 3-22: Multipath modeling

Referring to equation (27) and considering the small-targeted value of B, we represent the resulting received signal as:

$$r(t) = \sum_{i=0}^{M-1} \alpha_{2i+1} s(t - t_{2i+1}) + \sum_{j=1}^{N} \alpha_{2j} s\left(t - t_{2j}\right) + w(t) \tag{51}$$

Where t_{2i+1} stand for all the time of flight between A_1 and A_R, and t_{2j} stand for all the time of flight between A_2 and A_R.

The transfer function of the channel, in the base band representation, is written as:

$$H(f) = \sum_{i=0}^{M} \alpha_{2i+1} e^{j2\pi f t_{2i+1}} + \sum_{j=1}^{N} \alpha_{2j} e^{j2\pi f t_{2j}} \tag{52}$$

And its real part becomes:

$$H(f) = \alpha_1 + \alpha_2 \cos(2\pi f \tau) + \sum_{i=1}^{M} \alpha_{2i+1} \cos(2\pi f t_{2i+1}) + \sum_{j=2}^{N} \alpha_{2j} \cos\left(2\pi f t_{2j}\right) \tag{53}$$

where $\tau = t_2 - t_1$ is the TDOA of interest, and all the other combination of TDOAs are un-useful parasitic contributions that need to be mitigated.

3.6.2 **Emulating Multipath**

To emulate multipath, we add several path of several time of fight to the two LOS paths, already discussed in MISO configuration. Figure 3-23 shows the frequency response pf MP channel compared to free space channel. As expected this frequency selective channel exhibits multipath TDOAs corrupt the TDOA of interest.

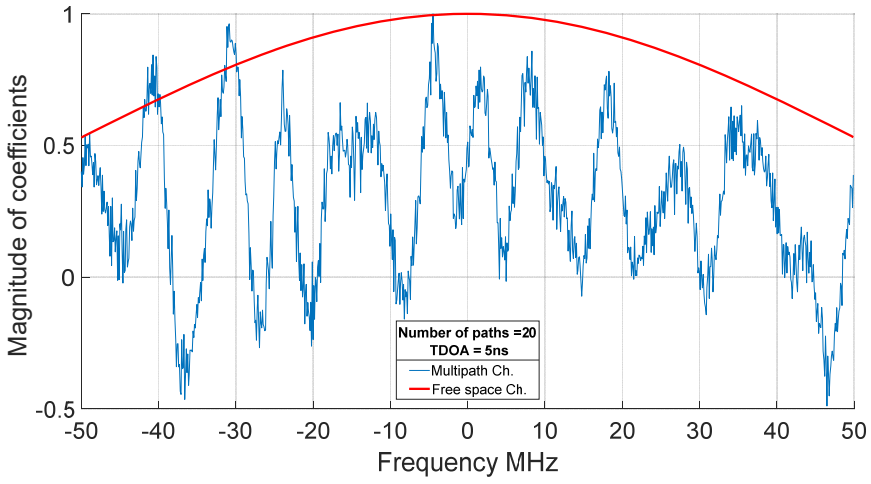

Figure 3-23: Channel estimation with multipath

As shown in Figure 3-24 and as expected, the multipath affects the performance of the estimator especially with small TDOA. This leads us to present in the next section our solution to deal with multipath.

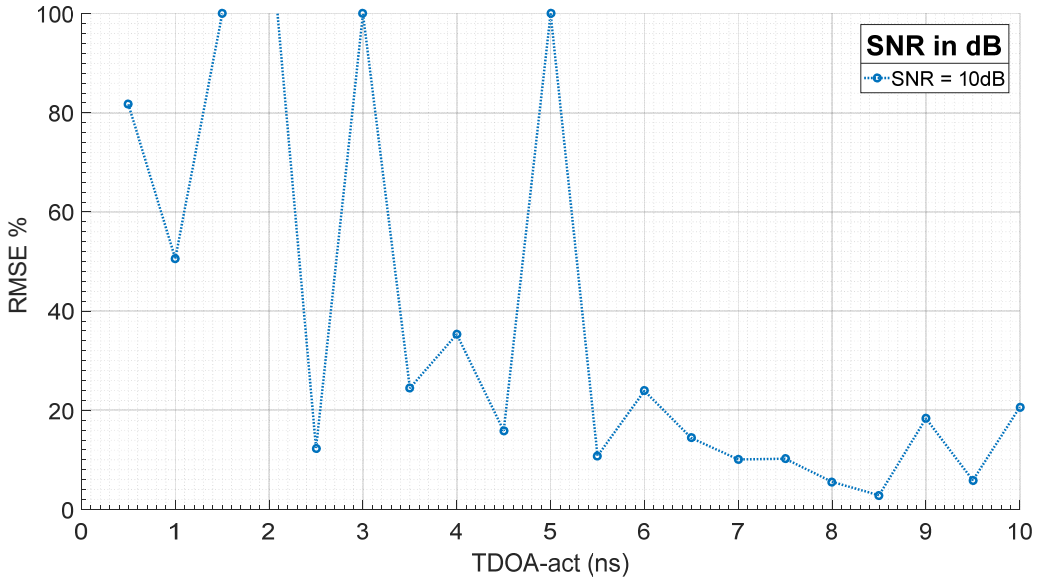

Figure 3-24: TDOA estimation with multipath efffect.

3.6.3 **Multipath effect reduction**

To solve the problem of multipath we classify all possible TDOAs into two main groups. The first group contains large TDOAs, generated by the combination between one LOS path from one transmitter and one reflected paths, or by the combination between different multipaths that are not close to each other. The effect of these TDOAs consists with a small-scale variation in the received spectrum and can hence be mitigated, by a simple filtering over the channel coherence bandwidth.

The second group encompasses small and very small TDOA, generally provided by multipath that has close times of flight. In the considered bandwidth, theses TDOAs produce large scale variation, comparable to the useful TDOA, and are hence difficult to mitigate by means of time discrimination. However their effects should be reduced by means of power discrimination. It is understood that such MP propagates along ways that are longer than those taken by direct path. Due to attenuation of propagation, MP signals are therefore weaker than

direct path and then should only slightly decrease the accuracy. This effect could be enhanced by using circular polarization.

Anyway, to assess those large scale multipath effects, we define the factor K as the ratio between the generated LOS paths that generates TDOA of interest and the multipath, given by:

$$K = \frac{\left|\alpha_1 + \alpha_2 e^{j2\pi f(t_2 - t_1)}\right|}{\left|\sum_{i=1}^{M} \alpha_{2i+1} \cos(2\pi f t_{2i+1}) + \sum_{j=2}^{N} \alpha_{2j} \cos(2\pi f t_{2j})\right|} \quad (54)$$

To investigate the effect of K, we performed simulation by adding multipath with several TDOAs with respect to the main LOS paths. One hundred trials are performed and we show in Figure 3-25 the cumulative distribution function of the obtained accuracy on the estimated TDOA.

It can be observed that, assuming a SNR = 20 dB, the error induced by the large scale MP signals is less than 10% with K factor superior to 9 dB. As mentioned before, high values of K factor can be obtained using circular polarization to reduce the power magnitude of MP.

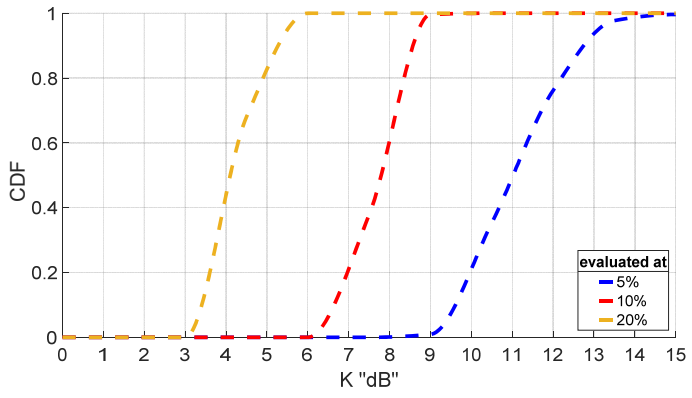

Figure 3-25: Fitted Normal Cumulative Distribution Function with different accepted error of the estimated value at $\tau_{opt} = 4.5\ ns$ ns, with SNR = 20 dB

This kind of power-based solution may improve the performance of the proposed solution when deployed in realistic channel. Moreover as the proposed solution targets millimeter wave scenario envisaged in the 5G networks, directional communication can also contribute to spatially discriminate MP.

3.7 Conclusion

In this chapter, different methods are proposed to extract TDOA information from OFDM signals. These methods use the already existing channel estimation, classically performed in OFDM schemes, limiting therefore any added complexity. The simulation, using MATLAB codes, is tested under several conditions of noise and multipath, and with varying different communication parameters dealing with pilots, roll off factor. Simulation results show good performance compared to Cramer Rao Lower Band, and the super-resolving character of the proposed solutions. The theoretical gain obtained, compared to conventional Fourier solution, is close to 20.

Such approach can be useful for several applications needing accurate positioning for indoor environment. The acquisition geometry requiring a MISO configuration may benefit from the future 5G standard and millimeter communications, to naturally reduce the size of the considered baseline.

Bibliography

[1] A. Quazi, "An overview on the time delay estimate in active and passive systems for target localization," *IEEE Trans. Acoust. Speech Signal Process,* vol. 29, no. 3, pp. 527-533, 1981.

[2] J. Chen, J. Benesty and Y. Huang, "Time Delay Estimation in Room Acoustic Environments: An Overview," *EURASIP Journal on Applied Signal Processing,* vol. 2006, no. 26503, pp. 1-19, 2006.

[3] C. Knapp and G. Carter, "The generalized correlation method for estimation of time del," *IEEE Transactions on Acoustics Speech & Signal Processing.,,* vol. 24, no. 4, pp. 320-327, 1976.

[4] F. Ge, D. Shen, Y. Peng and V. Li, "Super-resolution TDOA estimation based on eigenanalysis and sequential quadratic programming," *IEE Proc.-Radar Sonar Navig,* vol. 151, no. 4, pp. 197-202, 2004.

[5] M. Feder and E. Weinstein, "Parameter estimation of superimposed signals using the EM algorithm," *IEEE Trans. Acoust., Speech, Signal Process,* vol. 36, no. 4, pp. 477-487, 1988.

[6] A. Masmoudi, F. Bellili, S. Affes and A. Stephenne, "A maximum likelihood time delay estimator in a multipath environment using importance sampling," *IEEE Trans. Signal Process,* vol. 61, no. 1, pp. 182-193, 2013.

[7] A. Masmoudi, F. Bellili, S. Affes and A. Stephenne, "A non-data-aided maximum likelihood time delay estimator using importance sampling," *IEEE Trans. Signal Process,* vol. 59, no. 10, pp. 4505-4515, 2011.

[8] T. G. Manickam, R. J. Vaccaro and D. W. Tufts, "A least-squares algorithm for multipath time-delay estimation," *IEEE Trans. Signal Process,* vol. 42, no. 11, pp. 3229-3233, 1994.

[9] R. Wu and J. Lian, "Time-delay estimation via optimization highly oscillatory cost functions," *IEEE. J. Ocean. Eng,* vol. 23, no. 3, pp. 235-244, 1998.

[10] T. J. Shan, A. M. Bruckstein and T. Kailath, "The resolution of overlapping echoes," *IEEE Trans. Acoust. Speech Signal Process,* vol. 33, no. 6, pp. 1357-1367, 1985.

[11] H. Zi-Qiang and W. Zhen-Dong, "A new method for high resolution estimation of time delay," *in Proc. IEEE Int. Conf. Acoust., Speech, Signal Process. (ICASSP,* vol. 54, no. 6, pp. 1977-1986, 1982.

[12] F.-X. Ge, D. Shen, Y. Peng and V. O. K. Li, "Super-resolution time delay estimation in multipath environments," *IEEE Trans. Circuits Syst. I,* vol. 54, no. 9, pp. 1977-1986, 2007.

[13] H. Saarnisaari, "TLS-ESPRIT in a time delay estimation," *Proc.IEEE 47th Veh. Technol. Conf.,* vol. 3, pp. 1619-1623, 1997.

[14] J. Li and R.B.Wu, "An efficient algorithm for time delay estimation," *IEEE Trans. Signal Process.,* vol. 46, no. 8, pp. 2231-2235, 1998.

[15] Z. Q. Hou and Z. D.Wu, "A new method for high resolution estimation of time delay," *Proc. Int. Conf. on Acoustics, Speech and Signal Processing,* vol. 7, no. 3, pp. 420-423, 1982.

[16] M. Bocquet, C. Loyez and A. Benlarbi-Delai, "Using enhanced-TDOA measurement for indoor positioning," *IEEE Microwave and Wireless Components Letters ,* vol. 15, no. 10, pp. 612-614, 2005.

[17] S. STEIN, "Algorithms for Ambiguity Function Processing," *IEEE TRANSACTIONS ON ACOUSTICS, SPEECH, AND SIGNAL PROCESSING,,* Vols. ASSP-29,, no. 3, pp. 588-599, 1981.

Chapter 4: Experimental setup and results

In this chapter, a communication test-bench, designed specifically for measuring channel and estimating Time Differences of Arrival (TDOA) from OFDM signal, is presented and tested. The bench is implemented in the Electromagnetic and Electronics Laboratory at Sorbonne University.

The overall performances of the system are analyzed in a controlled electromagnetic environment experiment room, which has been built up to allow testing our method in both free space and multipath channels. The communication system is composed of one transmitter formed by two antennas, playing the role of Reference Unit (RU), and one single antenna receiver acting as a Mobile Unit (MU). The build and capture of the data signal is done automatically using computer software.

Prior to TDOA estimation, several logistic problems, mainly dealt with time management, had to be solved. They concern, for example, the time offset between the two transmitting antennas, which must be kept very low, and the time alignment in the receiver.

This chapter is organized as follows: section 4.1 presents the environment and global architecture of the system; section 4.2 tests the communication system performance; section 4.3 presents the experimental results for channel measurements and TDOA estimation, and finally, concluding remarks are exposed in section 4.4.

4.1 Presentation of the environment

To validate the simulation results discussed in the previous chapter 3, an experimental-test-bench has been set up. This bench consists of five major devices: the controlled electromagnetic room, radiating devices, amplifying devices, wave generator, and digital signal analyzer. In the next sections, we describe each of these devices.

4.1.1 The controlled electromagnetic room

As described in Figure 4-1, an electromagnetic environment experiment room is constructed over floor space: $\approx 7.5\ m^2$ and with height $\approx 2m$. Thus with this full Anechoic-Faraday Chamber (AFC), we have the ability to control finely the communication environment's parameters.

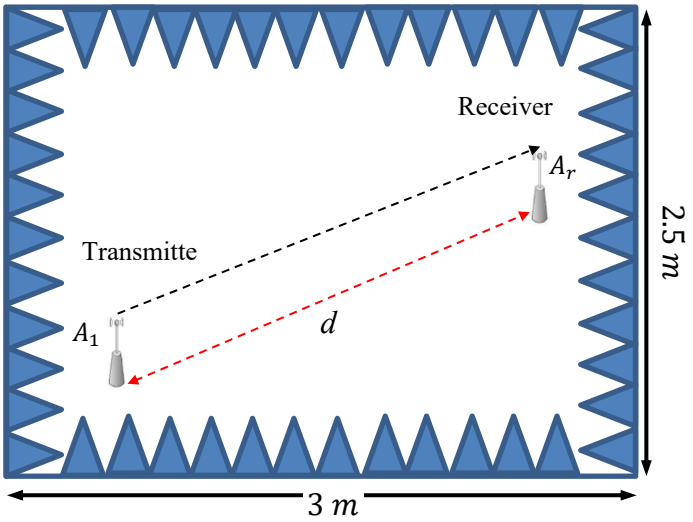

Figure 4-1: The Anechoic-Faraday Chamber.

The AFC creates an ideal environment to perform communication system by prohibiting external jammer and preventing wave reflection. In order to achieve this environment, the room is built up from walls of copper mesh, and the walls, ceiling, and floor of the room's interior are covered fully by a large number of electromagnetic wave-absorbing quadrangular pyramid shaped forms. They are made of carbon-coated foam that absorbs electromagnetic waves. The photograph of the AFC is shown in Figure 4-2(a) for room's interior and Figure 4-2(b) for room's exterior.

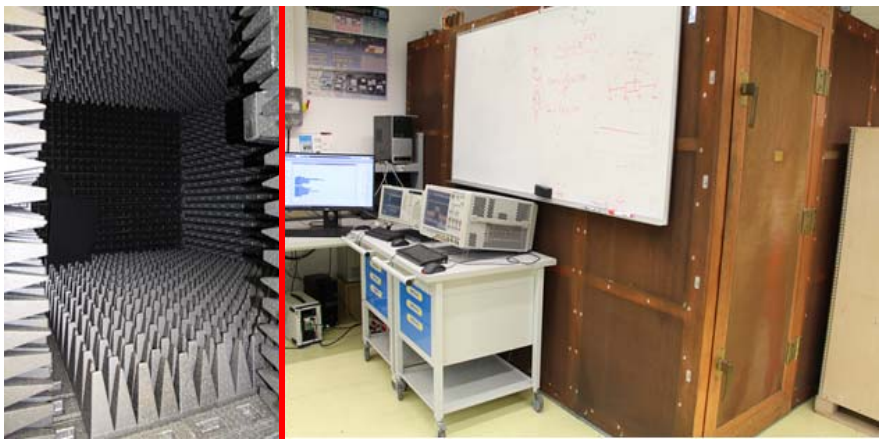

(a) (b)

Figure 4-2: Photograph of the Anechoic-Faraday Chamber
a) The room's interior. b) The room's exterior

This AFC enables a distance up to 2,5 m between the transmitter and the receiver, allowing thus far field measurement. So the distance d between the transmitting antenna and

the receiving antenna is set to 2.4 *m*. Let's note that the two antennas are installed on the same horizontal plane.

4.1.2 **Radiating devices**

The radiating devices are vertical dual band antenna, Figure 4-3 (a), operating in the frequency ranges (2.4-2.5 GHz) and (4.9-5.9 GHz) with a SWR < 2.0 and a maximum gain of 3dBi, and are compliant with IEEE 802.11a+b/g Wireless LAN. The radiation pattern of this kind of antenna is Omnidirectional in H plane as shown in Figure 4-3 (b).

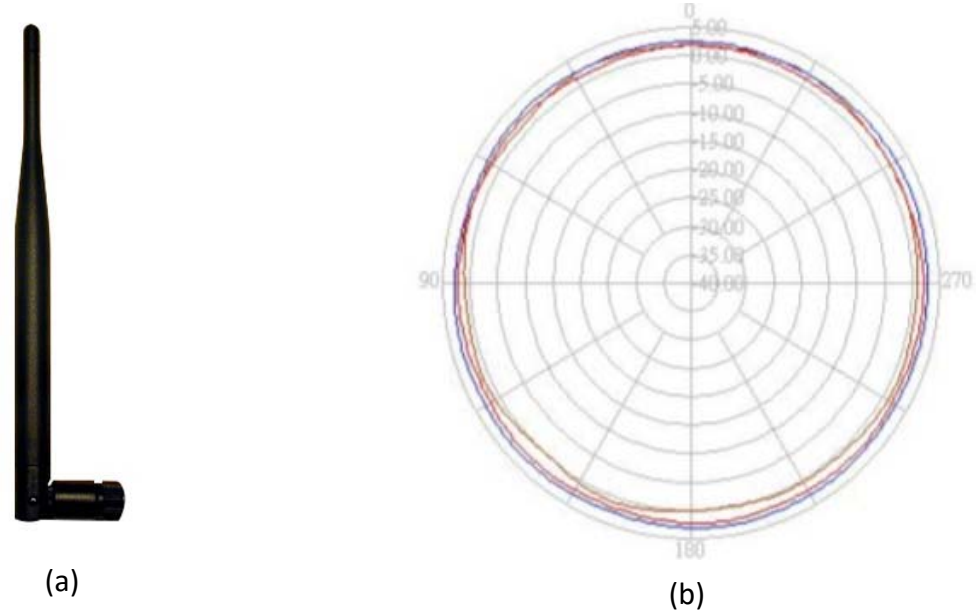

Figure 4-3: Radiating device
a) photograph of the used antenna, b) radiation pattern in H Plane

4.1.1 **Amplifier**

To increase the range of such communication system, we use a Low Noise Amplifier (LNA), type TA010-180-30-15, which has also the ability to act as a power amplifier thanks to its sufficient output power. So, for SISO scenario, one amplifier is inserted in the transmitter and one amplifier in inserted in the receiver, and for MISO scenario two amplifiers are inserted in the transmitter and one in the receiver. The features of such amplifier are listed below in Table 4-1.

Table 4-1 : LNA features

Features	Value
P_{-1} dB:	16 dBm
Noise Figure:	5 dB
Bias Condition:	230 mA @ 12V
Small Signal Gain:	31 dB

4.1.2 Arbitrary waveform generator

The arbitrary waveform generator AWG 7122B generates the transmitted signal. It generates complex wideband signals across a frequency range of up to 9.6 GHz under sampling frequency of 12GS/s or 24 GS/s when interleave mode is on. As it has 2-channel synchronized outputs, it acts like one dual transmitter. This solves naturally the problem of time offset between the transmitting antennas. The amplitude level is 3 dB higher when using differential (both) outputs. The user interface for the AWG is shown in the Figure 4-4.

Figure 4-4: The interface display of the AWG 7122B

By using a developed tool, the data and RF signal, built under MATLAB code, are sent via Local area network (LAN), to the AWG.

4.1.3 Digital storage oscilloscope

A digital storage oscilloscope DSO-91204A, with 12GHz bandwidth and a sampling frequency of 40GS/s, treat the received signal. A screen shot of the user interface of the DSO is plotted in the Figure 4-4. To get the signal, the MATLAB code captures the signal from the DOS and process it the way we need.

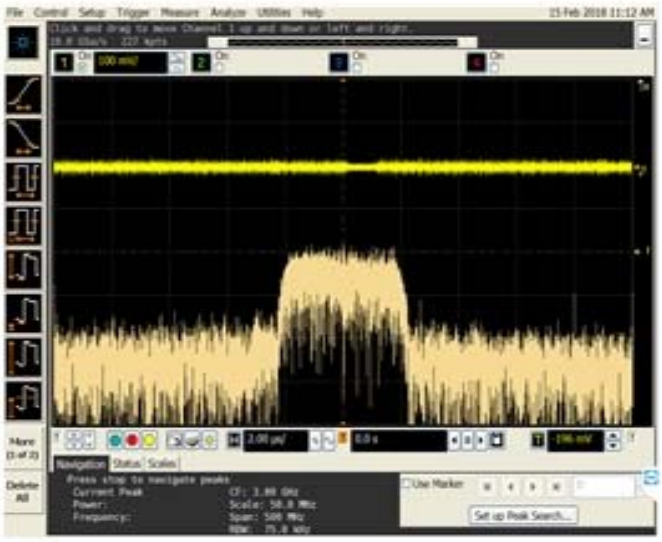

Figure 4-5: The interface display of the DSO-91204A

4.1.4 Conclusion

Prior to any measurement, we presented in this section the major devices used in our experimental study. The role of each device is well defined and their features are given. We show that their performances meet perfectly the experimental requirements, and their impacts on the quality of the measurement are taken into account in the calibration process. The next section presents the communication system setup and the preliminary results in term of communication performances dealing mainly BER vs. SNR and in terms of time management.

4.2 SISO communication system setup

Prior to TDOA estimation, it is necessary to test the communication system performance and behavior. This step is important since all the concept of our methods depends on the communication features. So this section provides a detailed description of the communication system setup. Starting by QPSK constellation diagram, the experimental results will be displayed, leading to the channel estimation. Some practical problems that we faced are also highlighted.

4.2.1 The transmitter

The block diagram of the transmitter already presented in chapter 2, is displayed at Figure 4-6

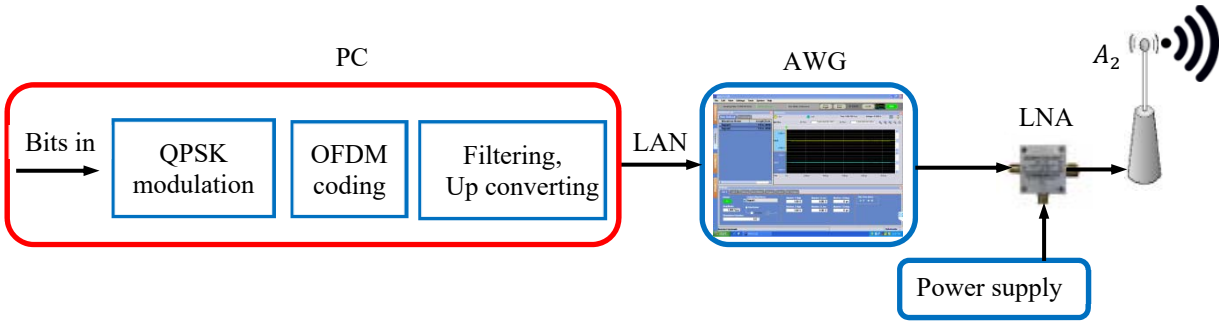

Figure 4-6: The transmitter block diagram

Using MATLAB, we first generate a random bit series, and then construct the QPSK symbols using the mapping table listed in chapter 2: table 2-1. To build up the OFDM frame, the QPSK symbols are converted from serial to parallel. The IFFT is applied on the parallel symbols, and then the result of the IFFT is converted from parallel to serial in order to form the OFDM signal.

To form the transmitted signal, the OFDM signal is filtered using the RRC filter and up converted to the carrier frequency f_c. Finally the transmitted signal is sent via LAN connection, to AWG to convert it into an analog signal, ready for propagation through antenna.

Figure 4-7 shows the representation of transmitted signal in frequency domain, and Figure 4-8 plots the I-Q components of the transmitted signal in time domain, respectively.

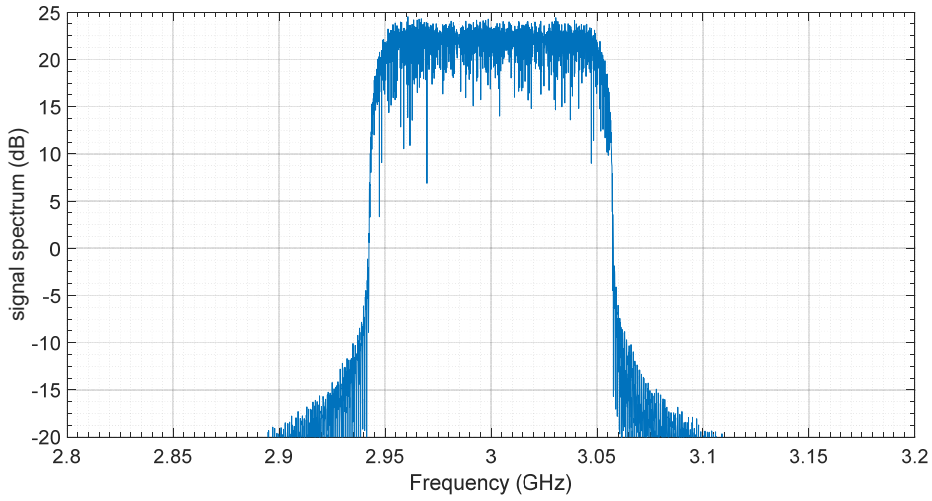

Figure 4-7: Experimental spectrum of the transmitted signal

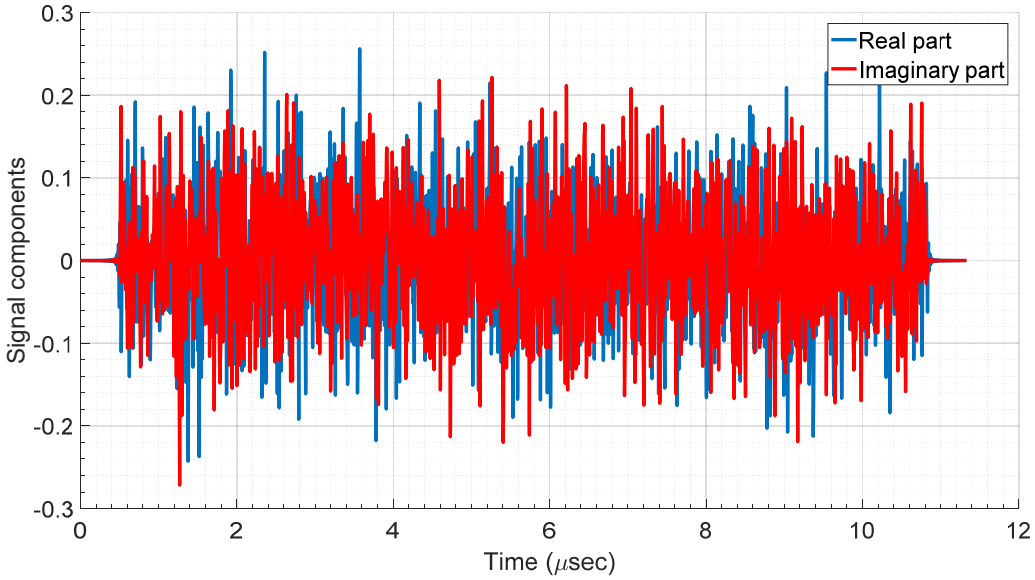

Figure 4-8: Experimental I-Q components of the transmitted signal in time domain

The signal is generated under the parameters listed in Table 4-2. Except the roll of factor β, these parameters will be fixed for all experimental testing.

Table 4-2 Values of the parameters

Parameter name	Parameter value
Number of bits to process	2048
Modulation type	QPSK
Bandwidth (f_d)	100 MHz
Sampling Frequency (f_s)	10 GHz
Carrier Frequency (f_c)	3 GHz
Filter Type	RRC
Roll off (β)	0.35
Number of carriers k	1024
Pilot number	1000

By this table we finished describing the transmitter side. In the next section we will see the receiver side and what problems that we faced.

4.2.2 **The receiver**

The block diagram of the receiver is described in Figure 4-9 below. The signal is collected by a single antenna, same type as at the transmitter side. The receiving antenna output signal is fed to the LNA, which is connected directly to the DSO. The DSO is

responsible of converting the received analog signal to digital. In order to get the OFDM frame, the signal is captured from the DSO via LAN connection. Then it is down converted from the carrier frequency f_c and filtered using the RRC filter.

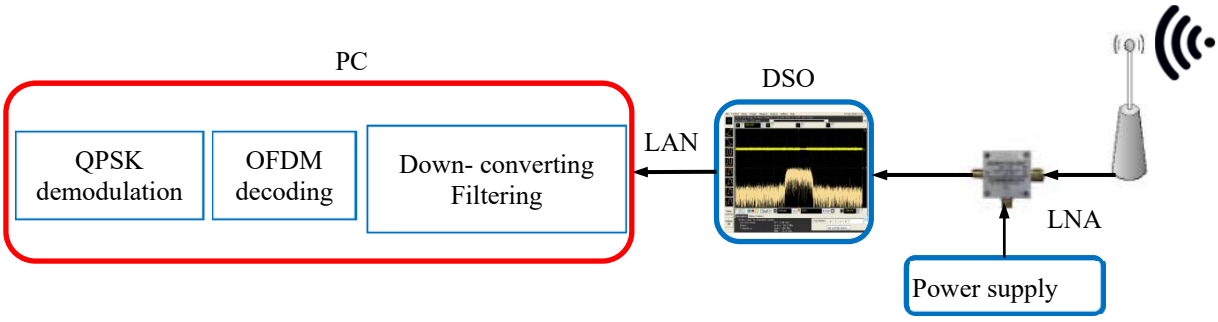

Figure 4-9: The receiver block diagram

Figure 4-10 shows the representation of received signal in frequency domain. The OFDM frame is converted from serial to parallel. The FFT is applied on the parallel data; the result of the FFT is converted from parallel to serial in order to form the QPSK symbols. Then the bits are recovered using the map Table 2-1 in chapter 2.

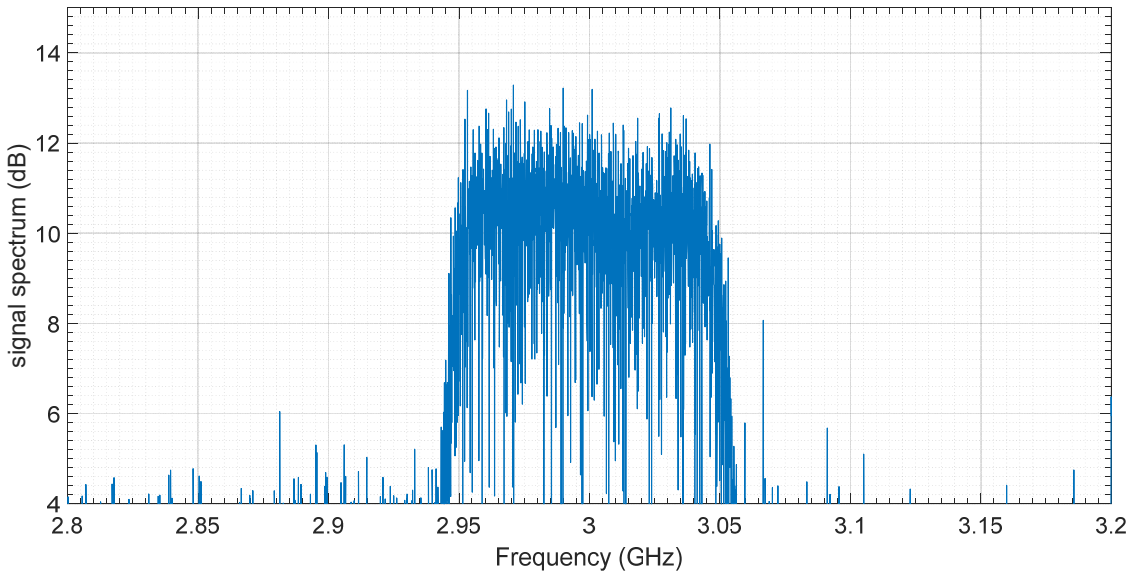

Figure 4-10: Experimental spectrum of the received signal

4.2.3 Signal acquisition and I-Q constellation

The constellation diagram is a way to test the validation of transmitting and receiving the symbols. At the transmitter the constellation is logically perfect. So by comparing it with one at the receiver we have the ability to evaluate the communication system performance.

We send an arbitrary data to the AWG; we capture the data from DSO and treat it in MATLAB. The Figure 4-11 shows that the received signal has not been captured at a right starting time.

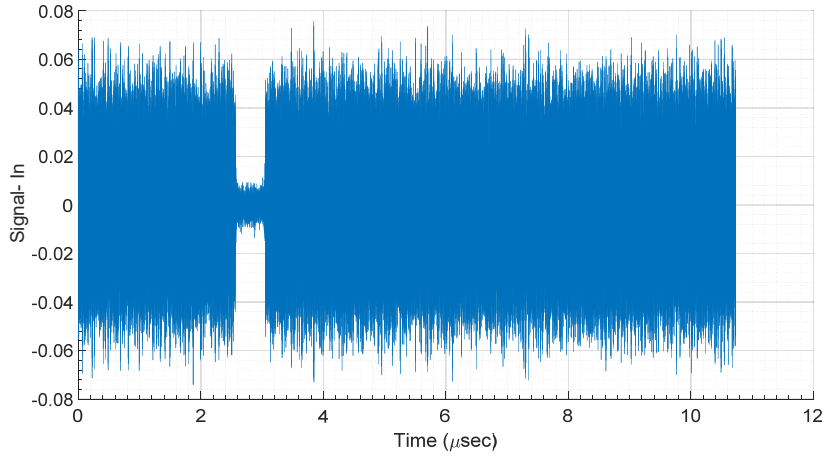

Figure 4-11: The received signal in time domain

This is because the DSO specifications do not include any routine for finding the starting time of the received signal. Indeed without this synchronization, the communication is no longer possible. We are facing here a time misalignment problem. To solve this problem, correlation between received signal and a copy of transmitted signal needs to be performed in MATLAB. This suggests to increase the depth memory of the DSO's buffer, and to set it at twice the length of the original signal. This offers us the possibility to have a full copy of received signal as shown in Figure 4-12.

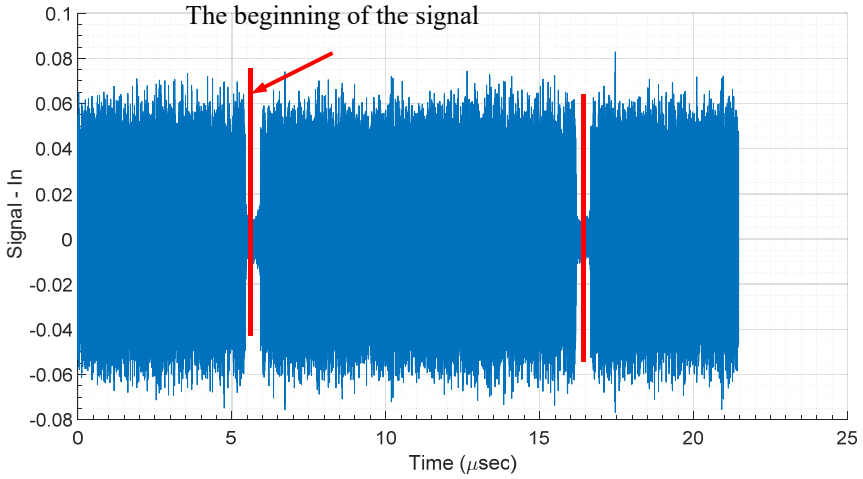

Figure 4-12: the received signal captured from DSO

Figure 4-13 shows the received signal, the transmitted signal, the results of correlation between them, and the received signal aligned, respectively. The received signal has double length of the original one, and is correlated with the transmitted signal. The correlation between the received signals and the transmitted signal, exhibits three peaks due to the three parts of the received signal.

The maximum of these peaks indicates the best similarity between the transmitted signal and the received signal. In the time vector of the correlation results, the maximum peak indicates the beginning of the full copy of the received signal. Simply, we cutoff the received signal aligned from the received signal by starting from that point until the end of the transmitted signal. This way is tested and validated several times and it works well.

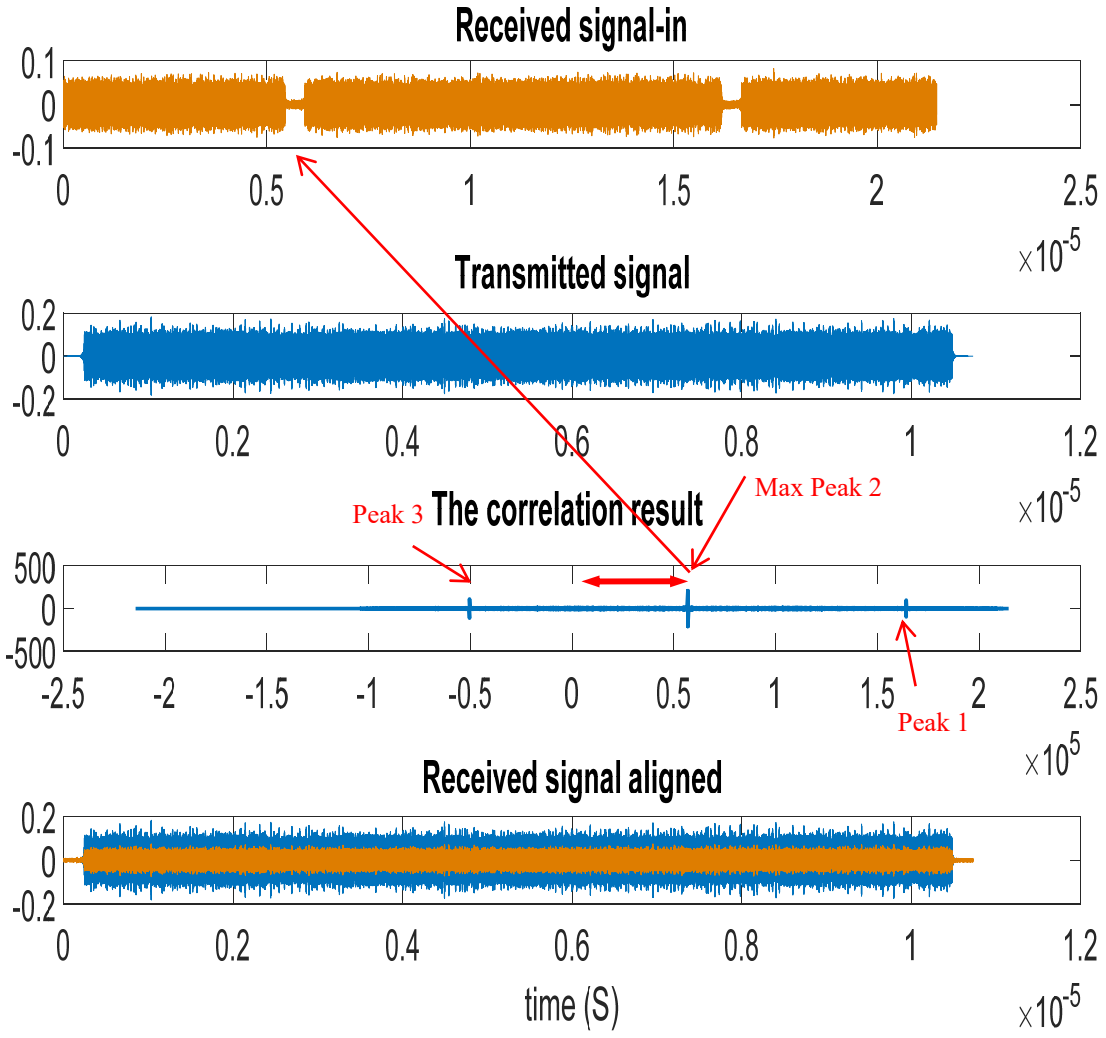

Figure 4-13: Received signal, transmitted signal, the correlation between them, and the RX signal aligned

Now we test the communication system by checking the constellation diagram at the receiver. The Figure 4-14 shows that the constellation diagrams of the transmitter and the receiver are almost at the same position. With this figure, we could conclude that the first part of the communication system is working well and we could proceed to the next step of OFDM testing and validation.

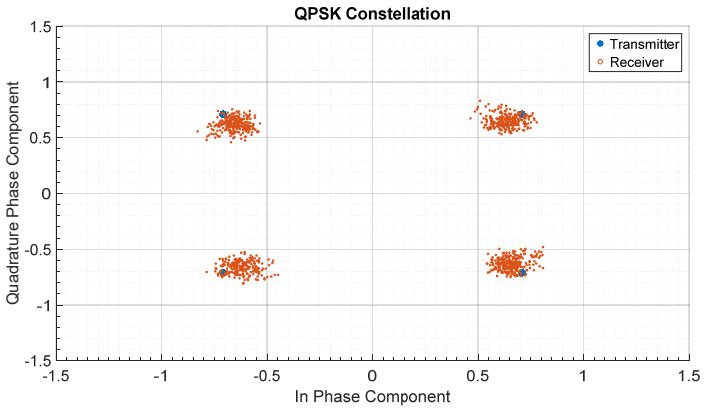

Figure 4-14: QPSK constellation diagram with SNR 20dB

4.2.4 **OFDM communication performances**

This section is the core of the communication system. It will be used later to perform the channel estimation. To measure the OFDM technique performance, usually the plot of BER, as a function of SNR, is used. To vary the SNR we attenuate the signal at the transmitter, and then we calculate the SNR at the receiver as explained in chapter 2 section 2.4.2. After running the system for 6 times with different transmitted signal attenuation, we observe Figure 4-15 as a plot of BER vs. SNR.

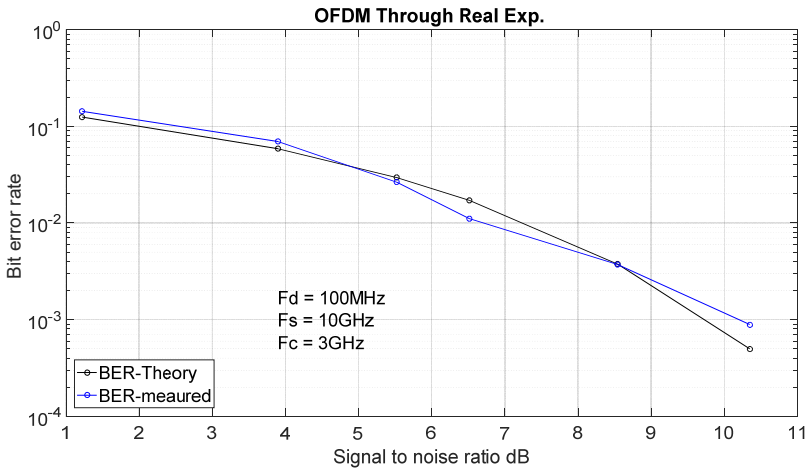

Figure 4-15: Experimental BER versus SNR for OFDM communication

We observe a good agreement between the theoretical BER and measured one. In another point of view, the constellation diagram over OFDM for each SNR is shown in Figure 4-16.

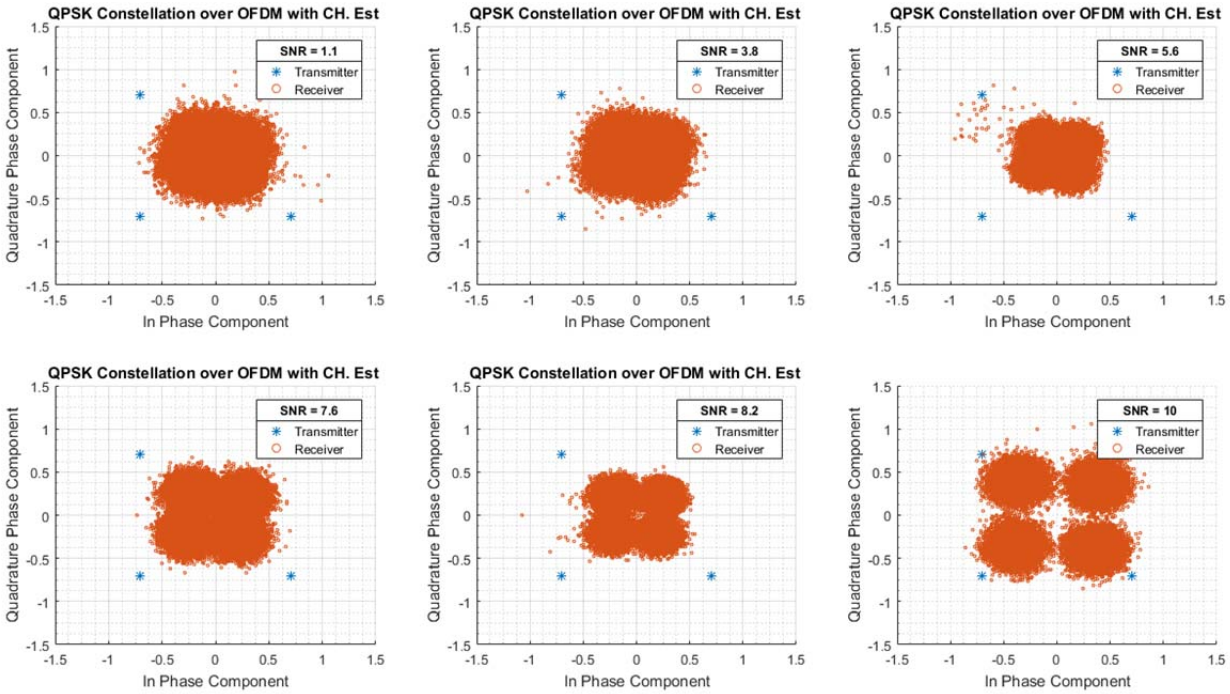

Figure 4-16: QPSK constellation diagram over OFDM

One can remark that the constellation I-Q is well reconstructed for SNR superior to 10dB. However if we perform some normalization and process in an ad hoc way the received data, the communication could be established, even if SNR is close to 5dB. Therefore, for all our experimental results, we set SNR superior to 5dB and less than 20dB.

After all that demonstration, the most important part in the communication signal, which concerns the channel estimation, will be presented in the next section.

4.2.5 **Channel estimation**

For our purpose, the channel estimation is the key part in the communication system that we need to cope with. We show hereafter how the channel estimation behaves in free space channel and in multipath channel. We start by SISO scenario for communication issue, and then study the MISO scenario for TDOA issue.

4.2.5.1 **SISO Free space channel**

In SISO free space channel testing, the channel is estimated by using one transmitting antenna and one receiving antenna. The Figure 4-17 below shows that the channel estimation amplitude in frequency domain is as expected almost flat.

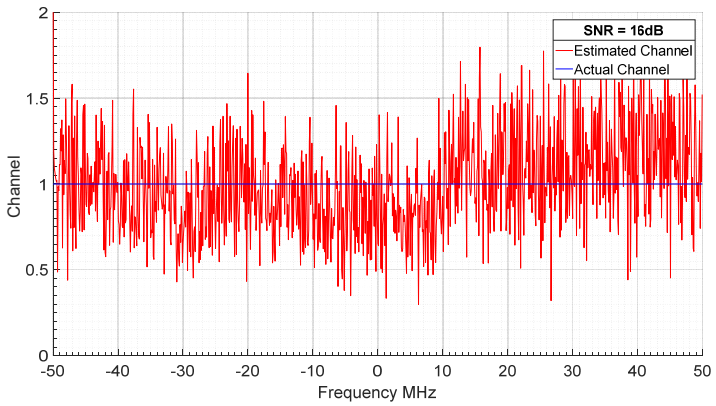

Figure 4-17: Normalized channel estimation in SISO free space channel

4.2.5.1 **SISO Multi path channel**

The multipath channel is generated randomly using MATLAB code. 21 paths with different time delays are emulated and the resulting digital signal is sent to AWG for analog transmission. The Figure 4-18 below shows that the normalized channel estimation amplitude in frequency domain is in good agreement with actual multipath channel, as well as for time domain representation.

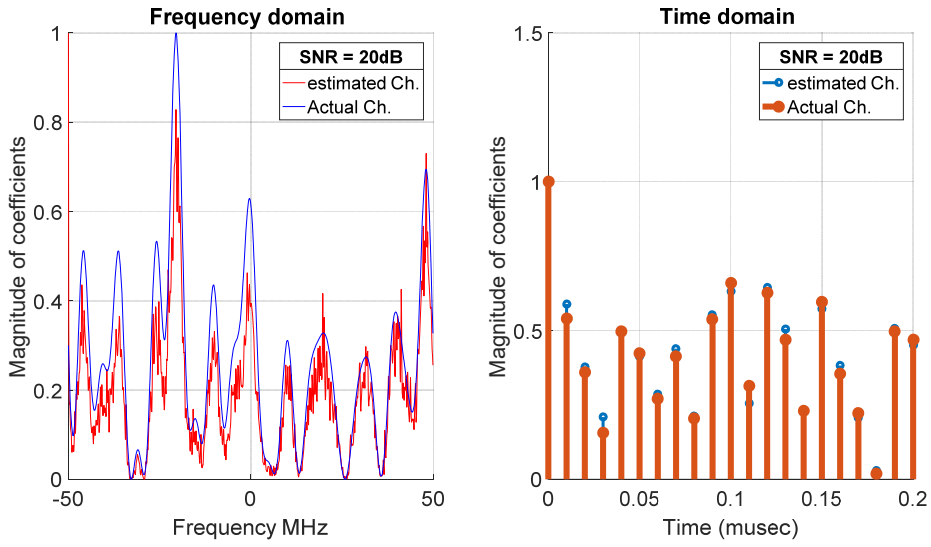

Figure 4-18: Normalized channel estimation in SISO multipath channel

We show through these measurements our ability to estimate properly the communication channel even in harsh environment. The following step is to apply such approach in MISO configuration for TDOA estimation.

4.3 Direct and Inverse models validation

All the previous work has been done for validation and tests simulation results, for communication issue, obtained in chapter 2. So this section will present the experimental results validating the simulation results discussed in chapter 3. Starting with MISO configuration, we give some guidelines for baseline dimensioning and then validate the direct and inverse problems.

4.3.1 MISO configuration

The TDOA estimation requires a MISO configuration as illustrated in Figure 4-19. The transmitter/receiver antennas are installed with a d =2.4m distance between them. In the receiving side we have one antenna acting as the Mobile Unit (MU), which needs to be localized, by means of TDOA. On the transmitting side, two antennas, separated by a distance B called baseline, act as the Reference Unit (RU). Let's note that due to the principle of reciprocity, this configuration remains valid even if the roles of transmitter and receiver are swapped.

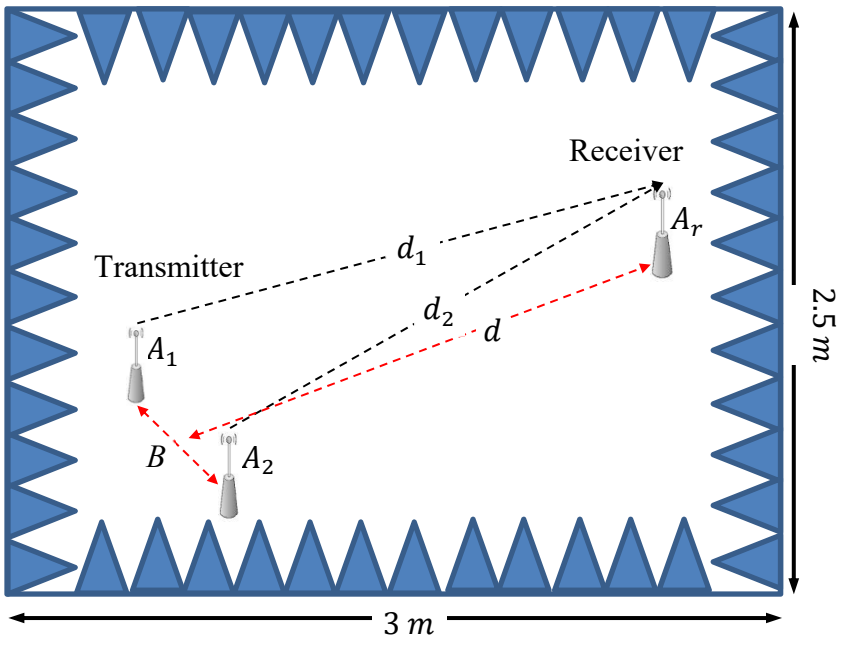

Figure 4-19: Anechoic Faraday Chamber and MISO configuration

We first test the situation leading to a null TDOA, where due to the symmetry of LOS path, the MISO channel behaves like SISO channel giving hence a flat frequency response. We show in Figure 4-20 (a) and (b), the real part and imaginary part of the channel frequency response.

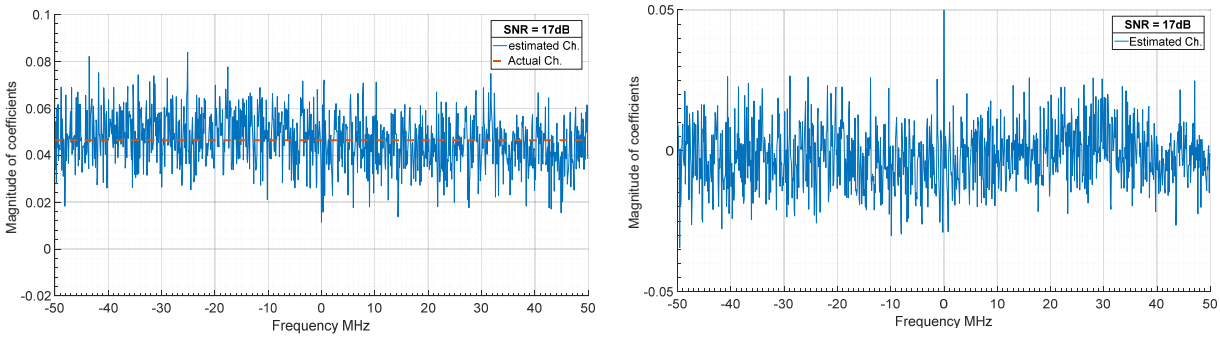

(a) (b)

Figure 4-20: MISO channel frequency response with equal LOS paths
a) real part and b) imaginary part

As seen, we didn't normalize the real and imaginary part of the channel, because we will use the real part in estimation of the coefficients α_1, α_2, already discussed in the direct model in chapter 3. These parameters will be used to extract the useful information as suggested in equation 14 in chapter 3.

4.3.2 **Baseline calculation**

Let's remember that we target in this work the estimation of TDOAs that are smaller than $1/f_d$. Using the relationship (1) between the baseline and the bandwidth, the baseline B should verify:

$$B < c \cdot \frac{1}{f_d} \tag{55}$$

With f_d =100MHz, the baseline is less than 3 meters, which is prohibitive for mobile devices. We showed in chapter 3 that minimum estimated TDOA is loosely $\frac{5}{f_s}$ with f_s the frequency sampling. Compared to f_d we gain a factor 20, which by turn may reduce the size of B which is now 15 cm.

Table 4-3: Baseline B in terms of available bandwidth f_d

	$f_d = 100\ MHz$	$f_d = 400\ MHz$	$f_d = 1\ GHz$
$\tau = \frac{1}{f_d}$	10 ns	2.5 ns	1 ns
B	3 m	75 cm	0.3 m
$\tau = \frac{1}{2*f_d}$	5 ns	1.25 ns	0.5 ns
B	1.5 m	0.375 m	0.15 m

Let's note that with wider bandwidth that, for example, used in millimeter wave communication or for 5G, makes B less than few centimeters as shown in Table 4-3

For the rest of the chapter, B is set to 20 cm. However to control in a proper way the actual TDOA, we choose to generate it in MATLAB, and to put the relative position of MU and RU in a fixed paraxial situation. Doing that, B will not impact the TDOA but makes the channel more realistic.

4.3.1 Calibration MISO system

We mean by calibration, the process to find the exact zero position of the MU with respect to the RU. In other words, the zero position is the paraxial position of the MU, where the two LOS paths d_1 and d_2, Figure 4-19 are equal. This means that the two branches are truly balanced. We aim here, by calibration, to reduce any imbalance between these two branches by compensating all the inserted delay time brought by the LAN and any other devices.

We do this simply by considering MISO configuration as the superposition of two SISO configurations i.e. SISO 1 between A_1 and A_r and SISO 2 between A_2 and A_r. So by measuring the signal power of each SISO and make a comparison between them we decide if the MU is in zero position or not. If the signal power of SISO 1 is bigger than the signal power from the SISO 2, then we move the MU one step to one direction, let's say right. If the in the next measure we still have the signal power from SISO 1 is bigger than the signal

power from the SISO 2 then we move the MU two step to the opposite direction, here is left, or if not we move it in the right once again. Doing that several times we could find almost an optimal position marked as zero position.

4.3.2 MISO configuration for TDOA estimation

The block diagram of the transmitter side is displayed at Figure 4-21

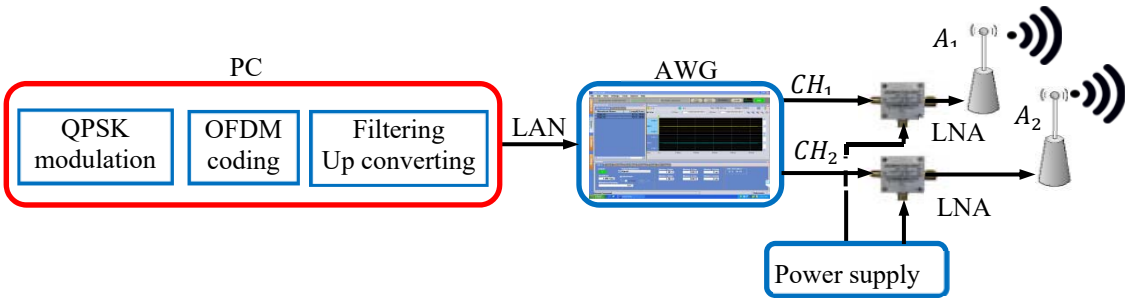

Figure 4-21: The transmitter block diagram

As described in chapter 2, the sounding OFDM signal is designed using MATLAB code, first by constructing the QPSK symbols, and then building up the OFDM frame. Finally, the resulting signal is filtered and up converted to the carrier frequency f_c=3GHz.

As mentioned earlier, the signal is replicated with a time delay acting as the TDOA of interest. For sake of clarity, the actual TDOA is set here to 10ns, so we can see the time shift in the Figure 4-22 below.

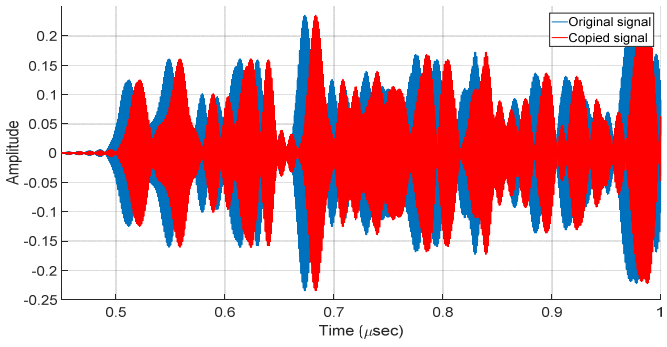

Figure 4-22: The transmitted signal and its delayed version using TDOA=10ns

For symmetry reasons, the actual TDOAs will be chosen in the interval $[\frac{1}{fs}, \frac{1}{f_d}]$. This interval is divided into 31 times, thus this will give us a graph with time scale of 31 points.

The setup of the devices of the communication system is plotted in the Figure 4-23.

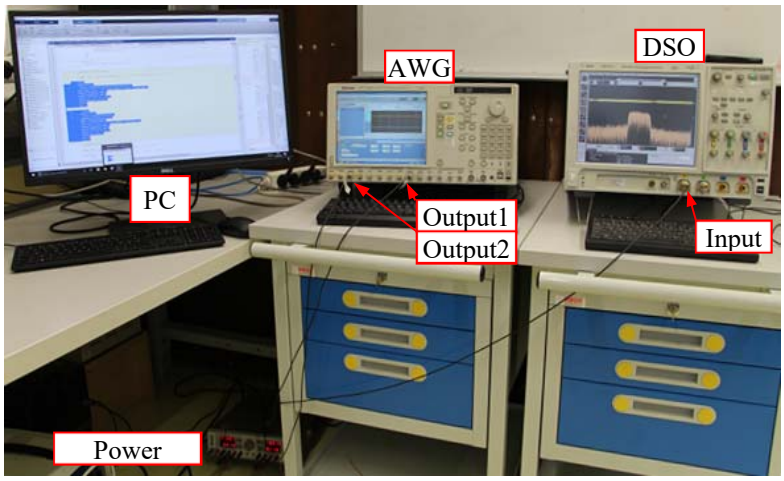

Figure 4-23: The OFDM communication setup for TDOA estimation

4.3.3 **Direct model validation**

To demonstrate the impact of the TDOA on the received signal spectrum, and validate the direct model, we plot it for several values of TDOA, considering the available bandwidth f_d, as shown in the figures below.

First we take the TDOA as four times the inverse of bandwidth $\tau = 4/f_d$, so we could see the periodicity. As clearly seen the shape of the received signal is modulated in amplitude by TDOA in the DSO Figure 4-24

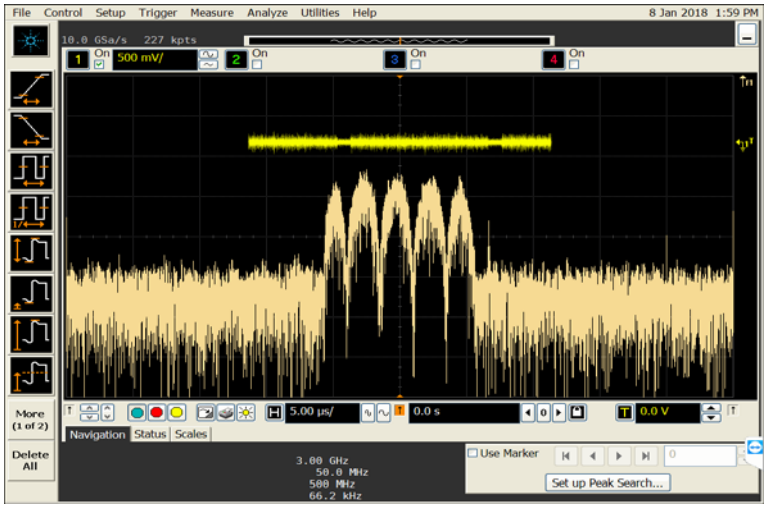

Figure 4-24: Experimental spectrum of the received signal displayed on the DSO with TDOA =40ns.

Also the channel estimation has the same periodicity in the frequency domain as shown in the Figure 4-25 below.

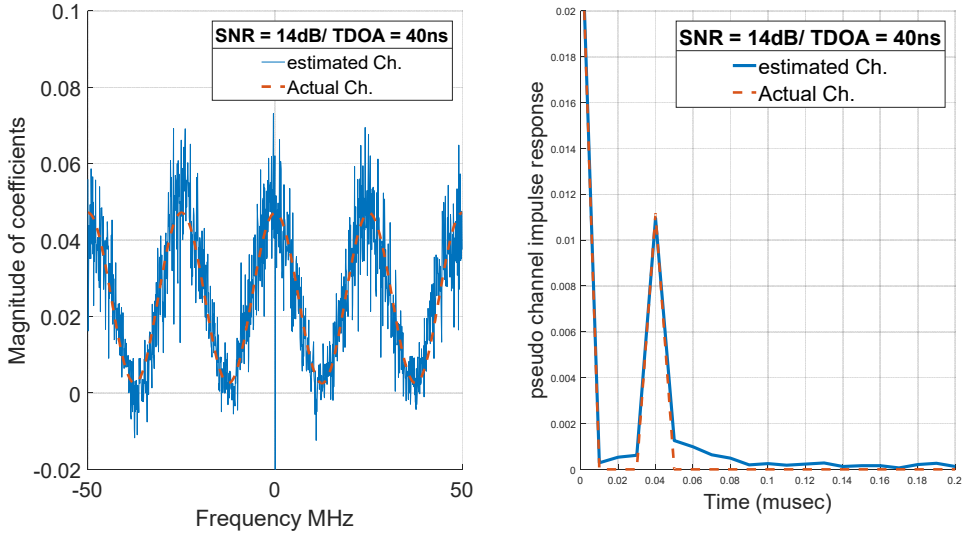

Figure 4-25 : Experimental Channel estimation and impulse response in TDOA domain, with TDOA = 40ns

As expected, by using the Fourier decomposition, one can access to a kind of "spoof" channel impulsive response, which is directly expressed in the domain of TDOA. The first non-zero line in this spectral analysis is the TDOA of interest = 40ns.

Now if we take TDOA less than the inverse of the bandwidth, let us take $\tau = \frac{0.5}{f_d}$, then no periodicity occurs in the spectrum of the received signal, as seen in Figure 4-26.

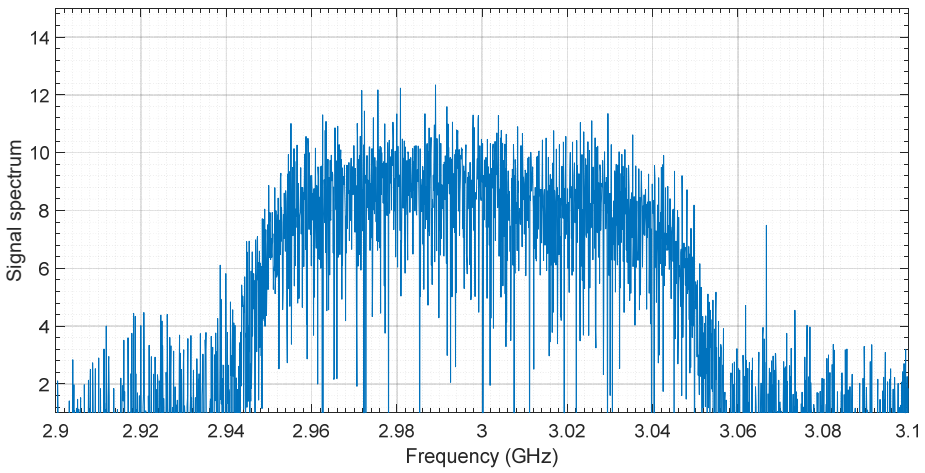

Figure 4-26: Experimental spectrum of the received signal with $= 0.5 / f_d$.

As the received spectrum is modulated by the TDOA then the channel frequency response will do as well. So we estimate the channel for the above received signal by using the method described in chapter 2.

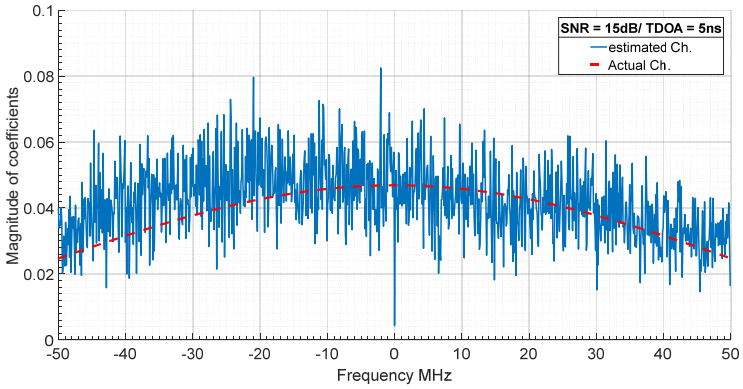

Figure 4-27 : Direct model validation with $\tau = 0.5 \,/\, f_d$

As depicted in Figure 4-27 the channel estimation has the same shape as the direct model.

4.3.4 **Inverse model validation**

In this section the mathematical derivation using the Useful Information $US_J(\tau)$, equation (43) is applied in a free space configuration. The curves shown in Figure 4-28 give the RMSE in TDOA estimation obtained for three values of SNR [6.5, 10, and 19] dB. The results are fairly good, but we see at higher TDOA values some kind of deviation in the three curves.

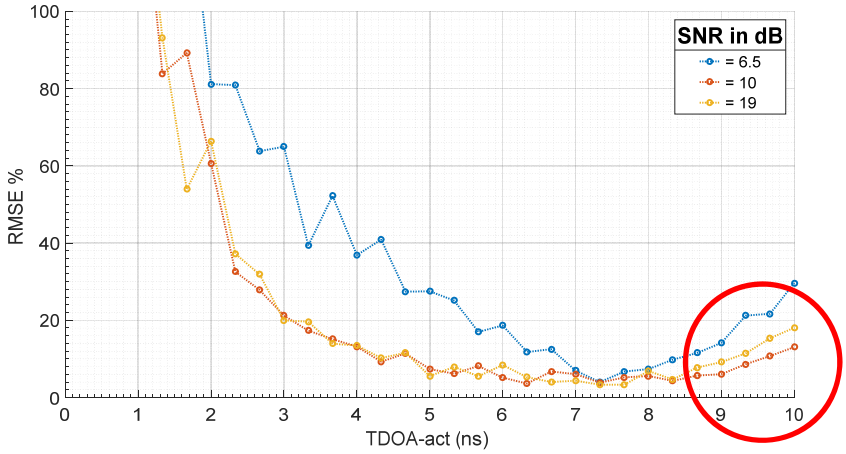

Figure 4-28: $US_J(\tau)$ estimator performance: RMSE vs. actual TDOA performance in free space.

These deviations are due to the error in estimating the coefficients of α_1, α_2. As we said former, the estimation of these parameters is not perfectly achieved.

So we apply the proposed solution in chapter 3 section 3.5.1, which is based on added time delay τ_p and phase demodulation. This solution solves the problem of α_1 estimation only. However this solution improved significantly the performance of our estimator and as seen in the figure the results over 8 ns in Figure 4-29 are better than in Figure 4-28.

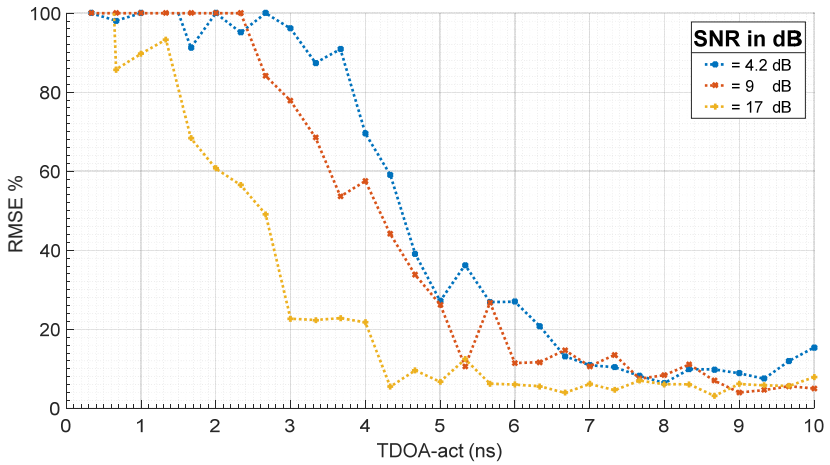

Figure 4-29 : $US_{Jdelay}(\tau)$ estimator performance: improved RMSE vs. actual TDOA in free space with τ_p= 100ns

It can be seen that when the signal-to-noise ratio is 17 dB, an error of less than 10% is obtained for TDOAs less than one half of the inverse of the available bandwidth, e.g. $\tau = 4.4ns$. This demonstrates that the approach makes possible to resolve small TDOA.

However these results are not as good as the simulation results, since there are some effects that need to be taken into account, such as the coefficient α_2. Prospective works need to focus on the calibration process to increase the performance of the estimator.

By this we finish testing our simulation in free space channel, and address in the next section the multipath channel.

4.3.5 **Multipath effects**

To deal with this situation we generate the multipath considering two ways.

4.3.5.1 **Generating multipath by MATLAB code**

As studied in chapter 3, MATLAB can help generating multipath by producing several delayed copies of the original signal, and adding them to the LOS path signals. We recall the definition of K factor as the ratio of signal power in LOS components over the signal power of NLOS components. The estimator is applied under different values of K factor belonging to the set [5, 15] dB and considering SNR set to 17dB. Figure 4-30 shows as expected that the performance of the estimator is getting better while the K factor increases.

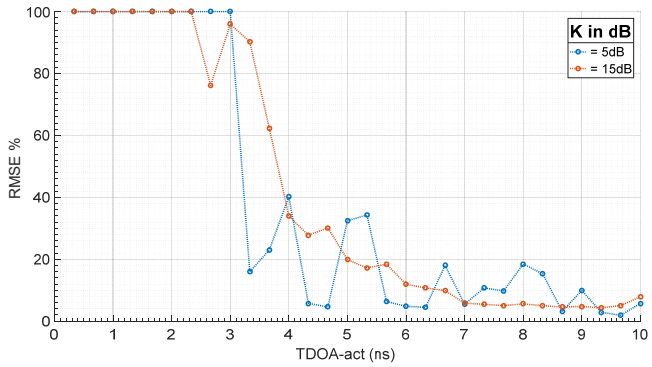

Figure 4-30: $US_J(\tau)$ estimator performance RMSE vs. actual TDOA in multipath scenario

As expect also, when K = 15 the estimator behaves almost like in free space channel, especially with higher values for TDOA.

4.3.5.2 **Generating multipath by installing a reflector in the AFC**

The second way to generate multipath, is by installing a reflector inside the AFC as depicted in Figure 4-31.

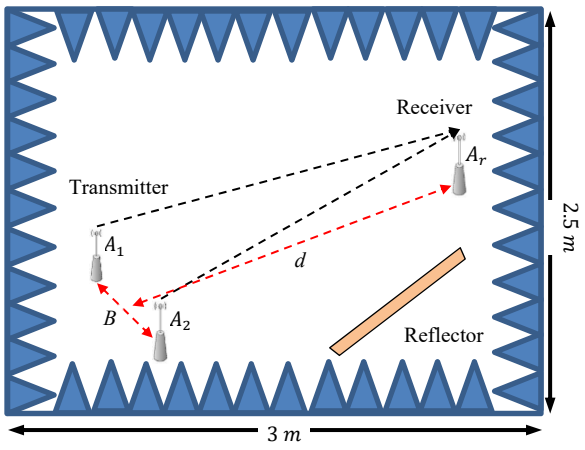

Figure 4-31 : Anechoic Faraday Chamber and MISO configuration with a reflector

The reflector is made of metallic sheet and installed vertically. This will generate a real multipath channel. The estimator is applied under SNR equal to 17 dB in mean value.

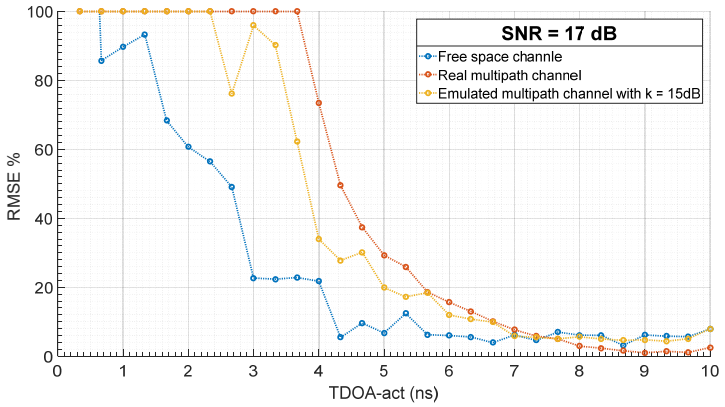

Figure 4-32: $US_J(\tau)$ estimator performance RMSE vs. actual TDOA in multipath scenario.

As seen in the figure above, the K factor plays an important role in estimation process. We also notice that the added reflector produces multipath that behaves like having a *K* factor = 15dB. This impact maybe reduced by using circular polarized antenna.

4.4 Conclusion

In this chapter we have test our methods to estimated TDOA using MISO configuration within an available bandwidth set to 100MHz. A test bench is presented and its performance tested under several conditions of propagation and of noise. We investigated the overall proposed method measurement using this setup. Its performances appeared to be good, proving that it is possible to have less than 10% of error of TDOA within a bandwidth less than what usually used. Nevertheless, with the used bandwidth, the current system is not yet capable of estimating TDOA under the condition of small baseline compliant with embedded mobile unit. Increasing the available bandwidth, as suggested for 5G new radio communications, may help in achieving this objective.

Conclusions and perspectives

Time delay estimation is an important area that attracts significant research interest. It is accomplished using UWB or Multicarrier signals to serve many applications, such as the indoor navigation, detection and tracking of persons or objects, and so on. The analysis of the state of the art of the time delay based indoor location systems and their forthcoming applications, in the context of 5G and beyond, encourages us investigating in this research domain.

The main objective of this work is to contribute to the field of TDOA estimation by proposing different solutions that overpassed the conventional resolution related to Fourier approach. We target in this report the TDOA estimation between two collocated antennas, acting as a Reference Unit (RU), and a single receiving antenna, acting as a Mobile Unit (MU). This states the MISO configuration we dealt with all along with this work.

Based on the deep understanding of the OFDM communication channel, the method proposed is led in the spectral domain. Using MISO channels, this new approach exploits the behavior of the received spectrum when multiple delayed signals are incoming on the MU.

We start this study by performing mathematical derivation to define the direct model linking the frequency response channel to the TDOA. The communication parameters dealing with roll off factor, pilots, SNR, multipath are all taken into account and their impact on the direct model clearly stated. Such approach has been simulated using MATLAB and experimentally validated with different channel configurations, and test conditions.

Once the channel estimation performed, the inverse problem consists in extracting TDOA information from the channel state information. TDOA estimation is obtained by using different approaches dealing with fitting the direct model, integration over the bandwidth of the complex frequency response of the channel or phase demodulation of the received signal. In each proposed estimator, the appropriate model is derived and evaluated. The performance of the best estimator is tested using both MATLAB code simulation and experiments in a controlled indoor environment. Its comparison with the Cramer Rao Lower Bound is performed when unbiased data are exploited.

In the free space channel and considering a SNR of 10dB, the simulation results show that despite a null-to-null bandwidth of 100 MHz, the TDOA can be estimated with an error less than 11%, up to 0.5 ns. This infers that the proposed method, qualified as super resolution, behaves like using a null-to-null bandwidth of 2 GHz leading to a gain of 20.

In the multipath channel, the preliminary results show that considering a SNR of 17dB, the TDOA can be estimated with an error less than 10%, up to 7 ns.

Future work

As mentioned before, the TDOA estimation within the OFDM signal in the multipath environments has recently attracted more and more research interests. It is thus clear that our work could not cover all the possible aspects of it. So we propose a few listed numbers of tasks and directions for the future research.

The Channel estimation improvement: since the proposed TDOA estimation depends primarily on the MISO channel estimation accuracy, improving its estimation is one of the most important ways to have accurate TDOA estimation. We indeed suggest to insert in the direct model the effect of the roll-off factor and to exploit maybe the phase of the frequency response channel.

The calibration process needs also to be addressed. As described in TDOA estimation, there are some dependent coefficients that need different SISO configurations to be well estimated. How to improve this, or better how to avoid this?

Influence of the Antenna Radiation Pattern: The radiation patterns of the antennas were not addressed in this work. However their influence is of prime importance since they condition the covered area, and by coupling effects in the RU, they contribute to decrease the estimator performance. It should be interesting to explore SIMO configuration for which the collocated antenna would be in the receiving part and coupling effects may be reduced.

To be 5G compliant, the proposed solution may address new radio solutions based on different multicarrier techniques dealing with FBMC for Filter Bank Multi-Carrier, UFMC, for Universal Filtered Multicarrier, GFDM for Generalized Frequency Division Multiplexing and Filtered OFDM.

List of publication

International conferences:

2016 Ahmed Abudabbousa, Sarrazin Julien , De Donker Philippe, Benlarbi-Delaï Aziz "Short Survey of Wireless Indoor Positioning TDOA", International Conference on Smart Cities Solutions 2016.

2017 Ahmed Abudabbousa, Sarrazin Julien , De Donker Philippe, Benlarbi-Delaï Aziz "Multicarrier Technique-Based Super-Resolution TDOA Estimation", MMS 2017

National conferences:

2017 Ahmed Abudabbousa, Sarrazin Julien , De Donker Philippe, Benlarbi-Delaï Aziz "Approche super-résolutive pour la mesure de la différence de temps d'arrivée (TDOA) à partir de trames OFDM", JNM 2017

Abbreviations

Abbreviation	Description
AFC	Anechoic-Faraday Chamber
AOA	Angle of arrival
AWG	arbitrary waveform generator
BER	Bit error rate
CCC	Cross-Correlation Computation
Cell-ID	Cell Identification
CFR	Channel frequency response
CN	Closest-neighbor
COO	Cell Of Origin
CP	Cyclic prefix
CRB	Cramer-Rao bound
CS	Cyclic suffix
CSI	Channel state information
DR	Dead Reckoning
DSO	Digital storage oscilloscope
EM	Expectation maximization
GCC	Generalized cross-correlation
ICT	Information and Communication Technology
IoP	Internet of Places
IoT	Internet of Things
IP	Indoor positioning
IR	Infrared
IRP	Indirect remote positioning
ISI	Inter symbol interference
ISP	Indirect self-positioning
KNN	K-nearest-neighbor
LAN	Local area network
LNA	Low Noise Amplifier
LOS	Line of sight
LS	Least Square
MC	Multicarrier
MISO	Multiple-Input Single-Output
ML	Maximal likelihood
MP	Multipath
MSE	Mean-square-error
MU	Mobile unit

NLOS	Non Line-of-sight
OFDM	Orthogonal Frequency Division Multiplexing
PNs	Personal Networks
POA	Phase of arrival
PSD	Power spectral density
QPSK	Quadrature phase shift keying
RF	Radio Frequency
RFID	Radio frequency identification
RRC	Root raised cosine
RSS	Received signal strengths
RTOF	Roundtrip Time of Flight
RU	Reference unit
RWGH	residual weighting
SIMO	Single-Input-Multiple-Output
SISO	Single-Input-Single Output
SMP	Smallest M-vertex polygon
SNR	Signal to noise ration
SVM	Support vector machine
TDOA	Time Difference Of Arrival
TOA	Time of arrival
UWB	Ultra-wideband
WLAN	Wireless local area network
WRELAX	weighted-Fourier-transform-based relaxation

List of Figures

Figure 1-1: Personal Networks (PNs). 5
Figure 1-2: Understanding Indoor Positioning System. 7
Figure 1-3: Example of IR Positioning system: The Firefly motion tracking architecture. 8
Figure 1-4: Flow Chart of general Indoor positioning system. 14
Figure 1-5: Time of arrival (ToA)-based approach. 15
Figure 1-6 Time difference of arrival (TDOA)-based approach. 17
Figure 1-7: Principle of carrier phase interferometry. 18
Figure 1-8: Example of RTOF system : Essensium Positioning System. 18
Figure 1-9: Basic AOA positioning. 19
Figure 1-10: General block diagram the proposed method. 22
Figure 2-1: The block diagram of TDOA estimation 29
Figure 2-2: Constellation diagram of QPSK, (a) transmitting side, (b) receiving side 33
Figure 2-3: Example of the spectrum of the received signal 35
Figure 2-4: QPSK Modulator/ Demodulator Block diagram 36
Figure 2-5: BER verses SNR – Performance curve for QPSK Modulation 37
Figure 2-6: Constellation diagram: (a) at the transmitter, (b) at the receiver for SNR = 30 dB, (c) for SNR = 15 dB, (d) for SNR = 1 dB 37
Figure 2-7: OFDM implementation (a) modulation (b) demodulation 39
Figure 2-8: Effect of a multipath channel on the received signal with CP: (a) OFDM symbols with CP (b) ISI effect of a multipath channel on OFDM symbols with CP length shorter than the maximum delay of the channel. 41
Figure 2-9: Frequency-domain equivalent model of OFDM system 42
Figure 2-10 Raised cosine window for OFDM symbol 43
Figure 2-11: OFDM symbol generation 44
Figure 2-12: Time and Frequency responses of transmitted signal $s(t)$ using a central frequency $fc = 3\ GHz$ 45
Figure 2-13: OFDM symbol reception. 45
Figure 2-14: Frequency responses of received signal (t) : (a) at A, and b) at B 46
Figure 2-15: BER vs. SNR – Performance curve for OFDM 46
Figure 2-16: Block-type pilot arrangement 48
Figure 2-17: Communication block diagram and channel estimation subsystem 50
Figure 2-18: Channel responses with multipath: (a) frequency domain (b) time domain 51
Figure 2-19 BER verses SNR – Performance curve with channel effect 51
Figure 3-1: MISO acquisition (a) and associated geometry (b) 57
Figure 3-2: Simulation block diagram of an OFDM based SISO communication emulating a MISO scenario 60
Figure 3-3: Examples of squared magnitude of the channel transfer function without noise. . 61
Figure 3-4: Roll of factor effect on the square of magnitude of the transfer function. Test parameters are reported in Table 3.1 and SNR = 20 dB 62
Figure 3-5: Channel estimation components for 3 different TDOA with β=0.15: a) Real part, b) Imaginary part 63
Figure 3-6: Channel estimation components for 3 different TDOA with β=0.15: 63
Figure 3-7: Two kinds of representation of the channel transfer function a) in the frequency domain, b) in the time difference of arrival domain. 65
Figure 3-8 : Square of magnitude of "edged" channel 66
Figure 3-9: Block diagram of TDOA estimation using $USSM(f, \tau)$ 67

Figure 3-10 : $USSM(f,\tau)$ estimator performance with SNR=10dB 68
Figure 3-11: Block diagram of TDOA estimation using $USI(f,\tau)$ and $USQ(f,\tau)$ 69
Figure 3-12 : $USI(f,\tau)$ and $USQf,\tau$ estimators performance with SNR=10dB 69
Figure 3-13: Block diagram of TDOA estimation using $US_J(f,\tau)$ function 71
Figure 3-14: $USJ(f,\tau)$ estimator performance 71
Figure 3-15 : $USJ(f,\tau)$ estimator performance with different SNR 72
Figure 3-16: Definition of the optimal added time delay around the inflexion point 73
Figure 3-17: Block diagram of TDOA estimation with τopt= 4.5 ns 73
Figure 3-18: $USJ(f,\tau)$ estimator performance with τopt= 4.5ns: The RMSE in % versus the actual TDOA. 74
Figure 3-19 : Estimator performance with τopt= 4.5ns: the RMSE in % versus the actual TDOA. 74
Figure 3-20: CRBL Theory and simulation results comparison for $USJ(f,\tau)$ based estimator 76
Figure 3-21: Estimator performance: The RMSE in % versus the actual TDOA 77
Figure 3-22: Multipath modeling 78
Figure 3-23: Channel estimation with multipath 80
Figure 3-24: TDOA estimation with multipath efffect. 80
Figure 3-25: Fitted Normal Cumulative Distribution Function with different accepted error of the estimated value at $\tau opt = 4.5\ ns$ ns, with SNR = 20 dB 81
Figure 4-1: The Anechoic-Faraday Chamber 86
Figure 4-2: Photograph of the Anechoic-Faraday Chamber 86
Figure 4-3: Radiating device a) photograph of the used antenna, b) radiation pattern in H Plane 87
Figure 4-4: The interface display of the AWG 7122B 88
Figure 4-5: The interface display of the DS0-91204A 89
Figure 4-6: The transmitter block diagram 90
Figure 4-7: Experimental spectrum of the transmitted signal 90
Figure 4-8: Experimental I-Q components of the transmitted signal in time domain 91
Figure 4-9: The receiver block diagram 92
Figure 4-10: Experimental spectrum of the received signal 92
Figure 4-11: The received signal in time domain 93
Figure 4-12: the received signal captured from DSO 93
Figure 4-13: Received signal, transmitted signal, the correlation between them, and the RX signal aligned 94
Figure 4-14: QPSK constellation diagram with SNR 20dB 95
Figure 4-15: Experimental BER versus SNR for OFDM communication 95
Figure 4-16: QPSK constellation diagram over OFDM 96
Figure 4-17: Normalized channel estimation in SISO free space channel 97
Figure 4-18: Normalized channel estimation in SISO multipath channel 97
Figure 4-19: Anechoic Faraday Chamber and MISO configuration 98
Figure 4-20: MISO channel frequency response with equal LOS paths a) real part and b) imaginary part 99
Figure 4-21: The transmitter block diagram 101
Figure 4-22: The transmitted signal and its delayed version using TDOA=10ns 101
Figure 4-23: The OFDM communication setup for TDOA estimation 102
Figure 4-24: Experimental spectrum of the received signal displayed on the DSO with TDOA =40ns. 102
Figure 4-25 : Experimental Channel estimation and impulse response in TDOA domain, with TDOA = 40ns 103

Figure 4-26: Experimental spectrum of the received signal with $= 0.5 / fd$ 103
Figure 4-27 : Direct model validation with $\tau = 0.5 / fd$ 104
Figure 4-28: $USJ(\tau)$ estimator performance: RMSE vs. actual TDOA performance in free space. 104
Figure 4-29 : $USJdelay(\tau)$ estimator performance: improved RMSE vs. actual TDOA in free space with τp= 100ns 105
Figure 4-30: $USJ(\tau)$ estimator performance RMSE vs. actual TDOA in multipath scenario 106
Figure 4-31 : Anechoic Faraday Chamber and MISO configuration with a reflector 106
Figure 4-32: $USJ(\tau)$ estimator performance RMSE vs. actual TDOA in multipath scenario. 107

List of Tables

Table 1-1 Comparison between Indoor Positioning Technologies. 13
Table 2-1 QPSK symbol mapping definition 32
Table 2-2 Parameters of QPSK simulation 36
Table 2-3 Numerical values for the OFDM parameters 44
Table 2-4 Simulation Parameters 50
Table 3-1 Test parameters 61
Table 3-2 Test parameters 67
Table 3-3 Simulation parameters for CRBL 75
Table 4-1 : LNA features 88
Table 4-2 Values of the parameters 91
Table 4-3: Baseline B in terms of available bandwidth fd 100

***Résumé** :*

Cette thèse présente une solution originale permettant d'extraire, à partir de signaux de communication OFDM, l'information liée à la différence de temps d'arrivée (TDOA) entre deux émetteurs très proches et un récepteur. Cette méthode, qui s'avère super-résolutive, permet d'extraire des TDOA en dessous de la limite de Rayleigh fixée par la bande passante utile.

1. Introduction

Les technologies des communications sans fil ont induit de nombreux usages et de nouveaux besoins fondés sur les données spatio-temporelles des objets connectés. L'information de localisation devient alors une donnée incontournable pour qui souhaite exploiter la dimension spatiale d'une communication sans fil à des fins d'augmentation de débit ou de focalisation de l'information. Elle est aussi centrale pour de nombreux algorithmes de routage avec comme but, le maintien de la connectivité dans les réseaux ad hoc et elle est naturellement à la base de toutes les applications géo contextualisées qui se retrouvent notamment dans le concept de l'internet des choses (*IoT*).

D'un point de vue technique, la localisation d'un objet connecté se fonde principalement sur quelques métriques dont les principales utilisent le temps de vol entre un émetteur et un récepteur synchronisés, ou les différences de temps d'arrivée entre un émetteur et deux récepteurs synchronisés. Le principe de réciprocité permet le cas échéant d'inverser les rôles entre émetteurs et récepteurs. D'autres métriques fondées sur le niveau de puissance reçue ou sur l'angle d'arrivée peuvent aussi être envisagées.

La qualité de l'information de localisation est, compte tenu du canal de propagation considéré, directement liée à la précision de mesure de la métrique retenue. On se propose dans cette thèse de définir une méthode originale permettant d'estimer la différence de temps d'arrivée (TDOA : *Time Difference of Arrival*) entre un émetteur formé d'un couple d'antennes et un récepteur à antenne unique. Dans cette configuration, appelée MISO (*Multiple Inputs Single Output*), des trames OFDM occupant une bande passante f_d autour d'une fréquence centrale f_c, assurent la communication sans fil et autorisent, par la même occasion, l'extraction de la TDOA.

2. *Principe de la méthode*

A partir de signaux de communication utilisant des trames OFDM, on se propose, en opérant avec une configuration MISO telle que sur la Figure 33, de déterminer, avec une résolution supérieure à celle susceptible d'être obtenue par des méthodes classiques utilisant l'analyse spectrale de Fourier, la différence de temps d'arrivée TDOA "τ" entre les antenns ($A_1 et\ A_2$) et l`antenne A_R.

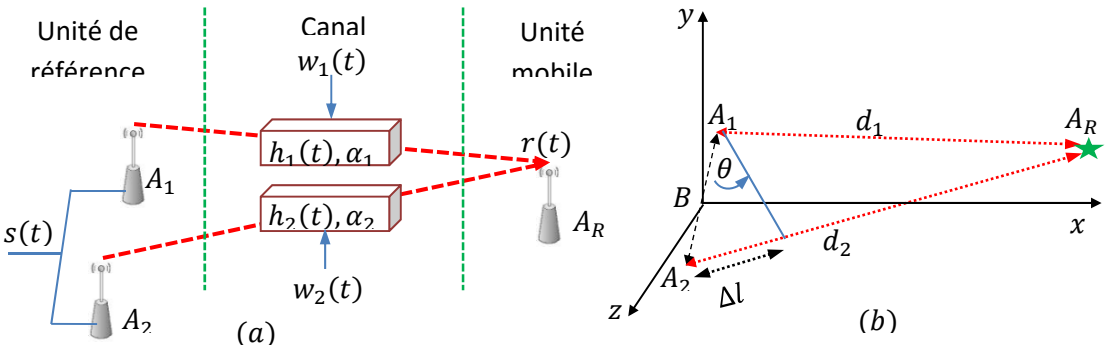

Figure 33. Géométrie d'acquisition MISO

2.1 *Définition du modèle direct*

On considère une trame OFDM $X(f)$ comportant M sous porteuses et occupant une bande passante f_d. Cette trame est transposée en fréquence autour de f_c et est émise par un couple d'antennes A_1 et A_2, séparées d'une distance B appelée « *baseline* ». A la réception, le signal s'écrit en bande de base et en présence d'un bruit blanc gaussien W de densité spectrale $N_0/2$:

$$Y(f) = H_1(f) \cdot X(f) + H_2(f) \cdot X(f) + W(f) = H(f) \cdot X(f) + W(f) \qquad (56)$$

avec $H_1(f) = \alpha_1 e^{-i2\pi f t_1}$ et $H_2(f) = \alpha_2 e^{-i2\pi f t_2}$, les fonctions de transfert vues respectivement entre A_R et A_1 et entre A_R et A_2 ,

Notons que l'effet du canal autour de la fréquence porteuse f_c a été reproduit en bande de base conservant ainsi l'information d'intérêt "τ".

2.2 *Détermination de la différence des temps d'arrivées*

Pour résoudre le problème inverse, consistant extraire à partir des mesures canal, la différence de temps d'arrivée, on se propose de minimiser l'une des fonctionnelles suivantes :

$$\mathcal{F}_1(\tau) = G_1\big(H(f,\tau)\big) - cos(2\pi f\tau) \quad \Rightarrow \quad \tau = argmin\,(\mathcal{F}_1(\tau)) \qquad (57)$$

$$\mathcal{F}_2(\tau) = G_2\big(H(f,\tau)\big) - sin(2\pi f\tau) \quad \Rightarrow \quad \tau = argmin\,(\mathcal{F}_2(\tau)) \qquad (58)$$

$$\mathcal{F}_3(\tau) = G\big(H(f,\tau)\big) - cos(2\pi f\tau) \quad \Rightarrow \quad \tau = argmin\,(\mathcal{F}_3(\tau)) \qquad (59)$$

Ou G_1, G_2, et Gsont différents fonctions appliqués à la fonction de transfert du canal pour s'approche du problème direct.

Les courbes de la Figure 34(a) montrent, en simulation, l'erreur relative commise dans la mesure de τ en utilisant la relation (5) en fonction de "τ", paramétrée par plusieurs valeurs du rapport signal à bruit (SNR). On voit que pour un rapport SNR de 20 dB, il est possible de mesurer "τ" jusqu'à 1 ns avec une erreur inférieure à 10%. Pour un SNR voisin de 10 dB, des valeurs de τ supérieures à 3 ns sont mesurables avec une erreur inférieure à 10% alors même que la bande passante utilisée, ici $f_d = 100MHz$, ne permettait de résoudre que des TDOA supérieures à 10 ns.

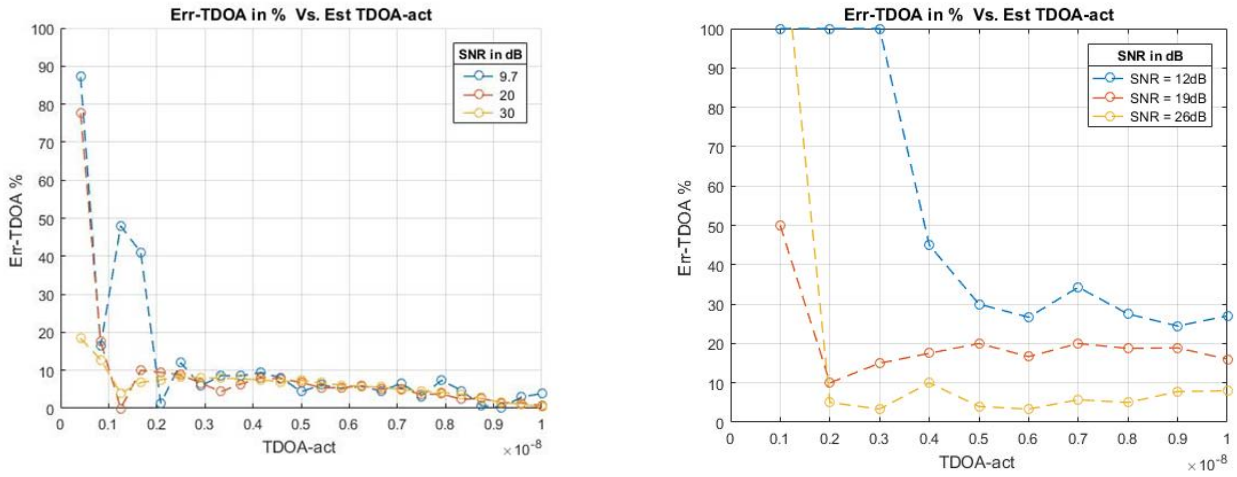

(a) (b)

Figure 34 Erreur relative en % sur $\tau_{\text{estimé}}$ en fonction de $\tau_{\text{réel}}$, pour différentes valeurs de rapport signal à bruit, f_d=100MHz, en utilisant la fonctionnelle $\mathcal{F}_3(\tau)$

Les courbes de la Figure 34 (b) montrent, sur le plan expérimentale, les TDOA retrouvés en fonction des TDOA générés dans Matlab pour différents niveaux de rapport signal à bruit. On montre bien que même des TDOA inférieurs à l'inverse de la bande passante utile peuvent être déterminées avec une bonne précision. On voit que lorsque le rapport signal à bruit est supérieur à 25dB, une erreur inférieure à 10% est obtenue pour des TDOA inférieurs au cinquième de l'inverse de la bande passante utile, soit $\tau = 2ns$. Cela

démontre que cette approche permet de résoudre des différences de temps d'arrivée susceptibles d'être obtenue par un système de bande passante équivalente à 500MHz.

3. Gestion des trajets multiples

La solution préconisée, utilisant des trames OFDM supportant des préfixes cycliques ad hoc, contribue naturellement à réduire drastiquement les effets des trajets multiples.

Toutefois des situations nouvelles, propres à la configuration MISO et à l'exploitation des différences de temps d'arrivée peuvent survenir et dégrader la précision de la mesure. En effet, si la différence des temps d'arrivée provenant des trajets multiples tombe dans l'intervalle utile défini par le Baseline *B,* alors la précision de la mesure sera considérablement dégradée. Pour s'en prémunir, des solutions de réduction de ces effets des trajets multiples peuvent être déployées.

En plus du filtrasse fréquentielle, l'utilisation de la polarisation circulaire permet de réduire, en plus de l'atténuation de propagation, logiquement plus grande pour les trajets multiples, et en vertu du facteur de polarisation croisée des antennes, d'au moins 15 à 20 dB supplémentaire le signal portant ces trajets multiples, réduisant ainsi leur impact sur la précision de la mesure.

4. Conclusion

Nous avons proposé une solution originale et simple à déployer pour extraire l'information de TDOA à partir de signaux OFDM. La géométrie d'acquisition requiert une configuration de type MISO qui, dans le cadre du futur standard 5G et des communications millimétriques, conduit naturellement à un encombrement réduit. Les résultats de simulation qui démontrent le caractère super-résolutif de la solution sont confrontés aux résultats expérimentaux et un bon accord est observé. L'erreur sur la mesure de la différence de temps d'arrivée et la plus petite TDOA mesurable montrent un gain d'au moins 5 pour la bande passante théoriquement requise.